The Scattering of Waves by An Elastic Floating Body on Water of Variable Depth

A thesis presented in partial fulfillment
of the requirement for the degree of
Master of Science
in the subject of
Mathematics

at Massey University, Albany, New Zealand

Synthia Dewi Darsono

2000

Abstract

For many years polar scientists and offshore engineers have studied the behavior of a floating body in the presence of ocean waves. A large floating structure, such as a floating runway or an ice sheet, is sufficiently thin so that elasticity is important. The solution of the motion can found by coupling the water and elastic plate equations. However these solutions have only been calculated when the water is of constant depth.

In this thesis we shall present a solution for wave scattering by an elastic body on water of variable depth. Our solution method involves partitioning the problem domain into finite and semi-infinite regions. In the semi-infinite region the solution is obtained using an integral equation. A boundary element method together with a Green's function for the thin plate is used to solve for the finite region. The separate solution are then coupled to give the solution for the full problem.

Acknowledgments

I would like to express my greatest gratitude for my supervisor Dr. Michael Meylan for his help and advice during the completion of this thesis. To me he is not only a supervisor but also a mentor and a friend who has given me all the support and encouragement that a master student needs. This thesis would not be possible without him.

I am also very grateful for the help and the time given by Mr. Adrian Swift and Judith Scheffer who have patiently proof read this thesis.

Finally I would like to thank my parents Lukman Darsono and Endang Sentyaningrum for their financial and emotional support during my postgraduate study.

Contents

List of Figures

Chapter 1
Introduction

For many years the study of ocean waves has been of interest in polar and offshore engineering. The object of the study is to find out how an arbitrary large floating body on the surface of the water behaves in the presence of an ocean wave. Some researchers are interested in the motion of the floating body while others study the motion of the water itself. Our main interest is to study the motion of the water in the presence of a floating body, by calculating the scattering of the water wave.

The scattering of the wave is influenced by many factors, the most important of which are the shape and the elasticity of the floating body. For example a round-shaped body rocks in different way from a flat-shaped body. A body of significant stiffness (such as a ship) is said to have small elasticity which is not important in determining the scattered wave, but for a sufficently thin body (such as a thin ice sheet) elasticity becomes important. We only consider a floating body which is flat, rectangular, and thin, so that elasticity is important. As well as the shape and elasticity of the floating body, the shape of the seabed also influences the behaviour of the wave. A constant bed topography (flat seabed) does not scatter the wave while a non-constant bed topography (varying seabed), such that the depth of the water is variable, scatters the wave. In this thesis we seek solutions for the scattering of waves by an elastic floating body on the surface of water with variable depth. The elastic floating body and the varying seabed are referred to as the scatterers.

The main reason for our interest is that, to our knowledge, no author has solved the scattering problem for the elastic floating body with varying seabed. However many publications have presented a number of solutions for simpler problems. There are two types of simplified problem, one which considers the elastic floating body only while the seabed is constant and the other one is to have a varying seabed with the surface of the water free. The first type of the simplified problem was solved by *Meylan* (1993) for an ice floe and by *Namba and Ohkusu* (1999) for a floating artificial island. Both used linear shallow water theory (*Stoker* (1957)). The second type of the simplified problem was solved by *Staziker, Porter and Stirling* (1997) for a localized bed topography with uniform depth at its ends. Their solution method used an integral equation and a Green's function.

In solving the problem of the wave scattering by an elastic body on water of variable depth we adopt the method used by *Liu and Liggett* (1982) and *Hazard and Lenoir* (1993). Both publications used artificial boundaries dividing the water domain into a finite and two semi-infinite domains. These boundaries are located at a sufficient distance from the scatterers so that the water depth is assumed constant; this method is called the far-field method, the solution being obtained using eigenfunction expansions. Then the far-field solution in the semi-infinite domain is matched with the solution in the finite domain. *Liu and Liggett* solved this using the boundary element method (BEM) and *Hazard and Lenoir* used the finite element method (FEM).

To solve the wave scattering problem by an elastic body floating on water of variable depth we use the far-field method and the BEM. Our solution technique involves two main steps. The first is to split the water domain into finite and semi-infinite domains. The

solution of the wave in the semi-infinite domain is obtained using appropriate separation of variables (leading to an eigenfunction expansion). From this solution we derive the coupling operator for the boundary condition at the artificial boundaries joining the finite and the semi-infinite domains. The solution for the wave in the finite domain cannot be solved exactly therefore we must solve it numerically. This leads us to the second step, the BEM, which involves transforming the wave problem into an integral equation together with the free-space Green's function.

The solution of the wave scattering problem is presented in terms of the wave potential, the techniques for which will be explained in detail in the first three chapters of the thesis. The first chapter explains the water domain and the governing equations for the wave scattering problem, including the derivation of the stationary model for the problem and the incident wave. The second chapter explains the reduction to finite and semi-infinite domains. In the first part of this chapter we derive the solution to the wave potential in the semi-infinite domain using separation of variables and the expression for the coupling operator for the boundary conditions. In the second part of chapter two we describe the BEM procedure for solving the wave potential in the finite domain. This procedure involves two integral equations (one is for the boundary condition underneath the elastic floating plate and one is for the solution of the wave potential) and two Green's functions (one for the elastic floating plate and the other the free space Green's function for the wave potential). Then in the third chapter we solve the integral equations from the second chapter numerically by solving an equivalent linear equation which involves matrices for the Green's

function and for the boundary conditions as well as vectors for the wave potential and the constant.

The next two chapters present the results of the implementation of the BEM. In the fourth chapter we define the reflected and the transmitted waves, which are useful for error checking in the numerical solution. In the fifth chapter we present some relevant results from the numerical computation of the wave potential. At the beginning of the chapter we test for convergence. This provide us with an appropriate choice of parameters used. Then we compare the results with the previous ones of *Meylan* [5], *Staziker, Porter and Stirling* [7], and *Namba and Ohkushu* [6].

Chapter 2
Introduction To The Wave Scattering Problem

In this chapter we will describe the wave scattering problem and derive the mathematical equation for it.

2.1 The Physical Description

The problem domain consists of a thin plate floating on the water surface above a seabed of variable depth. This domain is horizontally infinite and is bounded vertically by the water surface and the seabed. The water is assumed inviscid, incompressible, and its motion is irrotational. The seabed consists of three parts. Two regions of constant depth connected by a region of non-uniform depth profile. We call the region of non-uniform depth profile non-constant seabed. The thin plate that floats on the free surface of the water does not move horizontally (in other words, the plate only moves up and down). The immersed part of the thin plate is negligible compared to the depth of the water. We call the plate and the varying seabed *the scatterers*. This problem is shown in Figure 2.1. Since the domain is two dimensional, we use the Cartesian coordinates system with the x axis directed horizontally and the z axis directed vertically.

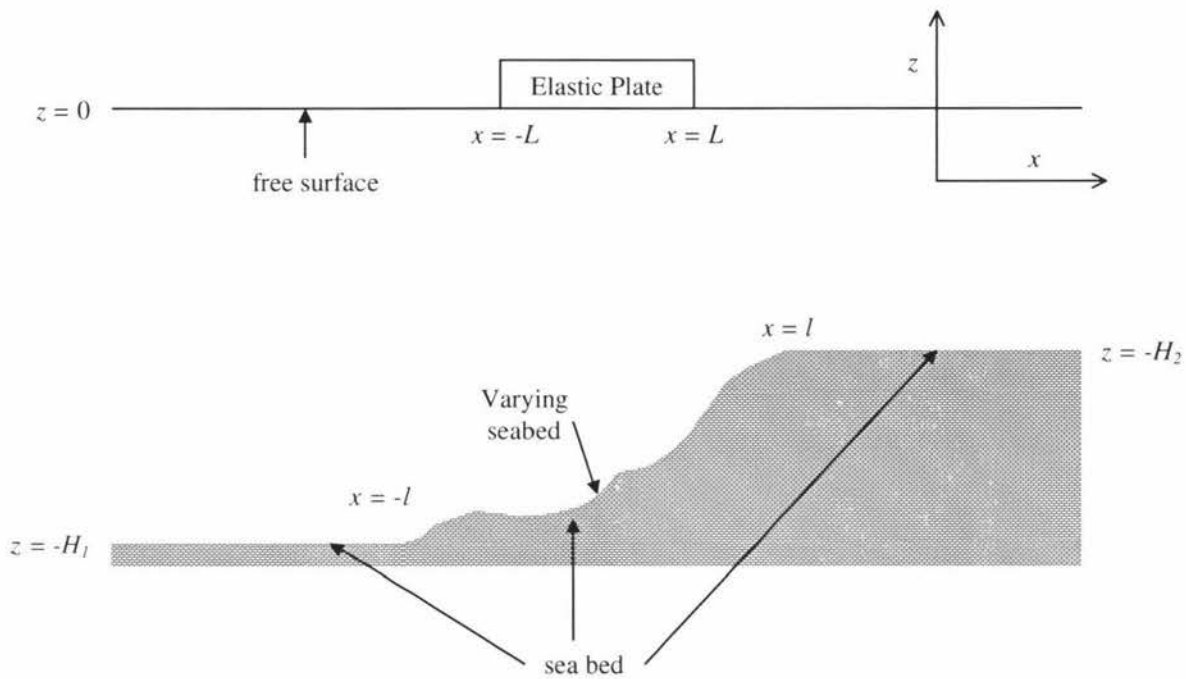

Figure 2.1. Physical description of the domain of the wave scattering problem containing a single floating thin plate and an arbitrary bed topography.

2.2 Mathematical Formulation of The Scattered Wave Problem

2.2.1 Equation of Wave's Motion

The domain of water in Figure 2.1 is denoted by Ω where $\Omega \subset \mathbb{R}^2$. The domain Ω is bounded by the water surface at $z = 0$ and the seabed at $z = \hat{d}(x)$. On the surface the plate occupies the region $x \in [-L, L]$. On the bottom the varying seabed occupies the region $x \in [-l, l]$ and it is described by a continuous function $d(x)$. Away from the varying seabed ($x \in (-\infty, -l)$ or $x \in (l, \infty)$) the water depth is uniform. Therefore the entire seabed can be described by the following function

$$\hat{d}(x) = \begin{cases} -H_1 & \forall x \in (-\infty, -l), \\ d(x) & \forall x \in [-l, l], \\ -H_2 & \forall x \in (l, \infty). \end{cases} \tag{2.2.1}$$

An incoming wave of small amplitude travels horizontally from negative infinity to positive infinity as shown in Figure 2.2. A result from this wave is a small vertical movement of the plate. As well as rocking the plate, the wave is also reflected and transmitted. This phenomenon can be described mathematically by a set of linearized equations involving the displacement of the plate $w(x)$ and the velocity potential of the wave $\Phi(x, z; t)$. On the surface of the water where the plate is floating, these two quantities are related by the equation $w(x) = -\nabla\Phi(x, z; t)$. This lead us to the equations of fluid flow for the time-dependent problem which are

$$\nabla^2\Phi = 0, \qquad \text{in } \Omega, \tag{2.2.2}$$

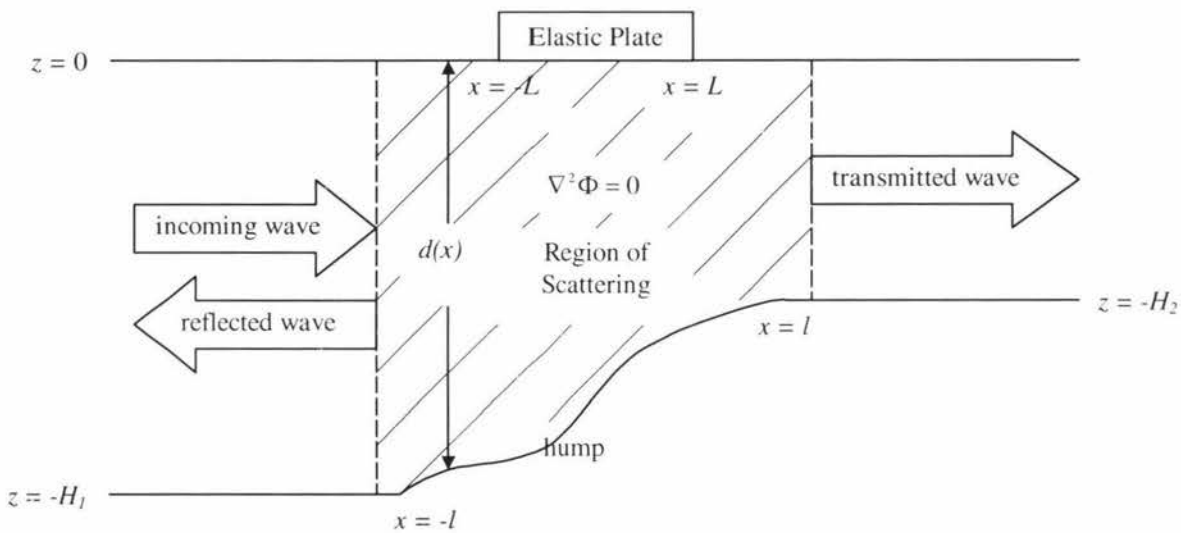

Figure 2.2. Schematic diagram for the wave scattering problem.

$$\frac{\partial^2 \Phi}{\partial t^2} + g \frac{\partial \Phi}{\partial n} = 0, \qquad \text{at } z = 0, \tag{2.2.3}$$

$$\frac{\partial \Phi}{\partial n} = 0, \qquad \text{at } z = \hat{d}(x), \tag{2.2.4}$$

$$\frac{\partial \Phi}{\partial n} = -\frac{\partial w}{\partial t}, \qquad \text{at } z = 0, \tag{2.2.5}$$

$$-\rho \left(g \frac{\partial \Phi}{\partial n} + \frac{\partial^2 \Phi}{\partial t^2} \right) = -\frac{\partial p}{\partial t}(x, z; t), \qquad \text{at } z = 0, \tag{2.2.6}$$

where ρ is the density of the water, p is the pressure on water surface, and g is the gravitational acceleration. Equation (2.2.2) is Laplace's equation which arises from incompressibility for an irrotational flow. Equation (2.2.3) is the boundary condition at the free surface deduced from Bernoulli's law and the fact that water particles stay on the surface. Equation (2.2.4) is the boundary condition for a physically fixed surface (in this case the seabed). The term $\frac{\partial w}{\partial t}$ in equation (2.2.5) denotes the free surface elevation (vertical speed) and is related to the wave potential as the negative of the normal derivative of Φ taken on the water surface. Equation (2.2.6) is derived from the linearized Bernoulli equation for pressure, $p(x, z; t) = -\rho \left(g\, w + \frac{\partial \Phi}{\partial t} \right)$ (*Stoker* [8]). Notice that all $\frac{\partial \Phi}{\partial n}$ is simply $= \frac{\partial \Phi}{\partial z}$.

For any point taken on the free surface away from the plate, i.e. $x \in (-\infty, -L) \cup (L, \infty)$, the pressure is equal to the constant atmospheric pressure. Hence the term $-\frac{\partial p}{\partial t}(x, z; t)$ is zero and so we can write (2.2.6) as

$$\rho \left(g \frac{\partial \Phi}{\partial n} + \frac{\partial^2 \Phi}{\partial t^2} \right) = 0, \qquad \forall x \in (-\infty, -L) \cup (L, \infty) \text{ and } z = 0.$$

The pressure and the displacement of the plate are described by the Bernoulli-Euler model for the plate. Neglecting gravity effects, the equation is

$$\rho' h \frac{\partial^2 w}{\partial t^2} + D \frac{\partial^4 w}{\partial x^4} = p, \qquad \forall x \in [-L, L] \text{ and } z = 0, \tag{2.2.7}$$

where ρ' is the density of the plate, h is its thickness, and

$$D = \frac{Eh^3}{12\left(1-\nu^2\right)}.$$

D is called the *bending rigidity of the plate per unit length,* E is *Young's modulus*, and ν is *Poisson's ratio.*

Differentiation of (2.2.7) once with respect to time gives

$$\frac{\partial p}{\partial t}(x,z,t) = -\rho' h \frac{\partial^3 w}{\partial t^3} + D\frac{\partial^5 w}{\partial t \partial x^4}. \tag{2.2.8}$$

We know from (2.2.5), $\dfrac{\partial \Phi}{\partial n} = -\dfrac{\partial w}{\partial t}$ at $z = 0$, $-L \leq x \leq L$. Using this, equation (2.2.8) can be written as

$$\frac{\partial p}{\partial t} = -\rho' h \frac{\partial^3 \Phi}{\partial t^2 \partial n} + D\frac{\partial^5 \Phi}{\partial x^4 \partial n}.$$

Therefore we can write (2.2.6) as

$$-\rho\left(g\frac{\partial \Phi}{\partial n} + \frac{\partial^2 \Phi}{\partial t^2}\right) = \begin{cases} 0, & x \in (-\infty, -L) \cup (L, \infty) \text{ and } z = 0, \\ \rho' h \dfrac{\partial^3 \Phi}{\partial t^2 \partial n} + D\dfrac{\partial^5 \Phi}{\partial x^4 \partial n}, & -L \leq x \leq L \text{ and } z = 0, \end{cases} \tag{2.2.9}$$

The bending moment and shear must vanish at both ends of the plate. Hence this gives the additional conditions

$$\frac{\partial^2 w}{\partial x^2} = \frac{\partial^3 w}{\partial x^3} = 0, \qquad \text{at } x = -L \text{ and } x = L.$$

By differentiating the equation above with time and applying (2.2.5), we get a condition specifying the behaviour of the wave potential at the edges of the plate

$$\frac{\partial^3 \Phi}{\partial x^2 \partial n} = \frac{\partial^4 \Phi}{\partial x^3 \partial n} = 0 \qquad \text{at } x = -L \text{ and } x = L. \tag{2.2.10}$$

2.2.2 Single Frequency Wave Problem

We simplify the model of the wave scattering problem by assuming that the plate is stationary. The solution to this model is then developed from the time-harmonic wave potential system with a monochromatic incident wave of frequency $\omega > 0$. This problem is relatively simple because we can write the wave potential as

$$\Phi(\mathbf{x};t) = \hat{\Phi}(\mathbf{x})\, e^{-i\omega t}, \tag{2.2.11}$$

and the displacement of the thin plate is

$$w(x) = \hat{w}(x)\; e^{-i\omega t},$$

where $\mathbf{x}$ is the position vector denoting the usual pair of (x, z).

Hence we may rewrite all time-dependent equations in (2.2.2) to (2.2.9). Equation (2.2.3) becomes

$$g\frac{\partial \hat{\Phi}}{\partial n} - \omega^2 \hat{\Phi} = 0, \tag{2.2.12}$$

and equation (2.2.9) becomes

$$-\rho\left(g\frac{\partial \hat{\Phi}}{\partial n} - \omega^2 \hat{\Phi}\right) = \begin{cases} 0, & \forall x \in (-\infty, -L) \cup (L, \infty) \text{ and } z = 0, \\ D\dfrac{\partial^5 \hat{\Phi}}{\partial x^4 \partial n} - \rho' h\, \omega^2 \dfrac{\partial \hat{\Phi}}{\partial n}, & \forall x \in [-L, L] \text{ and } z = 0. \end{cases} \tag{2.2.13}$$

2.2.3 The Incident Wave

The wave potiential function $\hat{\Phi}(\mathbf{x})$ is decomposed into two parts

$$\hat{\Phi}(\mathbf{x}) = \phi(\mathbf{x}) + \phi^I(\mathbf{x}), \tag{2.2.14}$$

with $\phi^I(\mathbf{x})$ the *potential of a single frequency incident wave* and $\phi(\mathbf{x})$ the *potential function of the transient wave*. The incident wave is one which enters the domain and the transient wave emerges from the scattering of this incident wave by the scatterers. We call $\hat{\Phi}$ the *full wave potential*.

The explicit expression for the velocity potential of the incident wave can be obtained by solving the following set of linearized equations

$$\begin{aligned} \nabla^2\phi^I &= 0, \qquad \text{in } \Omega, \\ \frac{\partial\phi^I}{\partial n} &= \nu\,\phi^I, \qquad \text{on } z=0, \qquad (2.2.15) \\ \frac{\partial\phi^I}{\partial n} &= 0, \qquad \text{on } z=-H_1, \qquad (2.2.16) \end{aligned}$$

where $\nu = \omega^2/g$ ($\nu \in \mathbb{R}^+$).

This problem can be solved using the separation of variables therefore we can write the incident wave potential as

$$\phi^I(\mathbf{x}) = f(x)\; g(z),$$

where $\mathbf{x} = (x, z)$. We easily obtain the solution for $f(x)$ as

$$f(x) = A\,e^{i\nu_0^{(1)}x} + B\,e^{-i\nu_0^{(1)}x},$$

where A, B are constants. The use of condition (2.2.16) gives

$$g(z) = \cosh\left(\nu_0^{(1)}\;(z+H_1)\right).$$

Since condition (2.2.15) must also be met then $\nu_0^{(1)}$ must satisfy the following condition

$$\nu_0^{(1)}\tanh\left(\nu_0^{(1)}H_1\right) = \nu, \qquad (2.2.17)$$

for the wave number $\nu_0 \in \mathbb{R}^+$. The subscript in $\nu_0^{(1)}$ indicates that the wave number belongs to the wave propagating on the left hand side of the scatterers (similarly a subscript (2) indicates that the wave number belongs to one on the right hand side of the scatterers and it also satisfies property (2.2.17) with H_2 replacing H_1). The wave number is related to the wavelength by the equation

$$\lambda^{(1)} = \frac{2\pi}{\nu_0^{(1)}}. \tag{2.2.18}$$

It is clear from the expression above that the wave frequency may be expressed in terms of the wavelength by the equation

$$\omega^2 = g\left(\frac{2\pi}{\lambda^{(1)}}\right)\tanh\left(\frac{2\pi\, H_1}{\lambda^{(1)}}\right), \tag{2.2.19}$$

and thus the wave period $T = 2\pi/\omega$ is related to the wavelength by the equation

$$T = \sqrt{\frac{2\pi\lambda^{(1)}}{g\,\tanh\left(\frac{2\pi\, H_1}{\lambda^{(1)}}\right)}}. \tag{2.2.20}$$

Note that the superscript in the parameters λ and ν_0 is to distinguish to which wave they belong. This is because the wavelength and the wave number of the wave to the left of the scatterers is different from one in the right-hand side since the water depth is different. However the frequency and hence the period stay the same.

The general solution for the incident wave problem is

$$\phi^I(x,z) = A\cosh\left(\nu_0^{(1)}(z+H_1)\right)e^{i\nu_0^{(1)}x} + B\cosh\left(\nu_0^{(1)}(z+H_1)\right)e^{-i\nu_0^{(1)}x}.$$

Since the incident wave travels towards the direction of positive x the second term in the equation above (corresponding to the exponential function) tends to zero as $x \to \infty$,

hence the potential of the incident wave can be expressed as the following

$$\phi^I(\mathbf{x}) = A\cosh\left(\nu_0^{(1)}(z+H_1)\right)e^{i\nu_0^{(1)}x}, \tag{2.2.21}$$

where $A \in \mathbb{C}$ is the amplitude of the velocity potential (*Hazard and Lenoir* [3]).

Chapter 3
Methodology for Solving The Wave Scattering Problem

In this chapter we present a solution for the wave scattering problem of a thin floating plate on water of variable depth. The method works by dividing the water domain into two semi-infinite regions connected by a finite region. The solution in the semi-infinite regions is found by an integral equation and the solution in the finite region is found by a Green's function (boundary element method (BEM)).

3.1 Reduction to Finite and Infinite Domain

A pair of vertical lines are located opposite to each other respectively at $x = a_1$ and $x = a_2$ in the domain Ω, where $a_1 < \min\{-L, -l\}$ and $a_2 > \max\{L, l\}$. The length of each line is equivalent to the depth of the water where it is located (the length of the line on the left-hand side is H_1 and the length of the one on the right-hand side is H_2). Therefore if we connect the edges of these lines then we will obtain a 'rectangular' area containing the scatterers. This situation is depicted in Figure 3.1.

The two vertical lines split the domain Ω into an inner bounded region $\hat{\Omega}$ and two outer semi-infinite regions, $\tilde{\Omega}_1$ and $\tilde{\Omega}_2$. These vertical lines are denoted by Σ_1 and Σ_2. In each of the semi-infinite domains we solve for the wave travelling in the outward direction (that is, the wave travelling towards $-\infty$ and the wave that travels towards ∞). This wave is the transient wave (this includes the travelling and the decaying waves) and the potential

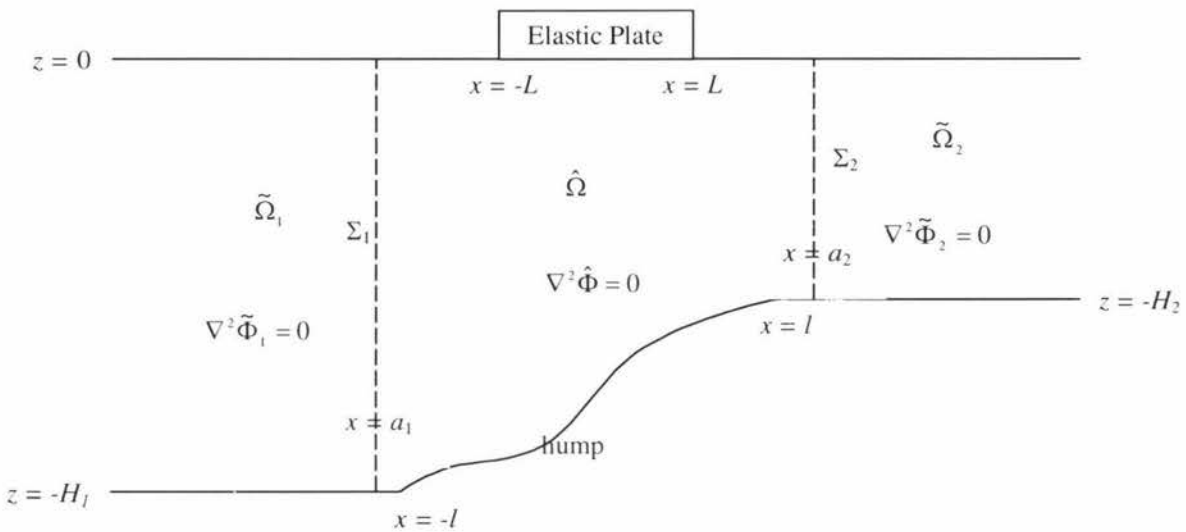

Figure 3.1. Schematic diagram of the finite and the infinite regions of the reduced water domain.

is denoted by $\tilde{\phi}_j\,(j=1,2)$ (with the full wave potential to be $\tilde{\Phi}_j=\tilde{\phi}_j^I+\tilde{\phi}_j$). In the outer regions we solve for the transient wave. In the bounded region we solve for the transient wave($\hat{\phi}$) plus the incident wave($\hat{\phi}^I$), and this full wave potential is denoted by $\hat{\Phi}$.

3.2 Solution on Unbounded Domain

In this section we solve for the transient waves $\tilde{\phi}_1$ and $\tilde{\phi}_2$ in the semi-infinite regions $\tilde{\Omega}_1$ and $\tilde{\Omega}_2$ using the method of separation of variables.

We derive a set of equations for the transient wave potential in the semi-infinite domain by substituting (2.2.14) into (2.2.2), (2.2.4) and (2.2.12).

$$\left.\begin{aligned} \nabla^2\tilde{\phi}_j&=0, \qquad \text{in } \tilde{\Omega}_j,\ j=1,2,\\ \frac{\partial\tilde{\phi}_j}{\partial n}-\nu\tilde{\phi}_j&=0, \qquad \text{at } z=0, \text{ and } -\infty<x<a_1 \text{ or } a_2<x<\infty,\\ \frac{\partial\tilde{\phi}_j}{\partial n}&=0, \qquad \text{at } z=-H_j,\ j=1,2,\\ \tilde{\phi}_j&=\psi(x), \qquad \text{at } \Sigma_j,\ j=1,2, \end{aligned}\right\} \tag{3.2.1}$$

where $\psi(x)$ is a continuous function defined on Σ_j.

To determine the boundary condition at Σ_1 and Σ_2 we define the coupling operator $Q_{j,\nu}$ by equation

$$Q_{j,\nu}\,\tilde{\phi}_j(\mathbf{x})=\frac{\partial\tilde{\phi}_j}{\partial n}(\mathbf{x}), \qquad \forall\mathbf{x}\in\Sigma_j. \tag{3.2.2}$$

where $\mathbf{x}=(x,z)$ and $\dfrac{\partial\tilde{\phi}_j}{\partial n}$ is the exterior normal derivative of the potential in domain $\tilde{\Omega}_j$.

To obtain an explicit expression for $Q_{j,\nu}$ we solve system (3.2.1) using separation of variables by writing the wave potential as $\tilde{\phi}_j=\chi_{j,\nu}(x)\ \tau_{j,\nu}(z)$. Using this wave potential function in (3.2.1) gives us a pair of Sturm-Liouville equations, which are to be solved

separately for functions $\chi_{j,\nu}(x)$ and $\tau_j, \nu(z)$

$$\mathcal{L}_1\left[\chi_{j,\nu}(x)\right] = -\mu\,\chi_{j,\nu}(x), \tag{3.2.3}$$

$$\mathcal{L}_2\left[\tau_{j,\nu}(z)\right] = -\mu\,\tau_{j,\nu}(z), \tag{3.2.4}$$

where $\mathcal{L}_1$ and $\mathcal{L}_2$, defined by $\mathcal{L}_1 = -\dfrac{d^2}{dx^2}$ and $\mathcal{L}_2 = \dfrac{d^2}{dz^2}$, are second order linear ordinary differential operators. By letting $\mu = \left(\eta_{j,\nu}^{(m)}\right)^2$ we obtain the general solutions to (3.2.3) and (3.2.4) as

$$\chi_{j,\nu}^{(m)}(x) = e^{(-1)^{j+1}\eta_{j,\nu}^{(m)}(x-a_j)}, \tag{3.2.5}$$

$$\tau_{j,\nu}^{(m)}(z) = \alpha_{j,\nu}^{(m)}\cos\left(\eta_{j,\nu}^{(m)}(z+H_j)\right) + \beta_{\nu}^{(m)}\sin\left(\eta_{j,\nu}^{(m)}(z+H_j)\right), \tag{3.2.6}$$

for $j = 1, 2$. Note that all $\eta_{j,\nu}^{(m)}$, $m \geq 0$, are the eigenvalues arising from the Sturm-Liouville problem with $\tau_{j,\nu}^{(m)}$ as their corresponding eigenfunctions.

Thus $\tilde{\phi}_{j,\nu}^{(m)}(x,z)$ can be expressed as

$$\tilde{\phi}_{j,\nu}^{(m)}(x,z) = e^{(-1)^{j+1}\eta_{j,\nu}^{(m)}(x-a_j)}\left[\alpha_{j,\nu}^{(m)}\cos\left(\eta_{j,\nu}^{(m)}(z+H_j)\right) + \beta_{j,\nu}^{(m)}\sin\left(\eta_{j,\nu}^{(m)}(z+H_j)\right)\right], \tag{3.2.7}$$

This leads us to the general solution for the wave potential function in terms of a series expansion of $\tilde{\phi}_{j,\nu}^{(m)}(x,z)$ which is

$$\tilde{\phi}(x,z) = \sum_m C^{(m)}\,\tilde{\phi}_{j,\nu}^{(m)}(x,z). \tag{3.2.8}$$

Since ν is real, then clearly both Sturm-Liouville operators are self-adjoint [*Zwillinger* [9]], hence the eigenvalues $\eta_{j,\nu}^{(m)}$ of $\mathcal{L}_1$ and $\mathcal{L}_2$ are real, and the eigenfunctions corresponding to distinct eigenvalues are orthogonal.

The condition $\dfrac{\partial \tilde{\phi}_j}{\partial n} = 0$ on $z = -H_j$ implies that $\beta_{j,\nu}^{(m)} = 0$ and (3.2.7) becomes

$$\tilde{\phi}_{j,\nu}^{(m)}(x,z) = e^{(-1)^{j+1}\eta_{j,\nu}^{(m)}(x-a_j)}\ \alpha_{j,\nu}^{(m)} \cos\left(\eta_{j,\nu}^{(m)}(z+H_j)\right).$$

By applying boundary condition $\dfrac{\partial \tilde{\phi}_j}{\partial z} - \nu\tilde{\phi}_j = 0$, at $z = 0$ in (3.2.7) we obtain the relationship between the eigenvalues of (3.2.7) and the frequency of the wave, as well as an equation for constants $\eta_{j,\nu}^{(m)}$. The result is expressed in the equation below

$$-\eta_{j,\nu}^{(m)} \tan\left(\eta_{j,\nu}^{(m)} H_j\right) = \nu. \tag{3.2.9}$$

We call this the *dispersion equation* and $\eta_{j,\nu}^{(m)}$ the roots. As proven by *Fox and Squire* [1] equation (3.2.9) has two pure imaginary roots corresponding to the travelling plane wave, and countably infinite number of real roots corresponding to the evanescent (decaying) modes of the wave. $\eta_{j,\nu}^{(m)}$ are chosen and ordered in a way such that $\eta_{j,\nu}^{(0)}$ is complex with positive imaginary part and $\eta_{j,\nu}^{(m)}$, $m \geq 1$, are negative real numbers of increasing magnitude. The real roots of the dispersion equation are depicted by the intersections of the curves of $\tan(\eta)$ and $-\nu/\eta$ in Figure 3.2. For $m = 0$, we can relate equation (3.2.9) to (2.2.17) by equation $\nu_0^{(j)} = -i\eta_{j,\nu}^{(0)}$.

All eigenfunctions $\tau_{j,\nu}^{(m)}$ are orthogonal, but they are not necessarily orthonormal. To achieve orthonormality, we normalize each $\tau_{j,\nu}^{(m)}$ using the condition

$$\left\langle \tau_{j,\nu}^{(m)}, \tau_{j,\nu}^{(n)} \right\rangle = \int_{-H_j}^{0} \tau_{j,\nu}^{(m)}\, \tau_{j,\nu}^{(n)}\, dz = \delta_{mn},$$

where δ_{mn} denotes the usual Kronecker delta. This condition can be satisfied if $\alpha_{j,\nu}^{(m)}$ is of the form

$$\alpha_{j,\nu}^{(m)} = \left(\frac{H_j}{2} + \frac{\sin\left(2\eta_{j,\nu}^{(m)} H_j\right)}{4\eta_{j,\nu}^{(m)}}\right)^{-\frac{1}{2}}. \tag{3.2.10}$$

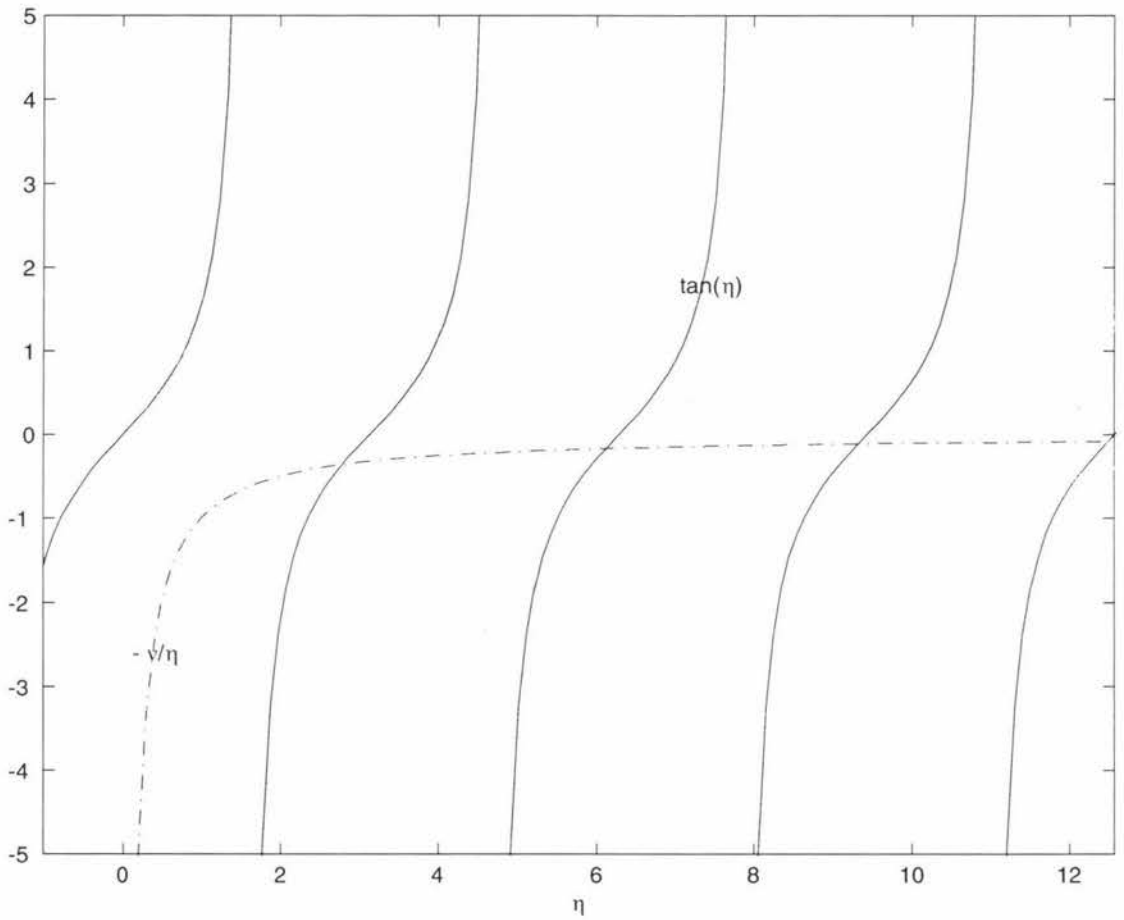

Figure 3.2. The real solution of the dispersion equation.

Finally the constant $C^{(m)}$ is determined by applying the orthogonality of $\tau_{j,\nu}^{(m)}$ to the last boundary condition of (3.2.1). The result is the following equation for $C^{(m)}$

$$C^{(m)} = \left\langle \tau_{j,\nu}^{(m)}(z), \psi(z) \right\rangle,$$

where the inner product term is the usual definite integral taken with respect of z with lower limit $z = -H_j$ and upper limit $z = 0$.

In conclusion we write the wave potential on domain $\tilde{\Omega}_j$ as the following

$$\tilde{\phi}_j(x,z) = \sum_m \left\langle \tau_{j,\nu}^{(m)}(z), \tilde{\phi}_j(a_j,z) \right\rangle \tau_{j,\nu}^{(m)}(z)\ e^{(-1)^{j+1}\eta_{j,\nu}^{(m)}(x-a_j)}. \tag{3.2.11}$$

We can derive the equation for the coupling operator by taking the normal derivative of (3.2.11). The result is

$$Q_{j,\nu}\tilde{\phi}_j(\mathbf{x}) = \sum_m (-1)^j\ \eta_{j,\nu}^{(m)}\ \left\langle \tau_{j,\nu}^{(m)}, \tilde{\phi}_j \right\rangle \tau_{j,\nu}^{(m)}(z), \qquad \forall \mathbf{x} \in \{(a_j,z) \in \Sigma_j,\ j = 1,2\}. \tag{3.2.12}$$

Recall from (3.2.2) our purpose for developing Q is to obtain the normal derivative at the artificial vertical boundaries which couples the outer and the inner regions of domain Ω. Therefore we may apply (3.2.12) to the bounded region to obtain boundary conditions at these vertical boundaries by taking the opposite sign of the normal derivative $\dfrac{\partial\tilde{\phi}_j}{\partial n}$. This gives

$$\frac{\partial}{\partial n}\hat{\phi}(\mathbf{x}) = -Q_{j,\nu}\tilde{\phi}_j(\mathbf{x}), \qquad \mathbf{x} \in \{(a_j,z) \in \Sigma_j,\ j = 1,2\}.$$

Using this result, we obtain the explicit expression for the coupling operator $Q_{j,\nu}$ in the domain $\hat{\Omega}$ as

$$Q_{j,\nu}\hat{\phi}(\mathbf{x}) = \sum_m \eta_{j,\nu}^{(m)} \left\langle \tau_{j,\nu}^{(m)}, \hat{\phi} \right\rangle \tau_{j,\nu}^{(m)}(z), \qquad \forall \mathbf{x} \in \{(a_j,z) \in \Sigma_j,\ j = 1,2\}. \tag{3.2.13}$$

3.3 Non-dimensionalization

All the parameters involved in our discussion so far retain their standard units in SI. To remove the units we non-dimensionalize them by taking the initial depth of the water on the left-hand side of the plate as the non-dimensionalization factor for the spatial parameters. This is shown in the following equations

$$\begin{aligned}
\bar{x} &= \frac{x}{H_1}, \\
\bar{z} &= \frac{z}{H_1}, \\
\bar{L} &= \frac{L}{H_1}, \\
\bar{H}_2 &= \frac{H_2}{H_1}, \\
\bar{l} &= \frac{l}{H_1}, \\
\bar{d}\,(x) &= \frac{d\,(x)}{H_1}.
\end{aligned}$$

The time parameter is non-dimensionalized by multiplying by the factor $\sqrt{\frac{g}{H_1}}$ to become

$$\bar{t} = t\sqrt{\frac{g}{H_1}},$$

and the dimensionless potential is

$$\bar{\Phi} = \frac{1}{H_1\sqrt{H_1 g}}\,\Phi,$$

where $\Phi = \phi^I + \phi$ and $\bar{\Phi} = \bar{\phi}^I + \bar{\phi}$.

In addition to the above, we define the dimensionless constants

$$\gamma = \frac{\rho' h}{\rho H_1},$$

$$\beta = \frac{D}{\rho g H_1^4}.$$

With the understanding that all variables have been non-dimensionalized, from now onwards we omit the overbar.

3.4 The Boundary Element Method for Laplace's Equation

In this section we aim to solve for the full wave potential $\hat{\Phi}$ in $\hat{\Omega}$ using the boundary element method.

The equations for the full wave potential in $\hat{\Omega}$ are

$$\nabla^2\hat{\Phi} = 0, \qquad \text{in } \hat{\Omega}, \tag{3.4.1}$$

$$\frac{\partial\hat{\Phi}}{\partial n} = \nu\hat{\Phi}, \qquad \text{at } x \in [a_1, -L] \text{ or } x \in [L, a_2] \text{ and } z = 0, \tag{3.4.2}$$

$$-\rho\left(g\frac{\partial\hat{\Phi}}{\partial n} - \omega^2\,\hat{\Phi}\right) = D\,\frac{\partial^5\hat{\Phi}}{\partial x^4\partial n} - \rho' h\,\omega^2\,\frac{\partial\hat{\Phi}}{\partial n}, \qquad \text{at } x \in [-L, L] \text{ and } z = 0, \tag{3.4.3}$$

$$\frac{\partial^3\hat{\Phi}}{\partial x^2\partial n} = \frac{\partial^4\hat{\Phi}}{\partial x^3\partial n} = 0, \qquad \text{at } x = -L \text{ and } x = L, \text{ and } z = 0, \tag{3.4.4}$$

$$\frac{\partial\hat{\Phi}}{\partial n} = 0, \qquad \text{at } x \in [a_1, a_2] \text{ and } z = \hat{d}\,(x)\,, \tag{3.4.5}$$

$$\frac{\partial\hat{\Phi}}{\partial n} = Q_{j,\nu}\,\hat{\Phi}, \qquad \text{at } x = a_j \text{ and } z \in \Sigma_j, \tag{3.4.6}$$

where $j = 1, 2$.

The boundary element method aims to transform the problem of solving Laplace's equation (3.4.1) with boundary conditions (3.4.2) to (3.4.6) into that of solving an equivalent integral equation. To achieve this integral equation we construct two Green's functions, one for the boundary condition under the plate and another for the potential.

3.4.1 Green's Function Solution for A Floating Thin Plate

We aim to express the boundary conditions underneath the plate by an integral equation involving a Green's function. This method is particularly useful when we come to discuss the numerical computation by the boundary element method.

The boundary condition for the plate (3.4.3) may be written as

$$\frac{\partial^4 \hat{\Phi}_n}{\partial x^4} - \alpha^4 \hat{\Phi}_n = \frac{\nu}{\beta} \hat{\Phi}, \qquad \text{at } x \in [-L, L] \text{ and } z = 0, \tag{3.4.7}$$

where $\hat{\Phi}_n = \dfrac{\partial \hat{\Phi}}{\partial n}$ and $\alpha^4 = (\gamma\nu - 1)/\beta$, together with the plate's boundary conditions at its edges (3.4.3)

$$\frac{\partial^2 \hat{\Phi}_n}{\partial x^2} = \frac{\partial^3 \hat{\Phi}_n}{\partial x^3} = 0, \qquad \text{at } x = -L,\ x = L, \text{ and } z = 0. \tag{3.4.8}$$

$\hat{\Phi}_n(x, 0) = \hat{\Phi}_z(x, 0)$ from (3.4.7) and (3.4.8) can be seen as 'a function of x' instead of 'a partial with respect to z'. Therefore we may view equation (3.4.7) as the fourth order ordinary differential equation for $\hat{\Phi}_n$ as the dependent variable. Equation (3.4.8) contains the boundary conditions for $\hat{\Phi}_n$. Together equations (3.4.7) and (3.4.8) are to be solved for $\hat{\Phi}_n$. For this purpose, we construct a Green's function that satisfies

$$\left.\begin{aligned} &\frac{\partial^4}{\partial x^4} G_{plate}(x, \xi) - \alpha^4 G_{plate}(x, \xi) = \frac{\nu}{\beta} \delta(x - \xi), \\ &\frac{\partial^2}{\partial x^2} G_{plate}(x, \xi) = \frac{\partial^3}{\partial x^3} G_{plate}(x, \xi) = 0, \qquad \text{at } x = -L,\ x = L. \end{aligned}\right\} \tag{3.4.9}$$

Then the solution for $\hat{\Phi}_n$ can be expressed as

$$\hat{\Phi}_n = \frac{\nu}{\beta} \int_{-L}^{L} G_{plate}(x, \xi)\ \hat{\Phi}(\xi)\ d\xi, \tag{3.4.10}$$

or, in terms of an operator, it may be written as

$$\hat{\Phi}_n = \mathbf{G}_{plate}\left[\hat{\Phi}\right].$$

More details of the method used to determine the solution of G_{plate} can be found in Appendix A.

3.4.2 Fundamental Solution of The Free-space Green's Function

In this section we want to express the wave potential in the bounded domain as an integral equation involving the Green's function. This Green's function arises from the fundamental solution for the Laplace differential operator and is expressed as a logarithmic function. We shall see this in the following explanation.

We redefine the linearized equations for the potential problem in domain $\hat{\Omega}$ to be the following

$$\left.\begin{aligned} \nabla^2\hat{\Phi} &= 0, && \text{in } \hat{\Omega}, \\ \frac{\partial\hat{\Phi}}{\partial n} &= -\nu\hat{\Phi}, && \text{at } x \in [a_1, -L] \text{ or } x \in [a_2, L], \text{ and } z = 0, \\ \frac{\partial\hat{\Phi}}{\partial n} &= \mathbf{G}_{plate}\left[\hat{\Phi}\right], && \text{at } x \in [-L, L] \text{ and } z = 0, \\ \frac{\partial\hat{\Phi}}{\partial n} &= 0, && \text{at } x \in [a_1, a_2] \text{ and } z = d(x), \\ \frac{\partial\hat{\Phi}}{\partial n} &= Q_{j,\nu}\hat{\Phi} && \text{at } x = a_j \text{ and } z \in \Sigma_j. \end{aligned}\right\} \tag{3.4.11}$$

where operator $\mathbf{G}_{plate}$ is defined by integral equation (3.4.10).

Then we construct a Green's function that satisfies

$$\nabla^2 G(\mathbf{x}, \mathbf{x}') = \delta_2(\mathbf{x} - \mathbf{x}'), \qquad \text{in } \hat{\Omega}. \tag{3.4.12}$$

By *Greenberg* the solution of (3.4.12) is the following equation

$$G(\mathbf{x}, \mathbf{x}') = \frac{1}{2\pi} \ln |\mathbf{x} - \mathbf{x}'|, \tag{3.4.13}$$

where $\mathbf{x} \in \{(x, z)\}$ is the coordinate of the field point and $\mathbf{x}'$ represent the 'source' or 'sink' point. $G(\mathbf{x}, \mathbf{x}')$ in (3.4.13) is commonly known as the *free-space Green's function* (*Greenberg* [2]).

For a 'rectangular' curve Σ encircling the inner bounded domain $\hat{\Omega}$ the Green's second identity in two-dimensions is

$$\iint_{\hat{\Omega}} \left(u\nabla^2 v - v\nabla^2 u\right) dA = \oint_{\Sigma} \left(u\frac{\partial v}{\partial n} - v\frac{\partial u}{\partial n}\right) ds.$$

Hence if we let $u = \hat{\Phi}(\mathbf{x}')$ and $v = G(\mathbf{x}, \mathbf{x}')$, the Green's second identity formula for $\hat{\Phi}(\mathbf{x}')$ and $G(\mathbf{x}, \mathbf{x}')$ can be written as

$$\iint_{\hat{\Omega}} \delta_2(\mathbf{x} - \mathbf{x}')\ \hat{\Phi}(\mathbf{x}')\ dA(\mathbf{x}') = \oint_{\Sigma} \left(\hat{\Phi}(\mathbf{x}')\ \frac{\partial}{\partial n} G(\mathbf{x}, \mathbf{x}') - G(\mathbf{x}, \mathbf{x}')\ \frac{\partial}{\partial n}\hat{\Phi}(\mathbf{x}')\right) ds(\mathbf{x}'), \tag{3.4.14}$$

since $\nabla^2 G(\mathbf{x}, \mathbf{x}') = \delta_2(\mathbf{x} - \mathbf{x}')$ and $\nabla^2 \hat{\Phi}(\mathbf{x}) = 0$ for all $\mathbf{x}$. [1]

Finally the left-hand side of equation (3.4.14) is defined (in *Zwillinger*) by the following equation

$$\iint_{\hat{\Omega}} \delta_2(\mathbf{x} - \mathbf{x}')\ \hat{\Phi}(\mathbf{x}')\ dA(\mathbf{x}') = \begin{cases} 0, & \text{if } \mathbf{x} \notin \hat{\Omega} \text{ and } \mathbf{x} \notin \Sigma, \\ \frac{1}{2}\hat{\Phi}(\mathbf{x}), & \text{if } \mathbf{x} \in \Sigma, \\ \hat{\Phi}(\mathbf{x}), & \text{if } \mathbf{x} \in \hat{\Omega}. \end{cases} \tag{3.4.15}$$

Subsequently we will omit the hat notation. In the next chapter we solve this problem numerically.

[1] The combination of equations (2.4.14) and (2.4.15) is sometimes called the direct boundary element method (*Zwillinger* [10]).

Chapter 4
Numerical Implementation

The goal of this chapter is to implement the boundary element method using the results obtained in the previous chapter.

4.1 The Numerical Integration Technique for The Integral Equations

First we divide Σ into six boundary segments consisting of: two vertical segments, Σ_1 and Σ_2, two free surface segments, Σ_3 and Σ_5, one segment under the plate, Σ_4, and one segment for the varying seabed, Σ_6. Figure 4.1 depicts the decomposition of boundary Σ.

Then we combine equations (3.4.14) and (3.4.15) to obtain the following equation

$$\frac{1}{2}\Phi\left(\mathbf{x}\right) = \sum_{j=1}^{6} \int_{\Sigma_j} \left(\frac{\partial}{\partial n} G\left(\mathbf{x}, \mathbf{x}'^{(j)}\right) \; \Phi\left(\mathbf{x}'^{(j)}\right) - G\left(\mathbf{x}, \mathbf{x}'^{(j)}\right) \; \frac{\partial}{\partial n} \Phi\left(\mathbf{x}'^{(j)}\right) \right) \; ds\left(\mathbf{x}'^{(j)}\right), \tag{4.1.1}$$

where $\mathbf{x}'^{(j)}$ is the 'source/sink' point at boundary Σ_j and $\mathbf{x}$ is the field point. Our aim is to solve equation equation (4.1.1) numerically.

To solve this first we discretize the region of integration by dividing it into a finite number of sufficiently small segments which we call *panels*. A panel on a straight-line boundary segment is denoted by $\Delta x_i'$ and a panel on the varying seabed is denoted by Δs_i. Figure 4.2 depicts $\Delta x_i'$ and Δs_i.

Next we notice that the free-space Green's function and its normal derivative in (4.1.1) are rapidly changing functions and have a singularity at $\mathbf{x} = \mathbf{x}'$, while the func-

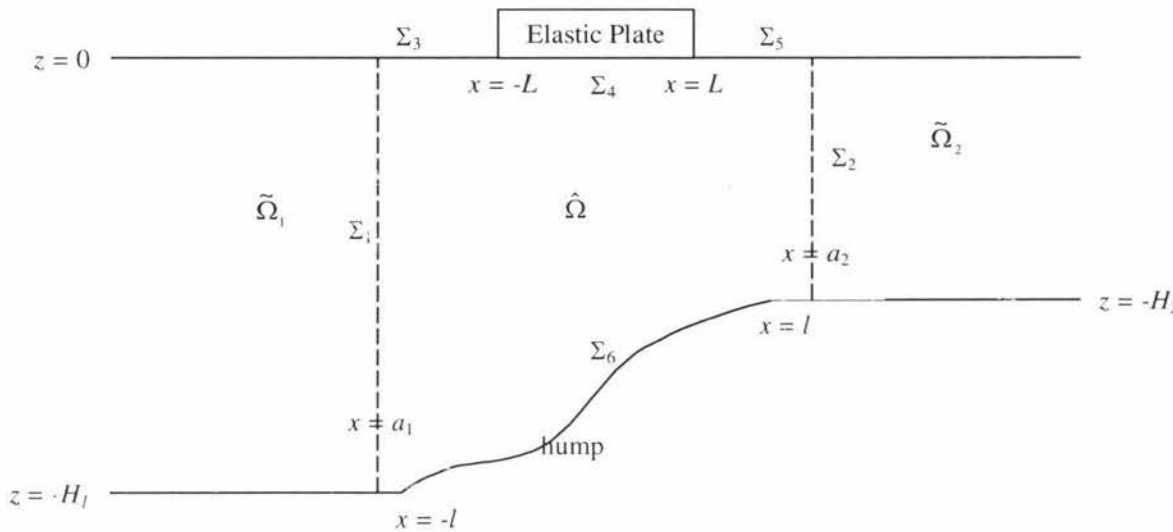

Figure 4.1. Notation diagram showing the segments of boundary Σ.

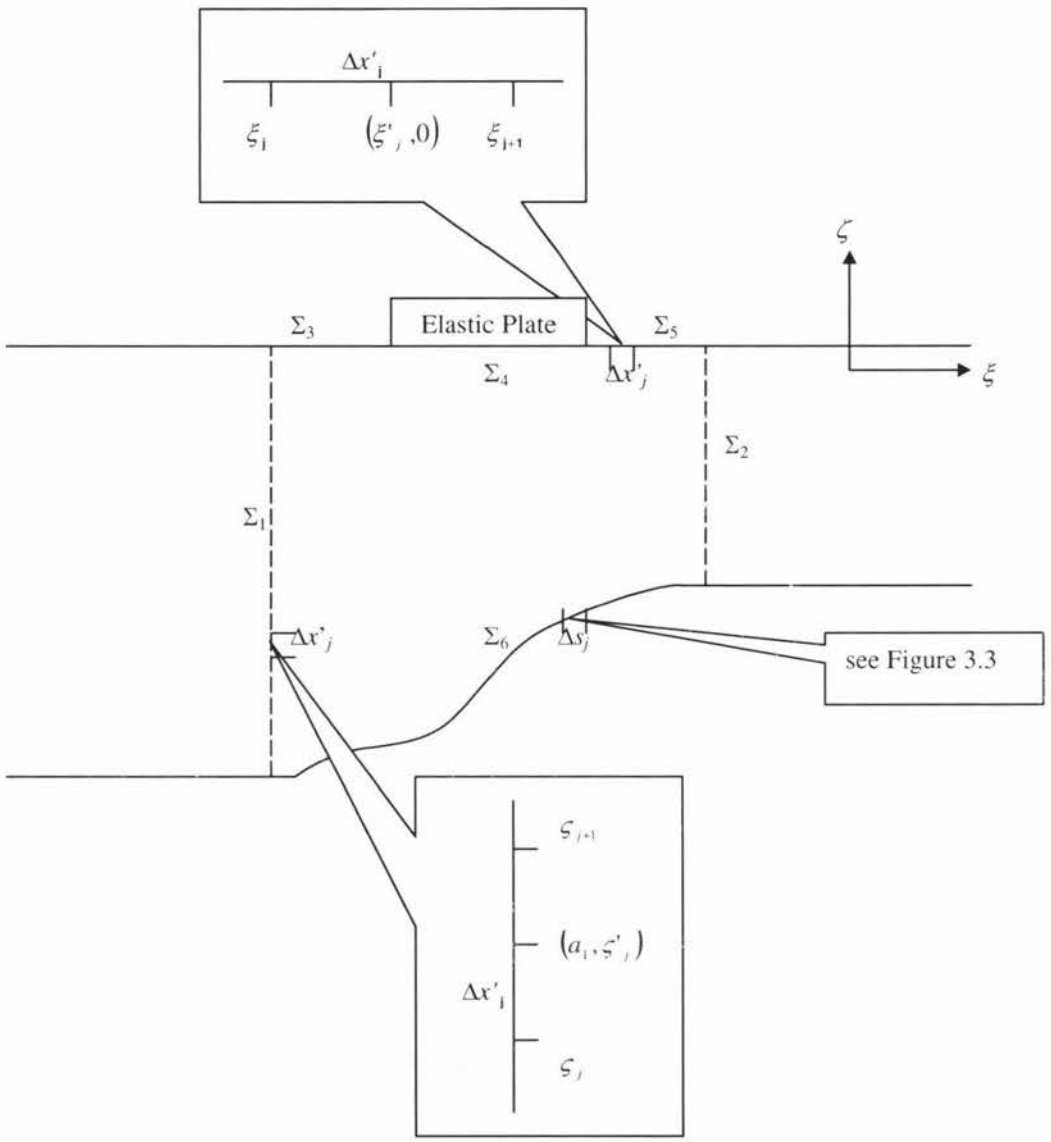

Figure 4.2. Pictorial description of panels $\Delta x'_i$ and Δs_i on various segment of boundary Σ.

tion Φ varies more slowly. Therefore we integrate G and $\dfrac{\partial G}{\partial n}$ exactly and assume Φ and Φ_n to be constants over each panel. This reduces (4.1.1) to a matrix equation

$$\frac{1}{2}\Phi = \mathbb{H}\,\Phi - \mathbb{G}\,\Phi_n, \tag{4.1.2}$$

where Φ and Φ_n are vectors of the potential and the normal derivative. $\mathbb{G}$ is the matrix with entries obtained from the exact integration of (3.4.13) and $\mathbb{H}$ is the matrix with entries from exact integration of the normal derivative of (3.4.13). We call $\mathbb{G}$ and $\mathbb{H}$ the *matrix operators for the free-space Green's function*. In the next section, we explain (4.1.2) in detail.

4.2 Matrix Operators for The Free-Space Green's Function

In this section we find explicit expression for the matrix operators introduced in the previous section.

The purpose of dividing the boundary Σ into 6 segments is because the results from integrating the Green's function and the normal derivative differ at distinct boundary segments. The numerical integration of each of the integrals in (4.1.1) is

$$\begin{aligned}
\int_{\Sigma_j} G\left(\mathbf{x}, \mathbf{x}'^{(j)}\right)\ \frac{\partial}{\partial n}\Phi\left(\mathbf{x}'^{(j)}\right)\ ds\left(\mathbf{x}'^{(j)}\right) &= \sum_{i=1}^{m_j} \frac{\partial}{\partial \xi}\Phi\left(\mathbf{x}_i'^{(j)}\right) \int_{\zeta_i}^{\zeta_{i+1}} G\left(\mathbf{x}, \mathbf{x}_i'^{(j)}\right)\, d\zeta, \\
\int_{\Sigma_j} \frac{\partial}{\partial n} G\left(\mathbf{x}, \mathbf{x}'^{(j)}\right)\ \Phi\left(\mathbf{x}'^{(j)}\right)\ ds\left(\mathbf{x}'^{(j)}\right) &= \sum_{i=1}^{m_j} \Phi\left(\mathbf{x}_i'^{(j)}\right) \int_{\zeta_i}^{\zeta_{i+1}} \frac{\partial}{\partial \xi} G\left(\mathbf{x}, \mathbf{x}_i'^{(j)}\right)\, d\zeta,
\end{aligned}$$

for $j = 1, 2$, and

$$\begin{aligned}
\int_{\Sigma_j} G\left(\mathbf{x}, \mathbf{x}'^{(j)}\right)\ \frac{\partial}{\partial n}\Phi\left(\mathbf{x}'^{(j)}\right)\ ds\left(\mathbf{x}'^{(j)}\right) &= \sum_{i=1}^{m_j} \frac{\partial}{\partial \zeta}\Phi\left(\mathbf{x}_i'^{(j)}\right) \int_{\xi_i}^{\xi_{i+1}} G\left(\mathbf{x}, \mathbf{x}_i'^{(j)}\right)\, d\xi, \\
\int_{\Sigma_j} \frac{\partial}{\partial n} G\left(\mathbf{x}, \mathbf{x}'^{(j)}\right)\ \Phi\left(\mathbf{x}'^{(j)}\right)\ ds\left(\mathbf{x}'^{(j)}\right) &= \sum_{i=1}^{m_j} \Phi\left(\mathbf{x}_i'^{(j)}\right) \int_{\xi_i}^{\xi_{i+1}} \frac{\partial}{\partial \zeta} G\left(\mathbf{x}, \mathbf{x}_i'^{(j)}\right)\, d\xi,
\end{aligned}$$

for $j = 3, 4, 5$, together with

$$\int_{\Sigma_6} G\left(\mathbf{x}, \mathbf{x}'^{(6)}\right) \frac{\partial}{\partial n}\Phi\left(\mathbf{x}'^{(6)}\right) ds\left(\mathbf{x}'^{(6)}\right) = \sum_{i=1}^{m_6} \frac{\partial}{\partial n}\Phi\left(\mathbf{x}_i'^{(6)}\right) \int_{\xi_i}^{\xi_{i+1}} G\left(\mathbf{x}, \mathbf{x}_i'^{(6)}\right) dh,$$

$$\int_{\Sigma_6} \frac{\partial}{\partial n} G\left(\mathbf{x}, \mathbf{x}'^{(6)}\right) \Phi\left(\mathbf{x}'^{(6)}\right) ds\left(\mathbf{x}'^{(6)}\right) = \sum_{i=1}^{m_j} \Phi\left(\mathbf{x}_i'^{(6)}\right) \int_{\zeta_i}^{\zeta_{i+1}} \frac{\partial}{\partial n} G\left(\mathbf{x}, \mathbf{x}_i'^{(6)}\right) dh,$$

where m_j denotes the maximum number of panels across Σ_j and $\mathbf{x}_i'^{(j)} = (\xi_i', \zeta_i')$ is the midpoint of panel $\Delta x_i'$ at Σ_j. ξ_i' and ζ_i' are defined in the following way

$$\xi_i' = \frac{\xi_i + \xi_{i+1}}{2},$$
$$\zeta_i' = \frac{\zeta_i + \zeta_{i+1}}{2}.$$

The variable h and n will be explained in Section 4.3.

Hence for a field point on the boundary $\left(\mathbf{x}_k^{(j)} = \mathbf{x}_k \in \Sigma_j\right)$ the potential is given by the product of the exact integration of the Green's function and its normal derivative, and the potential at the boundary point which is

$$\begin{aligned}
\frac{1}{2}\Phi\left(\mathbf{x}_k^{(j)}\right) = & \sum_{i=1}^{m_1} G_\xi^{(i)}\left(\mathbf{x}_k^{(j)}\right)\Big|_{\Sigma_1} \Phi^{(i)}\big|_{\Sigma_1} - \sum_{i=1}^{m_1} G^{(i)}\left(\mathbf{x}_k^{(j)}\right)\Big|_{\Sigma_1} \Phi_\xi^{(i)}\Big|_{\Sigma_1} \\
& + \sum_{i=1}^{m_2} G_\xi^{(j)}\left(\mathbf{x}_k^{(j)}\right)\Big|_{\Sigma_2} \Phi^{(i)}\big|_{\Sigma_2} - \sum_{i=1}^{m_2} G^{(i)}\left(\mathbf{x}_k^{(j)}\right)\Big|_{\Sigma_2} \Phi_\xi^{(i)}\Big|_{\Sigma_2} \\
& + \sum_{i=1}^{m_3} G_\zeta^{(i)}\left(\mathbf{x}_k^{(j)}\right)\Big|_{\Sigma_3} \Phi^{(i)}\big|_{\Sigma_3} - \sum_{i=1}^{m_3} G^{(i)}\left(\mathbf{x}_k^{(j)}\right)\Big|_{\Sigma_3} \Phi_\zeta^{(i)}\Big|_{\Sigma_3} \\
& + \sum_{i=1}^{m_4} G_\zeta^{(i)}\left(\mathbf{x}_k^{(j)}\right)\Big|_{\Sigma_4} \Phi^{(i)}\big|_{\Sigma_4} - \sum_{i=1}^{m_4} G^{(i)}\left(\mathbf{x}_k^{(j)}\right)\Big|_{\Sigma_4} \Phi_\zeta^{(i)}\Big|_{\Sigma_4} \\
& + \sum_{i=1}^{m_5} G_\zeta^{(i)}\left(\mathbf{x}_k^{(j)}\right)\Big|_{\Sigma_5} \Phi^{(i)}\big|_{\Sigma_5} - \sum_{i=1}^{m_5} G^{(i)}\left(\mathbf{x}_k^{(j)}\right)\Big|_{\Sigma_5} \Phi_\zeta^{(i)}\Big|_{\Sigma_5} \\
& + \sum_{i=1}^{m_6} G_n^{(i)}\left(\mathbf{x}_k^{(j)}\right)\Big|_{\Sigma_6} \Phi^{(i)}\big|_{\Sigma_6} - \sum_{i=1}^{m_6} G^{(i)}\left(\mathbf{x}_k^{(j)}\right)\Big|_{\Sigma_6} \Phi_n^{(i)}\big|_{\Sigma_6},
\end{aligned} \tag{4.2.1}$$

where

$$G_{\xi}^{(i)}\left(\mathbf{x}_k^{(j)}\right)\Big|_{\Sigma_{1,2}} = \int_{\zeta_i}^{\zeta_{i+1}} \frac{\partial}{\partial \xi} G\left(\mathbf{x}_k^{(j)}, (a_{1,2}, \zeta)\right)\, d\zeta, \tag{4.2.2}$$

$$G^{(i)}\left(\mathbf{x}_k^{(j)}\right)\Big|_{\Sigma_{1,2}} = \int_{\zeta_i}^{\zeta_{i+1}} G\left(\mathbf{x}_k^{(j)}, (a_{1,2}, \zeta)\right)\, d\zeta, \tag{4.2.3}$$

$$G_{\zeta}^{(i)}\left(\mathbf{x}_k^{(j)}\right)\Big|_{\Sigma_{3,4,5}} = \int_{\xi_i}^{\xi_{i+1}} \frac{\partial}{\partial \zeta} G\left(\mathbf{x}_k^{(j)}, (0, \xi)\right)\, d\xi, \tag{4.2.4}$$

$$G^{(i)}\left(\mathbf{x}_k^{(j)}\right)\Big|_{\Sigma_{3,4,5}} = \int_{\xi_i}^{\xi_{i+1}} G\left(\mathbf{x}_k^{(j)}, (0, \xi)\right)\, d\xi, \tag{4.2.5}$$

$$G_{n}^{(i)}\left(\mathbf{x}_k^{(j)}\right)\Big|_{\Sigma_6} = \int_{-\frac{|h_i|}{2}}^{\frac{|h_i|}{2}} \frac{\partial}{\partial n} G\left(\mathbf{x}_k^{(j)}, (h, 0)\right)\, dh, \tag{4.2.6}$$

$$G^{(i)}\left(\mathbf{x}_k^{(j)}\right)\Big|_{\Sigma_6} = \int_{-\frac{|h_i|}{2}}^{\frac{|h_i|}{2}} G\left(\mathbf{x}_k^{(j)}, (h, 0)\right)\, dh, \tag{4.2.7}$$

and

$$\Phi^{(i)}\big|_{\Sigma_j} = \Phi\left(\mathbf{x}_i^{\prime(j)}\right), \qquad \Phi_{\xi}^{(i)}\Big|_{\Sigma_j} = \frac{\partial}{\partial \xi}\Phi\left(\mathbf{x}_i^{\prime(j)}\right),$$

$$\Phi_{\zeta}^{(i)}\Big|_{\Sigma_j} = \frac{\partial}{\partial \zeta}\Phi\left(\mathbf{x}_i^{\prime(j)}\right), \qquad \Phi_{n}^{(i)}\big|_{\Sigma_j} = \frac{\partial}{\partial n}\Phi\left(\mathbf{x}_i^{\prime(j)}\right),$$

with $\mathbf{x}_i^{\prime(j)} \in \Sigma_j$, $1 \leq j \leq 6$.

If a set of points is taken from the same boundary segment, say Σ_p, then we have a set of equations in terms of equation (4.2.1) defined at different points. This set of k equations can be written in matrix notation as

$$\frac{1}{2}\Phi^{(p)} = \sum_{j=1}^{6} \mathbb{H}_j^{(p)}\, \Phi^{(j)} - \sum_{j=1}^{6} \mathbb{G}_j^{(p)}\, \Phi_n^{(j)}. \tag{4.2.8}$$

The dummy indices p and j in (4.2.8) indicate the boundary segment where the points lie. Vector $\Phi^{(j)}$ is

$$\Phi^{(j)} = \left[\Phi\left(\mathbf{x}\right)\big|_{\Sigma_j}\right], \tag{4.2.9}$$

with dimension k, and vector $\Phi_n^{(j)}$ is given by

$$\begin{aligned}
\Phi_n^{(j)} &= \left[\Phi_\xi(\mathbf{x})|_{\Sigma_j}\right], \qquad \text{for } j=1 \text{ or } j=2,\\
\Phi_n^{(j)} &= \left[\Phi_\zeta(\mathbf{x})|_{\Sigma_j}\right], \qquad \text{for } j=3,\ j=4, \text{or } j=5,\\
\Phi_n^{(j)} &= \left[\Phi_n(\mathbf{x})|_{\Sigma_j}\right], \qquad \text{for } j=6,
\end{aligned} \tag{4.2.10}$$

where the length of the vectors $\left[\Phi_\xi(\mathbf{x})|_{\Sigma_j}\right]$, $\left[\Phi_\zeta(\mathbf{x})|_{\Sigma_j}\right]$, and $\left[\Phi_n(\mathbf{x})|_{\Sigma_j}\right]$ are respectively m_1+m_2, $m_3+m_4+m_5$, and m_6. $\mathbb{G}_j^{(p)}$ is the matrix containing entries of the kind of equations (4.2.3), (4.2.5), and (4.2.7). $\mathbb{H}_j^{(p)}$ is the matrix with entries of the kind of equations (4.2.2), (4.2.4), and (4.2.6). The full expression for $\mathbb{G}_j^{(p)}$ at each boundary segment is given by

$$\mathbb{G}_j^{(p)} = \left[G\left(\mathbf{x}_k^{(p)}\right)\Big|_{\Sigma_j}\right], \qquad \text{for } 1 \le j,p \le 6, \tag{4.2.11}$$

and the full expression for $\mathbb{H}_j^{(p)}$ is given by

$$\begin{aligned}
\mathbb{H}_j^{(p)} &= \left[G_\xi\left(\mathbf{x}_k^{(p)}\right)\Big|_{\Sigma_j}\right], \qquad \text{for } j=1,2 \text{ and } 1 \le p \le 6,\\
\mathbb{H}_j^{(p)} &= \left[G_\zeta\left(\mathbf{x}_k^{(p)}\right)\Big|_{\Sigma_j}\right], \qquad \text{for } j=3,4,5 \text{ and } 1 \le p \le 6,\\
\mathbb{H}_6^{(p)} &= \left[G_n\left(\mathbf{x}_k^{(p)}\right)\Big|_{\Sigma_6}\right], \qquad \text{for } 1 \le p \le 6.
\end{aligned} \tag{4.2.12}$$

Both $\mathbb{G}_j^{(p)}$ and $\mathbb{H}_j^{(p)}$ have the dimension of $k \times m_j$.

Therefore for a set of points taken on all six boundary segments we have six equations (4.2.8) for six distinct p and we write this as the matrix equation

$$\frac{1}{2}\Phi = \mathbb{H}\,\Phi - \mathbb{G}\,\Phi_n,$$

where

$$\Phi = \begin{bmatrix} \Phi^{(1)} \\ \Phi^{(2)} \\ \Phi^{(3)} \\ \Phi^{(4)} \\ \Phi^{(5)} \\ \Phi^{(6)} \end{bmatrix}, \quad \Phi_n = \begin{bmatrix} \Phi_n^{(1)} \\ \Phi_n^{(2)} \\ \Phi_n^{(3)} \\ \Phi_n^{(4)} \\ \Phi_n^{(5)} \\ \Phi_n^{(6)} \end{bmatrix}, \tag{4.2.13}$$

$$\mathbb{G} = \begin{bmatrix} \mathbb{G}_1^{(1)} & \mathbb{G}_1^{(2)} & \mathbb{G}_1^{(3)} & \mathbb{G}_1^{(4)} & \mathbb{G}_1^{(5)} & \mathbb{G}_1^{(6)} \\ \mathbb{G}_2^{(1)} & \mathbb{G}_2^{(2)} & \mathbb{G}_2^{(3)} & \mathbb{G}_2^{(4)} & \mathbb{G}_2^{(5)} & \mathbb{G}_2^{(6)} \\ \mathbb{G}_3^{(1)} & \mathbb{G}_2^{(2)} & \mathbb{G}_3^{(3)} & \mathbb{G}_3^{(4)} & \mathbb{G}_3^{(5)} & \mathbb{G}_3^{(6)} \\ \mathbb{G}_4^{(1)} & \mathbb{G}_2^{(2)} & \mathbb{G}_4^{(3)} & \mathbb{G}_4^{(4)} & \mathbb{G}_4^{(5)} & \mathbb{G}_4^{(6)} \\ \mathbb{G}_5^{(1)} & \mathbb{G}_2^{(2)} & \mathbb{G}_5^{(3)} & \mathbb{G}_5^{(4)} & \mathbb{G}_5^{(5)} & \mathbb{G}_5^{(6)} \\ \mathbb{G}_6^{(1)} & \mathbb{G}_2^{(2)} & \mathbb{G}_6^{(3)} & \mathbb{G}_6^{(4)} & \mathbb{G}_6^{(5)} & \mathbb{G}_6^{(6)} \end{bmatrix}, \tag{4.2.14}$$

and

$$\mathbb{H} = \begin{bmatrix} \mathbb{H}_1^{(1)} & \mathbb{H}_1^{(2)} & \mathbb{H}_1^{(3)} & \mathbb{H}_1^{(4)} & \mathbb{H}_1^{(5)} & \mathbb{H}_1^{(6)} \\ \mathbb{H}_2^{(1)} & \mathbb{H}_2^{(2)} & \mathbb{H}_2^{(3)} & \mathbb{H}_2^{(4)} & \mathbb{H}_2^{(5)} & \mathbb{H}_2^{(6)} \\ \mathbb{H}_3^{(1)} & \mathbb{H}_3^{(2)} & \mathbb{H}_3^{(3)} & \mathbb{H}_3^{(4)} & \mathbb{H}_3^{(5)} & \mathbb{H}_3^{(6)} \\ \mathbb{H}_4^{(1)} & \mathbb{H}_4^{(2)} & \mathbb{H}_4^{(3)} & \mathbb{H}_4^{(4)} & \mathbb{H}_4^{(5)} & \mathbb{H}_4^{(6)} \\ \mathbb{H}_5^{(1)} & \mathbb{H}_5^{(2)} & \mathbb{H}_5^{(3)} & \mathbb{H}_5^{(4)} & \mathbb{H}_5^{(5)} & \mathbb{H}_5^{(6)} \\ \mathbb{H}_6^{(1)} & \mathbb{H}_6^{(2)} & \mathbb{H}_6^{(3)} & \mathbb{H}_6^{(4)} & \mathbb{H}_6^{(5)} & \mathbb{H}_6^{(6)} \end{bmatrix}. \tag{4.2.15}$$

The components of Φ are given by (4.2.9) and the components of Φ_n are given by (4.2.10). The entries of $\mathbb{G}$ are defined by (4.2.11) and the entries of $\mathbb{H}$ are defined by (4.2.12). $\mathbb{G}$ and $\mathbb{H}$ are square matrices with dimension $\sum_{j=1}^{6} m_j$. The solution of (4.2.2) to (4.2.7) is discussed in the next two sections.

4.3 Discretization Technique for Non-uniform Depth Profile

In this section we present a new coordinate system for the varying seabed. This will be used in the next section to integrate exactly the free-space Green's function and the normal derivative on the varying seabed.

From (3.4.13) the free-space Green's function depends only on the distance between points $\mathbf{x}$ and $\mathbf{x}'$. For the straight-line boundary segments the integral of this Green's function and the integral of its normal derivative can be done in a straightforward manner. For the varying seabed, the integration of the Green's function and its normal derivative is done with the help of a localized coordinate system which varies as we traverse the varying seabed.

The varying seabed, described by function $z = d(x)$, is divided into a finite number of equally spaced panels Δs_i. We set up the axes h and n in a way such that the origin coincides with the midpoint of Δs_i which is denoted by (ξ_i', ζ_i') (see Figure 4.3). The h axis is tangential to the curve and n axis is pointing downward in the normal direction to the curve. The coordinate system h and n is at an angle θ_i to the Cartesian coordinate system. The Cartesian coordinate system (x, z) is related to (h, n) by the following equations for panel j:

$$h = (x - \xi_i') \cos\theta_i + (z - \zeta_i') \sin\theta_i, \tag{4.3.1}$$

$$n = (x - \xi_i') \sin\theta_i - (z - \zeta_i') \cos\theta_i. \tag{4.3.2}$$

Hence the coordinate system changes for each Δs_i of the varying seabed. See Figure 4.3 for the direction of the $h^{(i)}$ and $n^{(i)}$ axes.

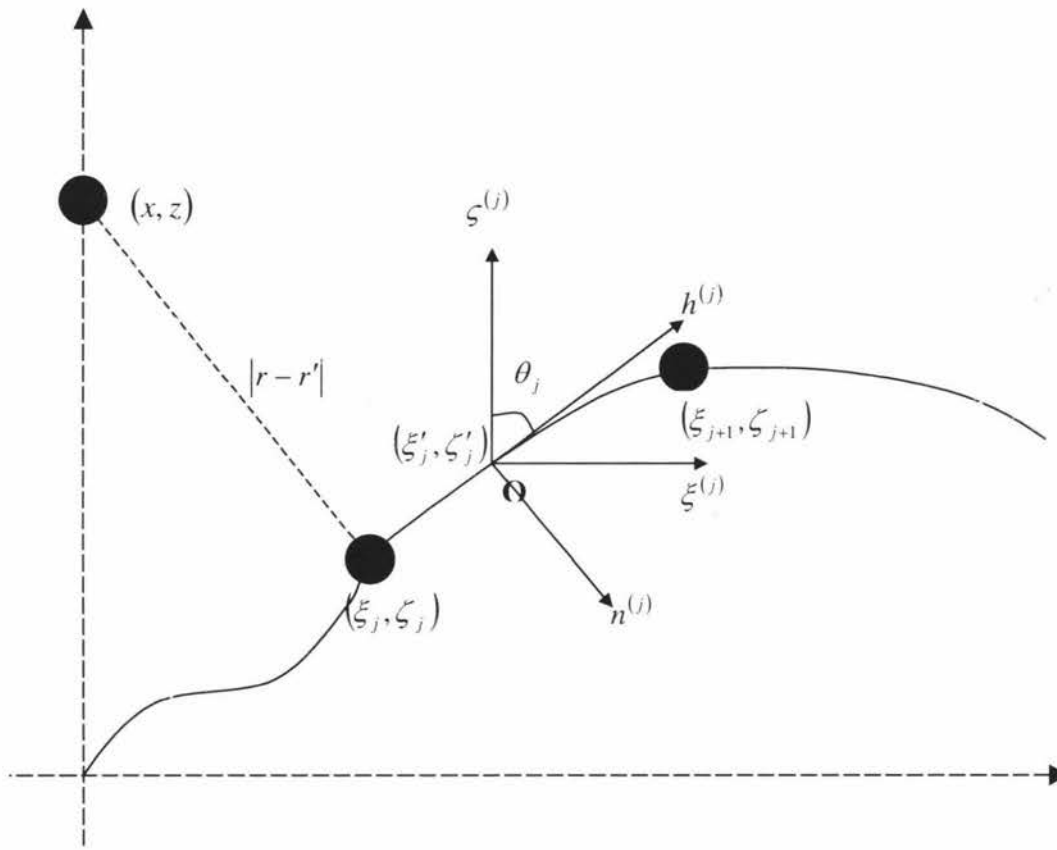

Figure 4.3. Schematic diagram of the localized coordinate system for node Δs_i taken on a seabed of arbitrary shape.

4.4 The Solution of The Free-space Green's Function

4.4.1 On Flat Boundary Segments

In this section we determine the analytic solutions of the integrals of the free-space Green's function and its normal derivative on flat boundary segments using the Cartesian coordinate system.

Since the Green's function and its normal derivative are singular at $\mathbf{x} = \mathbf{x}'$, we present the solution for several cases. First we consider the case for points which lie on Σ_1 or Σ_2 (the two lines are located respectively at a_1 and a_2) which have coordinate (a_j, ζ), $j = 1, 2$, where $H_j \leq \zeta \leq 0$.

$\frac{\partial G}{\partial n}$ on vertical segments is equivalent to G_ξ which is

$$G_\xi = -\frac{1}{2\pi} \frac{x - \xi}{(x - \xi)^2 + (z - \zeta)^2}. \tag{4.4.1}$$

Since (4.4.1) is zero when $x = \xi$ the solution of (4.2.2) is

$$\int_{\zeta_i}^{\zeta_{i+1}} G_\xi \left((x, z), (a_j, \zeta)\right) \, d\zeta = \begin{cases} 0, & \text{if } x = a_j, \\ (-1)^j \left[\frac{1}{2\pi}\left(\arctan\left(\frac{z-\zeta}{x-a_j}\right)\right)\right]_{\zeta_i}^{\zeta_{i+1}}, & \text{if } x \neq a_j. \end{cases} \tag{4.4.2}$$

When $x = \xi$ (3.4.13) becomes

$$G = \frac{1}{4\pi} \ln\left((z - \zeta)^2\right),$$

therefore the value of (4.2.3) is determined by the following formula

$$\int_{\zeta_i}^{\zeta_{i+1}} G\left((x,z),(a_j,\zeta)\right)\, d\zeta = \begin{cases} -\dfrac{1}{2\pi}\left[\zeta\right]_{\zeta_i}^{\zeta_{i+1}}, & \text{if } z=\zeta_i \text{ or } z=\zeta_{i+1}, \\ -\dfrac{1}{4\pi}\left[(z-\zeta)\,\ln(z-\zeta)+\zeta\right]_{\zeta_i}^{\zeta_{i+1}}, & \text{if } x=a_j, \\ -\dfrac{1}{4\pi}\left[(z-\zeta)\,\ln\left((x-a_j)^2+(z-\zeta)^2\right)\right. & \\ \left.+2\,(x-a_j)\,\tan^{-1}\left(\dfrac{z-\zeta}{x-a_j}\right)+2\zeta\right]_{\zeta_i}^{\zeta_{i+1}}, & \\ \text{if } x\neq a_j,\ z\neq\zeta_i \text{ and } z\neq\zeta_{i+1}. \end{cases} \tag{4.4.3}$$

Next we consider the case where the integrals are taken over the free surface and the contact surface between the floating plate and the water. All the points in this region are denoted by $(\xi,0)$, where $\xi\in[a_1,a_2]$. $\dfrac{\partial G}{\partial n}$ for the horizontal boundary segment is equivalent to G_ζ

$$G_\zeta = -\frac{1}{2\pi}\frac{z-\zeta}{(x-\xi)^2+(z-\zeta)^2}. \tag{4.4.4}$$

Equation (4.4.4) is zero when $z=\zeta$ for $x\neq\xi$ and hence this gives us the value of the integral (4.2.4) to be

$$\int_{\xi_i}^{\xi_{i+1}} G_\zeta\left((x,z),(\xi,0)\right)\, d\xi = \begin{cases} 0, & \text{if } z=0, \\ \left[\dfrac{1}{2\pi}\left(\tan^{-1}\left(\dfrac{x-\xi}{z-\zeta}\right)\right)\right]_{\xi_i}^{\xi_{i+1}}, & \text{if } z\neq 0. \end{cases} \tag{4.4.5}$$

When $z=\zeta$ equation (3.4.13) simplifies to

$$G=\frac{1}{4\pi}\ln\left((x-\xi)^2\right),$$

therefore the value of (4.2.5) is determined by the following formula

$$\int_{\xi_i}^{\xi_{i+1}} G\left((x,z),(\xi,0)\right)\, d\xi = \begin{cases} -\dfrac{1}{2\pi}\left[\xi\right]_{\xi_i}^{\xi_{i+1}}, & \text{if } x=\xi_{i+1} \text{ or } x=\xi_i, \\ -\dfrac{1}{4\pi}\left[(x-\xi)\,\ln(x-\xi)+2\xi\right]_{\xi_i}^{\xi_{i+1}}, & \text{if } z=0, \\ \frac{1}{4\pi}\left[(x-\xi)\ln\left((x-\xi)^2+z^2\right)+2z\,\tan^{-1}\left(\dfrac{x-\xi}{z}\right)+2\xi\right]_{\xi_i}^{\xi_{i+1}}, & \\ & \text{if } x\neq\xi_{i+1},\ x\neq\xi_i, \text{ and } z\neq 0. \end{cases} \tag{4.4.6}$$

4.4.2 On The Varying Seabed

In this section we use the localized coordinate system for the exact integration of the Green's function and the normal derivative on each panel Δs_i.

We write (3.4.13) in parameters h and n to be

$$G(\mathbf{x},\mathbf{x}') = \frac{1}{4\pi}\ln\left((H-h)^2+(N-n)^2\right),$$

and its integrals are written as

$$\int_{-\frac{|h|}{2}}^{\frac{|h|}{2}} G(\mathbf{x},\mathbf{x}')\, dh = \frac{1}{4\pi}\int_{-\frac{|h|}{2}}^{\frac{|h|}{2}} \ln\left((H-h)^2+(N-n)^2\right) dh, \tag{4.4.7}$$

$$\int_{h=-\frac{|h|}{2}}^{\frac{|h|}{2}} \frac{\partial}{\partial n} G(\mathbf{x},\mathbf{x}')\, dh = \frac{1}{2\pi}\int_{h=-\frac{|h|}{2}}^{\frac{|h|}{2}} \frac{(N-n)}{(H-h)^2+(N-n)^2}\, dh, \tag{4.4.8}$$

where $\mathbf{x}=(H,N)$ and $\mathbf{x}'=(h,n)$.

From Figure 4.3 it is clear that the coordinate system is set up in a way such that n is zero anywhere on the varying seabed. This simplifies (4.4.7) and (4.4.8) to

$$\int_{-\frac{|h|}{2}}^{\frac{|h|}{2}} G(\mathbf{x},\mathbf{x}')\, dh = \frac{1}{4\pi}\int_{-\frac{|h|}{2}}^{\frac{|h|}{2}} \ln\left((H-h)^2+N^2\right) dh, \tag{4.4.9}$$

$$\int_{h=-\frac{|h|}{2}}^{\frac{|h|}{2}} \frac{\partial}{\partial n} G(\mathbf{x},\mathbf{x}')\, dh = \frac{1}{2\pi}\int_{h=-\frac{|h|}{2}}^{\frac{|h|}{2}} \frac{N}{(H-h)^2+N^2}\, dh. \tag{4.4.10}$$

Formulas to determine the values of (4.4.9) and (4.4.10) then are as follows

$$\int_{-\frac{|h_i|}{2}}^{\frac{|h_i|}{2}} G(\mathbf{x},\mathbf{x}')\ dh = \begin{cases} -\frac{1}{2\pi}\left[h\right]_{-\frac{|h_i|}{2}}^{\frac{|h_i|}{2}}, & \text{if } H = \frac{|h_i|}{2} \text{ or } H = -\frac{|h_i|}{2}, \\ -\frac{1}{4\pi}\left[(H-h)\ln(H-h)+2h\right]_{-\frac{|h_i|}{2}}^{\frac{|h_i|}{2}}, & \text{if } N = 0, \\ \frac{1}{4\pi}\left[(H-h)\ln\left((H-h)^2+N^2\right)+2N\tan^{-1}\left(\frac{H-h}{N}\right)+2h\right]_{-\frac{|h_i|}{2}}^{\frac{|h_i|}{2}}, & \\ \qquad \text{if } H \neq \frac{|h_i|}{2},\ H \neq -\frac{|h_i|}{2}, \text{ and } N \neq 0. & \end{cases} \tag{4.4.11}$$

and

$$\int_{-\frac{|h_i|}{2}}^{\frac{|h_i|}{2}} \frac{\partial}{\partial n} G(\mathbf{x},\mathbf{x}')\ dh = \begin{cases} 0, & \text{if } N = 0, \\ \left[\frac{1}{2\pi}\left(\tan^{-1}\left(\frac{H-h}{N}\right)\right)\right]_{-\frac{|h_i|}{2}}^{\frac{|h_i|}{2}}, & \text{if } N \neq 0. \end{cases} \tag{4.4.12}$$

4.5 Matrix Operator for Boundary Conditions

In this section we discuss a matrix operator $\mathbb{A}$ relating the potential to its normal derivative.

We examine the boundary condition defined at Σ_1. Recall from Chapter 3 that the boundary condition on vertical segments may be deduced from the coupling operator $Q_{j,\nu}$ in (3.2.13). Since the boundary condition at Σ_1 is defined by $\dfrac{\partial}{\partial n}\phi = Q_{1,\nu}\,\phi = Q_{1,\nu}\,\Phi - Q_{1,\nu}\,\phi^I$, where ϕ is the transient wave and ϕ^I is the incident wave, we have

$$\Phi_n(a_1,z) - \phi_n^I(a_1,z) = Q_{1,\nu}\Phi(a_1,z) - Q_{1,\nu}\phi^I(a_1,z).$$

$Q_{1,\nu}\phi^I\,(a_1, z)$ is referred to as the driving force due to the incident wave. This driving force can be calculated exactly using $\phi_n^I = Q_{1,\nu}\phi^I\,(a_1, z)$ and it is

$$Q_{1,\nu}\,\phi^I = -i\nu_0\,\cosh\left(\nu_0^{(1)}\,(z+1)\right)\,e^{i\nu_0^{(1)}a_1},$$

and hence the boundary condition at Σ_1 is

$$\Phi_n\,(a_1, z) = Q_{1,\nu}\Phi\,(a_1, z) - 2i\nu_0\,\cosh\left(\nu_0^{(1)}\,(z+1)\right)\,e^{i\nu_0^{(1)}a_1}. \tag{4.5.1}$$

From (3.2.13) the coupling operator $Q_{1,\nu}$ is

$$Q_{1,\nu}\,\Phi\,(a_1, z) = \sum_m \eta_{1,\nu}^{(m)}\,\left\langle \tau_\nu^{(m)}, \Phi\right\rangle\,\tau_\nu^{(m)}\,(z),$$

where $\eta_{1,\nu}^{(m)}$ are the roots of dispersion equation (3.2.9). $\tau_{1,\nu}^{(m)}\,(z)$ are orthogonal functions defined by equation (3.2.7), with $\beta_{1,\nu}^{(m)} = 0$, and $\alpha_{1,\nu}^{(m)}$ is derived from (3.2.10). By writing the inner product as an integral, we find an explicit expansion of the integral equation (3.2.13) which is

$$Q_{1,\nu}\,\Phi\,(a_1, z) = \sum_m \eta_{1,\nu}^{(m)}\,\alpha_{1,\nu}^{(m)}\,\cos\left(\eta_{1,\nu}^{(m)}\,(z+1)\right)\int_{-1}^{0}\alpha_{1,\nu}^{(m)}\,\cos\left(\eta_{1,\nu}^{(m)}\,(z+1)\right)\,\Phi\,(a_1, z)\;dz. \tag{4.5.2}$$

Numerical integration of (4.5.2) gives

$$\int_{d(x)}^{0}\cos\left(\eta_{1,\nu}^{(m)}\,(z+1)\right)\,\Phi\,(a_1, z)\;dz = \sum_{i=1}^{m_1}\Phi\,(a_1, z_i')\int_{\zeta_i}^{\zeta_{i+1}}\cos\left(\eta_{1,\nu}^{(m)}\,(z+1)\right)\,dz,$$

where the term $\int_{\zeta_i}^{\zeta_{i+1}}\cos\left(\eta_{1,\nu}^{(m)}\,(z+1)\right)\;dz$ is the weight function which can be found analytically to obtain $\dfrac{1}{\eta_{1,\nu}^{(m)}}\left[\sin\left(\eta_{1,\nu}^{(m)}\,(z+1)\right)\right]_{\zeta_i}^{\zeta_{i+1}}$. Therefore the coupling operator for

boundary segment Σ_1 can be expressed as

$$Q_{1,\nu}\,\Phi\left(a_1,z\right)=\sum_{m}\left(\alpha_{1,\nu}^{(m)}\right)^2\cos\left(\eta_{1,\nu}^{(m)}\left(z+1\right)\right)\sum_{i=1}^{m_1}\Phi\left(a_1,z_i'\right)\left[\sin\left(\eta_{1,\nu}^{(m)}\left(z+1\right)\right)\right]_{\zeta_i}^{\zeta_{i+1}}. \tag{4.5.3}$$

For the normal derivative of the potential taken at a set of k points on Σ_1, where each is represented by (a_1,z_k), we obtain a set of k equations in terms of (4.5.3). This reduces (4.5.3) to

$$\Phi_n^{(1)}=\mathbb{Q}_{1,\nu}\Phi^{(1)}-2i\nu_0\,\Phi^{I(1)}, \tag{4.5.4}$$

where $\Phi_n^{(1)}$ is defined in (4.2.10), $\Phi^{I(1)}$ is the vector containing $\phi^I\left(a_1,z_k\right)\ \left(1\leq k\leq m_1\right)$, and $\mathbb{Q}_{1,\nu}$ is a matrix composed from the two other matrices, $\mathbb{S}_{1,\nu}$ and $\mathbb{R}_{1,\nu}$, defined by

$$\mathbb{Q}_{1,\nu}=\mathbb{S}_{1,\nu}\,\mathbb{R}_{1,\nu}, \tag{4.5.5}$$

where the components of these matrices are expressed as

$$S_{km}^{(1)} = \cos\left(\eta_{1,\nu}^{(m)}\left(z_k+1\right)\right), \tag{4.5.6}$$

$$R_{mi}^{(1)} = \alpha_{1,\nu}^{(m)}\left[\sin\left(\eta_{1,\nu}^{(m)}\left(\zeta+1\right)\right)\right]_{\zeta_i}^{\zeta_{i+1}}. \tag{4.5.7}$$

$S_{1,\nu}$ has dimension $m_1\times m$ and $\mathbb{R}_{1,\nu}$ has dimension $m\times m_1$ where m is the number of modes used. Therefore $\mathbb{Q}_{1,\nu}$ is square matrix with dimension m_1.

By applying the same techniques to the normal derivative of the potential at Σ_2 we obtain a linear matrix equation for the boundary condition at Σ_2 which is

$$\Phi_n^{(2)}=\mathbb{Q}_{2,\nu}\Phi^{(2)}, \tag{4.5.8}$$

where $\mathbb{Q}_{2,\nu}$ is the square matrix operator composed by matrices $\mathbb{S}_{2,\nu}$ and $\mathbb{R}_{2,\nu}$ which are defined by the equations

$$S_{km}^{(2)} = \cos\left(\eta_{2,\nu}^{(m)}\left(z_k + H_2\right)\right), \tag{4.5.9}$$

$$R_{mi}^{(2)} = \alpha_{2,\nu}^{(m)}\left[\sin\left(\eta_{2,\nu}^{(m)}\left(\zeta + H_2\right)\right)\right]_{\zeta_i}^{\zeta_{i+1}}, \tag{4.5.10}$$

and H_2 is the non-dimensionalized height of the water on the right-hand side of the plate. The dimension of $\mathbb{Q}_{2,\nu}$ is m_2. Notice that there is no driving force from the right-hand since the incident wave travels from $-\infty$. Hence the incident wave term is zero $\left(Q_{2,\nu}\,\phi^I = 0\right)$.

The boundary conditions on the free water surface at Σ_3 and Σ_5 is derived from

$$\Phi_n + \phi_n^I = \nu\Phi\left(x, 0\right) + \nu\phi^I.$$

Since $\phi_n^I = \nu\phi^I$ the incident wave potential term may be cancelled. Therefore the boundary condition at Σ_3 and Σ_5 is written in vectorial form as

$$\Phi_n^{(j)} = \nu\,\Phi^{(j)}, \tag{4.5.11}$$

for $j = 3, 5$.

At Σ_4 the boundary condition is defined by (3.4.10)

$$\Phi_n\left(x, 0\right) = \frac{\nu}{\beta}\int_{-L}^{L} G_{plate}\left(x, \xi\right)\ \Phi\left(\xi\right)\ d\xi,$$

where G_{plate} is explained in Appendix A.

The integral $\int_{-L}^{L} G_{plate}\left(x, \xi\right)\ \Phi\left(\xi\right)\ d\xi$ is done numerically by integrating G_{plate} exactly and holding Φ constant over each panel to give

$$\Phi_n\left(x, 0\right) = \frac{\nu}{\beta}\sum_{i=1}^{m_4}\phi\left(\xi_i', 0\right)\int_{\xi_i}^{\xi_{i+1}} G_{plate}\left(x, \xi\right)\ d\xi.$$

For a set of Φ_n taken over all points at Σ_4, we have a vector $\Phi_n^{(4)}$ that is

$$\Phi_n^{(4)} = \mathbb{G}^{plate}\, \Phi^{(4)}, \tag{4.5.12}$$

where $\mathbb{G}^{plate}$ is the square matrix of dimension m_4 and is composed of all the integrals of G_{plate}

$$\mathbb{G}^{plate} = \left[\frac{\nu}{\beta} \int_{\xi_i}^{\xi_{i+1}} G_{plate}\left(x_k, \xi\right)\, d\xi \right].$$

On the bottom boundary segment the condition is

$$\Phi_n^{(6)} = \mathbf{0}. \tag{4.5.13}$$

Finally we substitute (4.5.4), (4.5.8), (4.5.11), (4.5.12), and (4.5.13) into Φ_n in (4.2.13). This gives us

$$\Phi_n = \begin{bmatrix} \Phi_n^{(1)} \\ \Phi_n^{(2)} \\ \Phi_n^{(3)} \\ \Phi_n^{(4)} \\ \Phi_n^{(5)} \\ \Phi_n^{(6)} \end{bmatrix} = \begin{bmatrix} \mathbb{Q}_{1,\nu}\, \Phi_1 - 2i\nu_0\, \Phi_1^I \\ \mathbb{Q}_{2,\nu}\, \Phi_2 \\ \nu\, \Phi_3 \\ \mathbb{G}^{plate}\, \Phi_4 \\ \nu\, \Phi_5 \\ 0 \end{bmatrix}.$$

We write this in matrix equation form as

$$\Phi_n = \mathbb{A}\, \Phi - F,$$

where

$$\mathbb{A} = \begin{bmatrix} \mathbb{Q}_{1,\nu} & & & & & \\ & \mathbb{Q}_{2,\nu} & & & & \\ & & \nu\, \mathbb{I} & & & \\ & & & \mathbb{G}^{plate} & & \\ & & & & \nu\, \mathbb{I} & \\ & & & & & 0 \end{bmatrix}, \tag{4.5.14}$$

is the block-diagonal matrix called the *matrix operator for the boundary conditions*, and the constant vector F is defined by

$$F = \begin{bmatrix} 2i\nu_0\,\Phi_1^I \\ 0 \\ \cdot \\ \cdot \\ \cdot \\ 0 \end{bmatrix}. \tag{4.5.15}$$

We call F the *driving vector.*

Hence equation (4.1.2) becomes

$$\left(\frac{1}{2}\mathbb{I} - \mathbb{H} + \mathbb{G}\mathbb{A}\right)\Phi = -F,$$

where $\mathbb{I}$ is the identity matrix, $\mathbb{H}$ is defined by (4.2.15), $\mathbb{G}$ is defined by (4.2.14) and F is defined by (4.5.15). The dimension of Φ is equal to $\sum_{j=1}^{6} m_j$.

Chapter 5
The Reflected and Transmitted Waves

The scattering of wave occurs when the incident wave meets the floating plate on the water surface and the varying seabed on the bottom (recall that the plate and the varying seabed are called the scatterers). After the impact the wave is split into two parts; one will rebound to travel in the opposite direction and the other will continue travelling in the same direction. We call them, respectively, the *reflected* and *transmitted waves*. Provided that $|x|$ is large, i.e. away from the influence of scatterers, both waves can be written in the form $A\,e^{i\left(\pm\nu_0^{(j)}x-\omega t\right)}$, where A is the amplitude and $j = 1, 2$. The reflection and transmission of the wave is depicted by Figure 5.1. Bear in mind that we impose the condition on incident wave to be of unit amplitude ($A = 1$).

In this chapter we derive the scattered wave by solving for the reflection and the transmission amplitude using the result for Φ. Then we relate the amplitude of the transmitted and reflected waves to the amplitude of the incident wave by the energy flux equation. This is a check on the correctness of the numerical computation. Finally we relate the reflected and transmitted wave in the mirror image domains using the theory of Stokes time reversal (this is used in optics). The mirror image domains are domains that behave as if one is a 'mirror image'of the other. The result of the time reversal is particularly interesting and it is useful to check the solution for Φ.

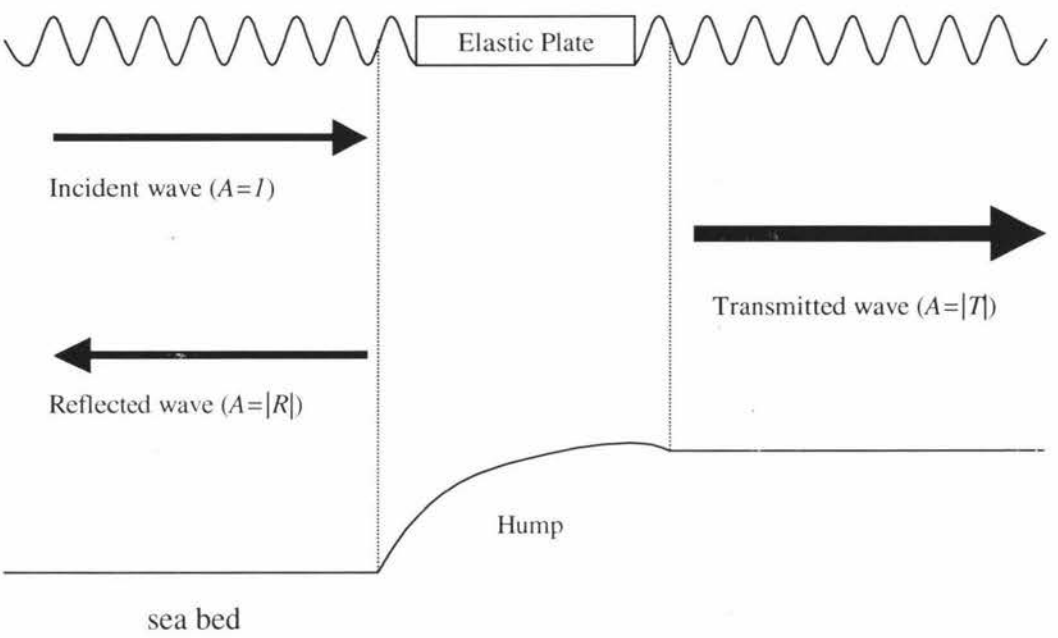

Figure 5.1. Schematic diagram of the scattered wave.

5.1 Determination of R and T

In this section our goal is to obtain explicit formulations for R and T from the result of Chapter 3.

On the left-hand side of the scatterers ($\tilde{\Omega}_1$) the wave (of potential Φ) that travels in the direction *towards* $-\infty$ is called the reflected wave (it is directed away from Σ_1). On the right-hand side of the scatterers ($\tilde{\Omega}_2$) the wave that travels in the direction *towards* ∞ is called the transmitted wave (it is directed away from Σ_2). Figure 5.1 depicts the reflected and the transmitted waves.

First we solve for the reflected wave. In $\tilde{\Omega}_1$ there are two types of waves travelling in different direction, one is the incident wave (from $-\infty$) and the other is the transient wave (towards $-\infty$). Since the reflected wave is travelling towards $-\infty$, then its potential Φ^R is equal to $\tilde{\phi}_1$. From Chapter 3 $\tilde{\phi}_1$ can be expressed using (3.2.11) as

$$\Phi^R(x,z) = \tilde{\phi}_1 = \sum_m \left\langle \tau_{1,\nu}^{(m)}, \tilde{\phi}_1(a_1,z) \right\rangle \tau_{1,\nu}^{(m)}(z)\ e^{\eta_{1,\nu}^{(m)}(x-a_1)}, \tag{5.1.1}$$

where $\tau_{1,\nu}^{(m)}$ is defined by (3.2.6).

To obtain the explicit expression for the reflected coefficient R we solve the transient wave potential $\tilde{\phi}_1$. $\tilde{\phi}_1$ is related to the incident wave potential and the full wave potential by equation (3.2.11). Hence we may write (5.1.1) as

$$\begin{aligned}
\tilde{\phi}_1(x,z) &= \sum_m \left\langle \tau_{1,\nu}^{(m)}, \left(\Phi(a_1,z) - \phi^I(a_1,z)\right) \right\rangle \tau_{1,\nu}^{(m)}(z)\ e^{\eta_{1,\nu}^{(m)}(x-a_1)} \\
&= \sum_m \left[\left\langle \tau_{1,\nu}^{(m)}, \Phi(a_1,z) \right\rangle - \left\langle \tau_{1,\nu}^{(m)}, \phi^I(a_1,z) \right\rangle \right] \tau_{1,\nu}^{(m)}(z)\ e^{\eta_{1,\nu}^{(m)}(x-a_1)}.
\end{aligned} \tag{5.1.2}$$

From (2.2.21) we notice that ϕ^I is orthogonal to $\tau_{1,\nu}^{(m)}$ and their inner product is equal to zero for all $m \neq 0$. This reduces (5.1.2) to

$$\tilde{\phi}_1(x,z) = \sum_m \left\langle \tau_{1,\nu}^{(m)}, \Phi(a_1,z) \right\rangle \tau_{1,\nu}^{(m)}(z)\ e^{\eta_{1,\nu}^{(m)}(x-a_1)} - e^{i\nu_0^{(1)}x}\ \tau_{1,\nu}^{(0)}(z)\ e^{\eta_{1,\nu}^{(0)}(x-a_1)}. \tag{5.1.3}$$

We separate the term corresponding to $m = 0$ from the series on the right-hand side of (5.1.3) to give us

$$\begin{aligned}\tilde{\phi}_1(x,z) &= \left\langle \tau_{1,\nu}^{(0)}, \Phi(a_1,z) \right\rangle \tau_{1,\nu}^{(0)}(z)\ e^{\eta_{1,\nu}^{(0)}(x-a_1)} + \sum_{m\geq 1} \left\langle \tau_{1,\nu}^{(m)}, \Phi(a_1,z) \right\rangle \tau_{1,\nu}^{(m)}(z)\ e^{\eta_{1,\nu}^{(m)}(x-a_1)} \\ &\quad -e^{i\nu_0^{(1)}x}\ \tau_{1,\nu}^{(0)}(z)\ e^{\eta_{1,\nu}^{(0)}(x-a_1)}.\end{aligned} \tag{5.1.4}$$

The first term on the left-hand side of (5.1.4) is the travelling plane wave and the terms in the series are the evanescent modes. These evanescent modes decay as the wave moves further away from the scatterers (or Σ_1). Hence as $x \to -\infty$ the series for $m \geq 1$ in (5.1.4) vanishes, reducing (5.1.4) to

$$\tilde{\phi}_1(x,z) = \left[\left\langle \tau_{1,\nu}^{(0)}, \Phi(a_1,z) \right\rangle - e^{i\nu_0^{(1)}x}\right] \tau_{1,\nu}^{(0)}(z)\ e^{\eta_{1,\nu}^{(0)}(x-a_1)}. \tag{5.1.5}$$

Equation (5.1.5) may be written as

$$\tilde{\phi}_1(x,z) = R\,\tau_{1,\nu}^{(0)}(z)\ e^{\eta_{1,\nu}^{(0)}(x-a_1)},$$

where R is the reflection coefficient (or reflection amplitude) and is of the form

$$R = \left[\left\langle \tau_{1,\nu}^{(0)}, \Phi(a_1,z) \right\rangle - e^{i\nu_0^{(1)}x}\right].$$

In practice the reflection amplitude is measured right at the $x = a_1$ and this implies

$$R = \left[\left\langle \tau_{1,\nu}^{(0)}, \Phi(a_1,z) \right\rangle - e^{i\nu_0^{(1)}a_1}\right]. \tag{5.1.6}$$

The inner product term in (5.1.6) can be replaced by an integral which gives us

$$R = \left(\alpha_{1,\nu}^{(0)}\right)^2 \int_{-1}^{0} \cos\left(\eta_{1,\nu}^{(0)}(\zeta+1)\right)\ \Phi(a_1,\zeta)\ d\zeta - e^{i\nu_0^{(1)}a_1}. \tag{5.1.7}$$

We numerically integrate the integral in (5.1.7) by integrating $\int_{-1}^{0} \cos\left(\eta_{1,\nu}^{(0)}(\zeta+1)\right)\ dz$ exactly and holding Φ constant over a panel $\Delta x_a'$ (the definition of $\Delta x_a'$ is given in Chapter 4). The result is

$$R = \left(\alpha_{1,\nu}^{(0)}\right)^2 \left[\sum_{i=1}^{m_1} \left[\sin\left(\eta_{1,\nu}^{(0)}(\zeta+1)\right)\right]_{\zeta_i}^{\zeta_{i+1}}\ \Phi(a_1,\zeta_i')\right] - e^{i\nu_0^{(1)}a_1}. \tag{5.1.8}$$

Next we solve the transmitted wave. In $\tilde{\Omega}_2$ the incident wave and the transient wave travel in the same direction (towards ∞). Hence the transmitted wave is the incident wave plus the transient wave, and therefore the potential is equal to that of the full wave which is given by

$$\Phi^T(x,z) = \sum_m \left\langle \tau_{2,\nu}^{(m)}, \Phi(a_2,z)\right\rangle\ \tau_{2,\nu}^{(m)}\, e^{-i\eta_{2,\nu}^{(m)}(x-a_2)}, \tag{5.1.9}$$

where Φ is the full wave potential function.

To obtain the transmission coefficient we solve for Φ^T. By separating the term corresponding to $m=0$, equation (3.2.11) becomes

$$\Phi^T(x,z) = \left\langle \tau_{2,\nu}^{(0)}, \Phi(a_2,z)\right\rangle\ \tau_{2,\nu}^{(0)}(z)\ e^{-\eta_{2,\nu}^{(0)}(x-a_2)} + \sum_{m\geq 1} \left\langle \tau_{2,\nu}^{(m)}, \Phi(a_2,z)\right\rangle\ \tau_{2,\nu}^{(m)}(z)\ e^{-\eta_{2,\nu}^{(m)}(x-a_2)}, \tag{5.1.10}$$

where $\tau_{2,\nu}^{(m)}$ is defined by (3.2.6).

The first term on the left hand side of (5.1.10) is the travelling plane wave and the term in the series are the evanescent modes which decays as the wave moves further away from the scatterers (or Σ_2). Therefore as $x \to \infty$ the evanescent modes in (5.1.10) vanish

and (5.1.10) becomes

$$\Phi^T(x,z) = \left\langle \tau_{2,\nu}^{(0)}, \Phi(a_2,z) \right\rangle \tau_{2,\nu}^{(0)}(z)\ e^{-\eta_{2,\nu}^{(0)}(x-a_2)}. \tag{5.1.11}$$

As in the case of finding the reflection coefficient above, we may write (5.1.11) into

$$\Phi^T(x,z) = T\,\tau_{2,\nu}^{(0)}(z)\ e^{-\eta_{2,\nu}^{(0)}(x-a_2)},$$

where T is the transmission coefficient (or transmission amplitude) and has the form of

$$T = \left\langle \tau_{2,\nu}^{(0)}, \Phi(a_2,z) \right\rangle. \tag{5.1.12}$$

By replacing the inner product term in (5.1.12) with an integral and integrating it numerically we obtain

$$T = \left(\alpha_{2,\nu}^{(0)}\right)^2 \sum_{i=1}^{m_2} \left[\sin\left(\eta_{2,\nu}^{(0)}(\zeta + H_2)\right)\right]_{\zeta_i}^{\zeta_{i+1}} \Phi(a_2,\zeta_a'), \tag{5.1.13a}$$

since $\cosh\left(\nu_0^{(2)}(z+H_2)\right) = \cos\left(\eta_{2,\nu}^{(0)}(z+H_2)\right)$, where H_2 is the non-dimensionalized water height on the right hand-side of the plate and the varying seabed.

5.2 Energy Transfer Across The Boundary

The reflection and the transmission coefficients must satisfy the energy flux equation, that is

$$|R|^2 + |T|^2 = 1,$$

for water of constant depth. Our goal in this section is to reach similar conclusion for water of variable depth by relating the amplitudes of the reflected wave, the transmitted wave, and the the incident wave by energy equation. This will provide us a strategy to check the solution for the reflection and the transmission coefficient.

We give a general expression for the time-dependent potential of the reflected, the transmitted, and the incident waves. These are, respectively

$$\phi^R(x,z) = R\cosh\left(\nu_0^{(1)}(z+1)\right)e^{i\left(\nu_0^{(1)}x-\omega t\right)}, \tag{5.2.14}$$

$$\phi^T(x,z) = T\cosh\left(\nu_0^{(2)}(z+2)\right)e^{i\left(\nu_0^{(2)}x-\omega t\right)}, \tag{5.2.15}$$

$$\phi^I(x,z) = \cosh\left(\nu_0^{(1)}(z+1)\right)e^{i\left(\nu_0^{(1)}x-\omega t\right)}. \tag{5.2.16}$$

For energy stored in $\hat{\Omega}$, bounded by Σ, the energy flux across the boundary is given by the equation (*Stoker* [8])

$$E = \rho' \int_t^{t_0+t_{final}} \left(\int_\Sigma \phi_t \frac{\partial\phi}{\partial n}\, dS\right) dt, \tag{5.2.17}$$

where ϕ is one of (5.2.14), (5.2.15), or (5.2.16).

It is assumed that there is no energy transfer across Σ_3, Σ_4, Σ_5, and Σ_6. Energy transfer only occurs across Σ_1 and Σ_2. Therefore solving equation (5.2.17) using the spatial integrals taken at Σ_1 and Σ_2 gives us E_R, E_T, and E_I which are

$$E_R = \rho' \int_t^{t_0+t_{final}} \left(\int_{\Sigma_1} \phi_t^R \frac{\partial\phi^R}{\partial n}\, dS\right) dt, \tag{5.2.18}$$

$$E_T = \rho' \int_t^{t_0+t_{final}} \left(\int_{\Sigma_2} \phi_t^T \frac{\partial\phi^T}{\partial n}\, dS\right) dt, \tag{5.2.19}$$

$$E_I = \rho' \int_t^{t_0+t_{final}} \left(\int_{\Sigma_1} \phi_t^I \frac{\partial\phi^I}{\partial n}\, dS\right) dt. \tag{5.2.20}$$

Using definition (5.2.14) equation (5.2.18) becomes

$$E_R = R^2\,\omega\,\rho'\,\nu_0^{(1)}\left[\frac{1}{2}+\frac{\sinh\left(2\nu_0^{(1)}\right)}{4\nu_0^{(1)}}\right]\int_{t_0}^{t_0+2\pi/\omega} e^{2i\left(\nu_0^{(1)}x-\omega t\right)}\, dt,$$

which is the energy flux per unit length across the boundary segment Σ_1 in time $t_{final} = 2\pi/\omega$. Notice that the function $e^{2i\left(\nu_0^{(1)}x-\omega t\right)}$ is periodic with period $2\pi/\omega$. Thus the average

flux per unit time is given by the following equation

$$E_R = \frac{R^2\,\omega\,\rho'\,\nu_0^{(1)}}{4}\left[1+\frac{\sinh\left(2\nu_0^{(1)}\right)}{2\nu_0^{(1)}}\right]. \tag{5.2.21}$$

Using definition (5.2.15) and by the same method as above, we may express (5.2.19) as equation

$$E_T = \frac{1}{4}T^2\,\omega\,\rho'\,\nu_0^{(2)}H_2\left[1+\frac{\sinh\left(2\nu_0^{(2)}\,H_2\right)}{2\nu_0^{(2)}\,H_2}\right], \tag{5.2.22}$$

and equation (5.2.20) becomes

$$E_I = \frac{1}{4}\,\omega^{(1)}\,\rho'\,\nu_0^{(1)}\left[1+\frac{\sinh\left(2\nu_0^{(1)}\right)}{2\nu_0^{(1)}}\right].$$

By virtue of energy conservation, the incoming energy into the domain $\tilde{\Omega}$ must total the outgoing energy (in other words $E_I = E_R + E_T$). Hence this gives us the equation

$$C\left(H_1\right) = |R|^2\,C\left(H_1\right) + |T|^2\,C\left(H_2\right), \tag{5.2.23}$$

where the constant function $C\left(H_j\right)$ is defined by the equation

$$C\left(H_j\right) = \frac{1}{4}\,\omega\,\rho'\,\nu_0^{(j)}H_j\left[1+\frac{\sinh\left(2\nu_0^{(j)}\,H_j\right)}{2\nu_0^{(2)}\,H_j}\right],$$

where $H_j,\ j=1,2$, is the dimensionless constant $\left(H_1=1\right)$.

If we take the dimensionless constants $H_1 = H_2\,(=1)$ the constant function $C\left(H_2\right)$ is equal to $C\left(H_1\right)$. This simplifies (5.2.23) to

$$|R|^2 + |T|^2 = 1, \tag{5.2.24}$$

which agrees with *Meylan* [5].

5.3 Reversed Time

In this section we shall show an interesting result about the reflected and the transmitted coefficients which is useful as another strategy to verify the solution to the reflection and the transmission amplitudes. We use Stoke's time reversal theory to relate the wave scattering problem in two mirror image domains. Two domains are called mirror images if one can be 'reflected' by a vertical line (or a mirror) to depict the other.

The seabed is of arbitrary shape. Then an incident wave of amplitude 1 travels from left to right of the scatterers (the plate and the varying seabed). This is depicted by the Figure 5.2 (a). We call this problem 1.

Problem 2 is when the same plane wave travels in the same direction but in the domain which is the mirror image of the water domain in Problem 1 (it means that if we 'reflect' the domain in problem 2 over a vertical line then we will obtain the domain in problem 1). This is depicted by Figure 5.2 (b).

To relate quantities R_1 and T_1 to R_2 and T_2 we apply Stokes time reversal, used in optics, to problem 1. The time reversal results in the 'reversed' wave functions involving $A^* e^{-i\left(\nu_0^{(j)} x - \omega t\right)}$, where A^* is the complex conjugate of amplitude A. We call this system 1. Then we notice that the reversed reflection amplitude can also be obtained by multiplying the amplitude of the incident wave in problem 1 by R_1. This give rise to system 2 where $R_1^* T_1$ is the amplitude for the transmitted wave and $|R_1|^2$ is the amplitude of the reflected wave. In order for this system to agree with system 1 we take the negative of all amplitudes in system 2 and add them to system 1. This gives us system 3 where the reflection coeffi-

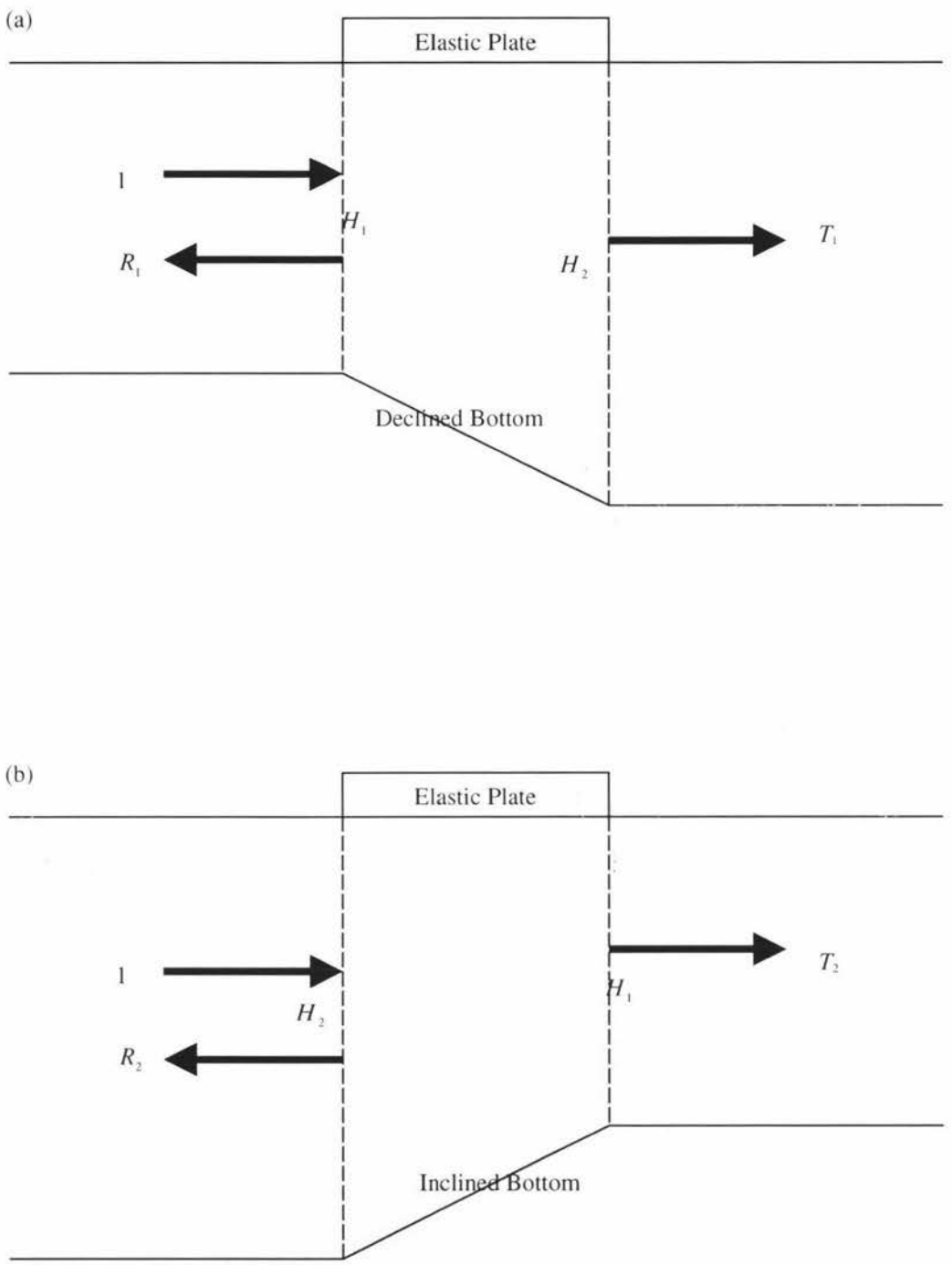

Figure 5.2. The distribution of amplitudes of the wave before and after the impact with the scatterers where the domain in (b) is the mirror image of the domain in (a).

cient is $-\frac{R_1^* T_1}{T_1^*}$ and the transmission coefficient is $\frac{1-|R_1|^2}{T_1^*}$. The process of time reversal is summarized by a chart in Figure 5.3.

By comparing the result in system 3 to problem 2 clearly R_2 and T_2 must satisfy the relationships

$$|R_2| = \left|\frac{R_1^* T_1}{T_1^*}\right| = |R_1|, \tag{5.3.1}$$

$$|T_2| = \left|\frac{1-|R_1|^2}{T_1^*}\right|. \tag{5.3.2}$$

Hence regardless of the direction of the incident wave the resulting amplitudes of the reflected waves on both sides of the scatterers are equal by equation (5.3.1), and the amplitudes of the transmitted waves on both sides of the scatterers must satisfy equation (5.3.2). This property applies to any arbitrary seabed shape.

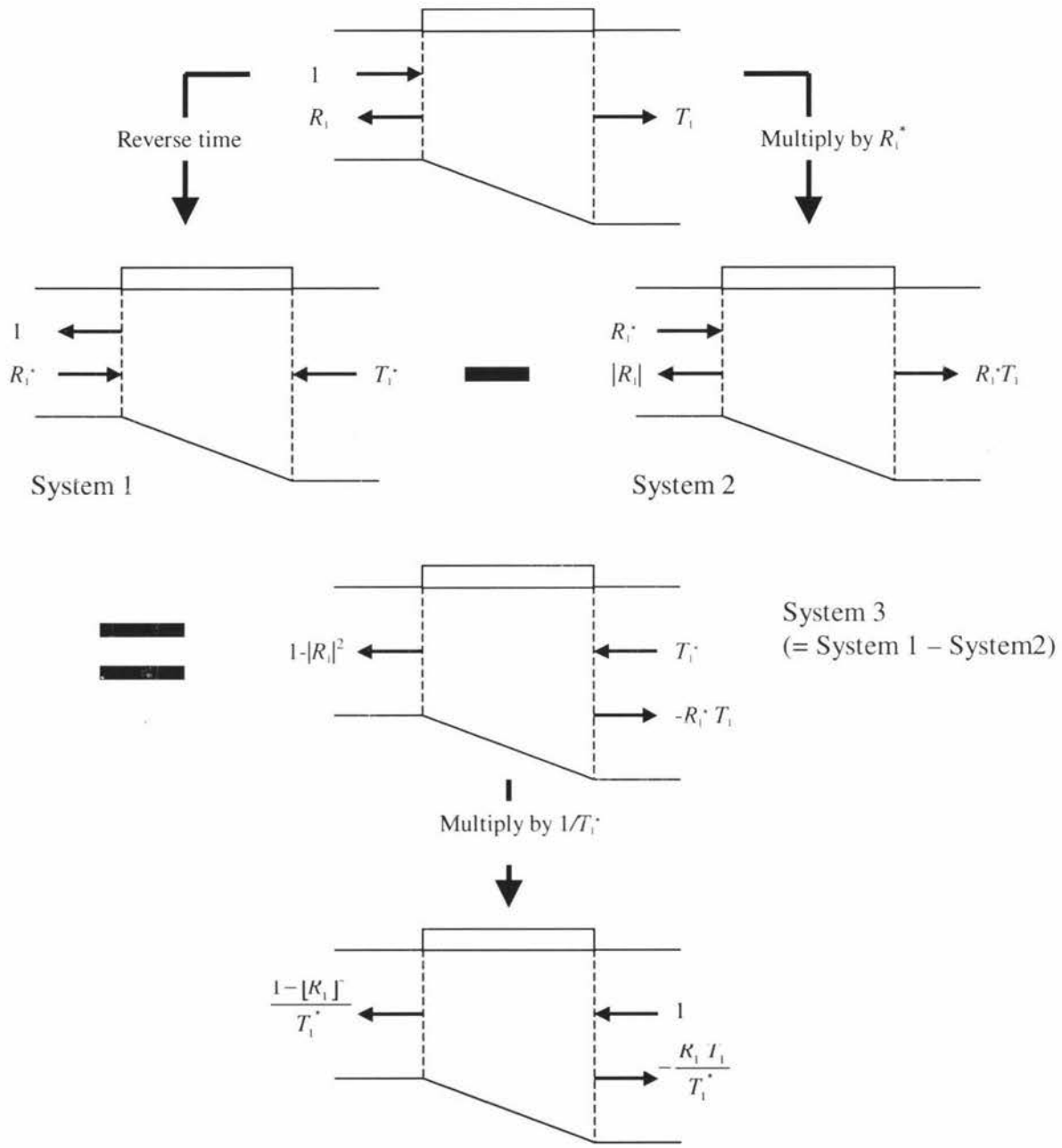

Figure 5.3. Flowchart showing mathematical technique derived from Stokes time reversal theory to relate the reflection and the transmission coefficients in two mirror image domains.

Chapter 6
Numerical Results

In this chapter we use numerical methods to solve the problems from previous chapters. These codes are tested against the known results from *Meylan* [5] and *Staziker, Porter, and Stirling* [7]. Meylan presented the result for the wave scattering by an ice sheet on water of constant depth, whereas Staziker presented the result for the wave scattering by a varying seabed (of uniform ends, i.e. $H_1 = H_2$). Notice that both problems have a simpler domain than ours because our water domain has both the plate and the varying seabed with possibly different depth at its ends.

For the first experiment we shall use the problem in Meylan. There are four tasks in this experiment. The first task is to show convergence for different numbers of the evanescent modes of the wave. The second task is to show convergence for different discretization step sizes (this is done with respect to the depth of the water). The third task is to reproduce the result presented by Meylan. The last task is to present the solution of the same problem for a different wavelengths.

In the second experiment we shall reproduce the results for two of Staziker's problems and compare them. We also present the solution for a depth profile with non-uniform ends (the height of the water before and after the varying seabed is different).

Finally in the last experiment we combine the problem from Meylan and Staziker by solving the potential with a plate and a varying seabed. The result is classified according to the material of the plate. There are two types of material of the plate. One is the ice

in Meylan's problem and the other is an artificial island (in the form of a floating runway) which was used in *Namba and Ohkusu* [6]. Under each material the result is further classified according to the shape of the varying seabed. One is the Staziker's depth profile and the other is one with non-uniform ends.

The plate is $x \in [-L, L]$ (the length of the plate is $2L$). The shape of the varying seabed is described by a function $d(x)$ and $x \in [-l, l]$ (the length of the varying seabed is $2l$). The boundary segments Σ_1 $(x = a_1)$ and Σ_2 $(x = a_2)$ are located right at both ends of the varying seabed and their position is symmetric $(a_1 = -a_2)$. The water is assumed to be inviscid and incompressible, and the motion is irrotational. The incident wave of unit amplitude (with respect to the height of the water) always travels from $-\infty$.

6.1 Single Ice Sheet on Water of Constant Depth

The aim of this experiment is to check our solution by solving the problem in *Meylan* [5] and comparing the result. The problem domain consists of an ice sheet floating on the surface of water of constant depth. There are four sections representing four tasks of this experiment. The first section shows the convergence of the solution for different number of evanescent modes of the wave. The second section shows the convergence of the solution for various magnitude of the discretization step size. The third section reproduces the result given in Meylan. The fourth section shows the result for Meylan's problem under various wavelengths.

The parameters for the ice sheet are: Young's modulus $E = 6$ G Pa, the sea ice density $\rho' = 922.5\,\text{kg/m}^3$, Poisson's ratio $\nu = 0.3$, and the thickness of the ice sheet is

$h = 1$ m. The bending rigidity for sea ice is $D = \frac{1}{12} E h^3 / (1 - \nu^2)$. The density of sea water is $\rho = 1025.0\,\text{kg/m}^3$. Since the water is of uniform depth then $H_1 = H_2$.

6.1.1 Convergence Test for The Evanescent Modes of The Wave

In this section we show the convergence of the solution for different number of evanescent modes of the wave. The test will be carried out using an inelastic (stiff) and immovable plate and an ice sheet. This helps us choosing the appropriate number of evanescent modes for later tests. The parameters used are: $L = 100$ m (length of plate is 200 m), the wavelengths $\lambda = 50$ m and $\lambda = 100$ m, and 1 m discretization step size (we assume this is sufficiently accurate and later we will show this true in the convergence test for the discretization step size). The result is presented in the following table which shows the absolute magnitude of the reflection amplitudes for different number of evanescent modes at $H_1 = H_2 = 5$ m and $H_1 = H_2 = 20$ m, $h = 1$ m for stiff and immovable plate ($\Phi_n = 0$ at $x \in [-L, L]$). The recorded results are rounded to 5 digits accuracy.

Table 6.1.1. Convergence of Evanescent Modes for a stiff and immovable plate of thickness $h = 1$ m.at $H_1 = H_2 = 5$ m and 20 m.

number of evanescent modes	5 m		20 m	
	$\lambda = 50$ m	$\lambda = 100$ m	$\lambda = 50$ m	$\lambda = 100$ m
0	0.9968	0.9875	0.9950	0.9868
1	0.9968	0.9875	0.9969	0.9877
2	0.9968	0.9875	0.9969	0.9877
5	0.9968	0.9875	0.9969	0.9877

For a stiff and immovable plate on shallow water (5 m) we see that the number of evanescent modes does not influence the solution. For the same plate on water of 20 m depth we see that the result requires more than one mode to achieve convergent. Note that zero evanescent mode means there is only the travelling wave in the solution.

A similar table is also presented for the case of a non-rigid ice sheet at $H_1 = H_2 = 5$ m and $H_1 = H_2 = 20$ m Bending rigidity constant for sea ice is $D = 5.4945 \times 10^8$ Pa.m^3.

Table 6.1.2. Convergence of Evanescent Modes for a non-rigid ice sheet with bending rigidity constant of $D = 5.4945 \times 10^8$ Pa.m^3 at $H_1 = H_2 = 5$ m and 20 m.

number of evanescent modes	5 m		20 m	
	$\lambda = 50$ m	$\lambda = 100$ m	$\lambda = 50$ m	$\lambda = 100$ m
0	0.2752	0.1871	0.6345	0.2592
1	0.2746	0.1871	0.6455	0.2610
2	0.2745	0.1871	0.6469	0.2611
5	0.2747	0.1872	0.6474	0.2612
10			0.6476	0.2613
15			0.6478	0.2613

For $H_1 = H_2 = 5$ m we see that 5 is the required number of the evanescent modes and for $H_1 = H_2 = 20$ m the required number of the evanescent modes is 15.

Note that the number of evanescent modes is proportional to the number of panels we use to discretize the vertical boundary segments (result from experiments). For discretization step size 1 m and $H_1 = 5$ m, 5 evanescent modes gives a sufficiently accurate result.

6.1.2 Convergence Test for The Magnitude of The Discretization Step Size

In this section we show the convergence of the solution for different magnitudes of the discretization step size. The parameters used are: wavelength $\lambda = 100$ m, $H_1 = 5$ m, and 5 evanescent modes. The result is presented in Figure 6.1 as a plot for the reflection coefficient versus the length of the plate at thickness $h = 1$ m. We can see that use of a step size too large leads to an incorrect result.

From the convergence test it is clear that the accuracy of the solution is determined by the discretization step size. The step size is related to the water depth so if the water is shallow then the step size must be relatively small (for example, water of depth 2 m will not be discretized using a 1 m step size) because a large step size can lead to the result being inaccurate. This is shown in Figure 6.1.

We see from Figure 6.1 that discretization step size of 1 m is sufficient to produce accurate result for the depths used here. Subsequently we shall use 1 m discretization step size unless H_1 and H_2 are not of multiple 1 m (for example, 2.3 m if divided by 1 m yields 0.3 m remainder).

6.1.3 Reflection Amplitude

In this section we reproduce the result presented in *Meylan* [5]. The parameters used are: wavelength $\lambda = 100$ m, $H_1 = 5$ m, and 5 evanescent modes with mixed discretization steps of 0.05 m, 0.1 m, and 0.5 m. The result is shown in Figure 6.2 as a plot for the reflection

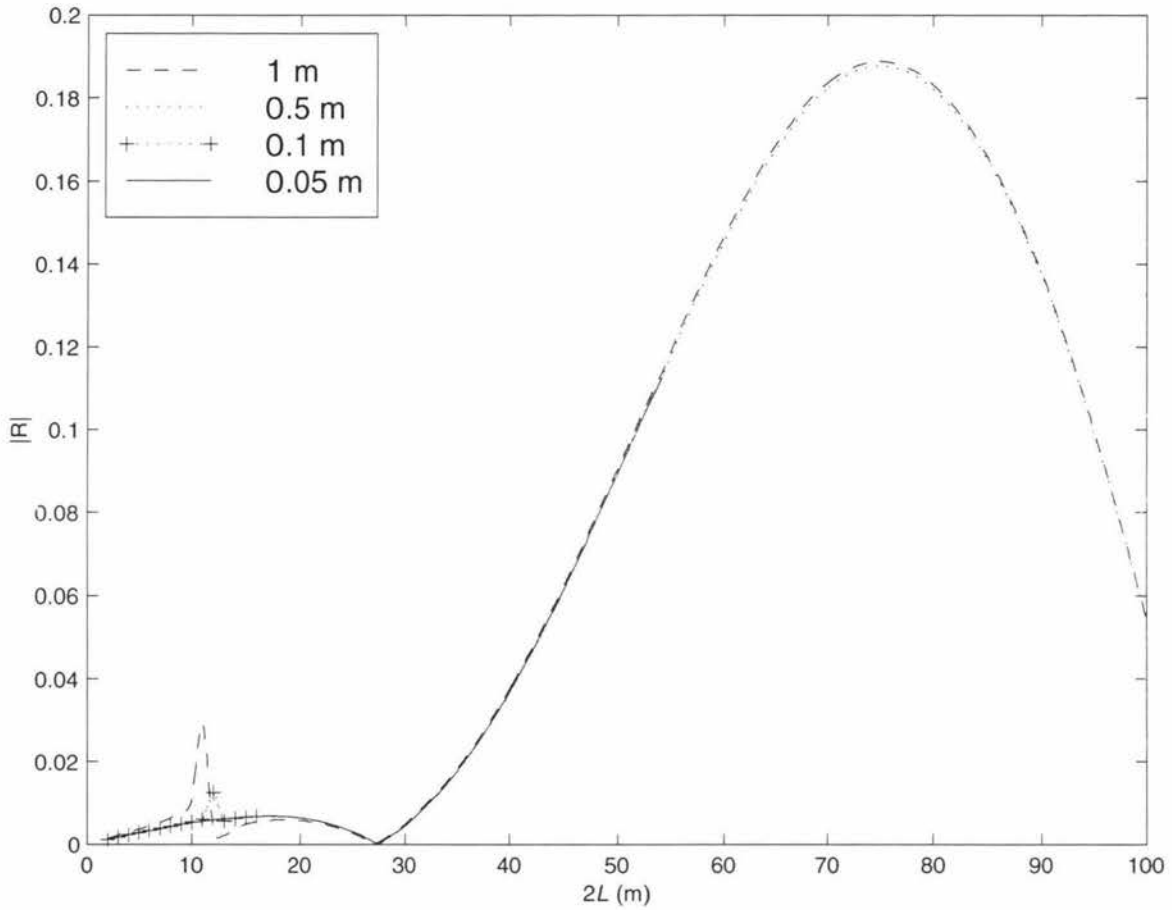

Figure 6.1. The reflection amplitude $|R|$ versus the length of the ice sheet $2L$ for the convergence test of discretization step size with $H_1 = H_2 = 5$ m, $\lambda = 100$ m and, 5 evanescent modes.

amplitude versus the length of the ice sheet. This result is identical to the result by Meylan and validates our numerical method.

Perfect resonance (transmission) occurs when the wave is only transmitted without being reflected. This is explained in great detail by *Meylan* [5]. The interval of perfect resonance is half the wavelength in the bounded region ($\hat{\Omega}$).

In Figure 6.2 the perfect resonance is represented by points where $|R| = 0$. The first point is at $2L = 27.2$ m and the next is at $2L = 105$ m. Then for every 60 m increase in the length we have $|R| = 0$.

6.1.4 Wavelength

In this section we present the solution to Meylan's problem for various magnitudes of the wavelength . The parameters used are: $H_1 = 5$ m, $L = 100$ m, 5 evanescent modes, and 1 m discretization. The result is shown in Figure 6.3 as a plot of the reflection amplitude versus the wavelength.

From Figure 6.3 we see that points of $|R| = 0$ no longer occur at uniform intervals as in Figure 6.2. For a sufficiently short wavelength ($\lambda < 100$ m) the ice sheet affects the reflected wave. For a sufficiently large wavelength ($\lambda > 500$ m) the reflected amplitude converges to zero which means all the wave is transmitted, and therefore the ice sheet on the surface is no longer important.

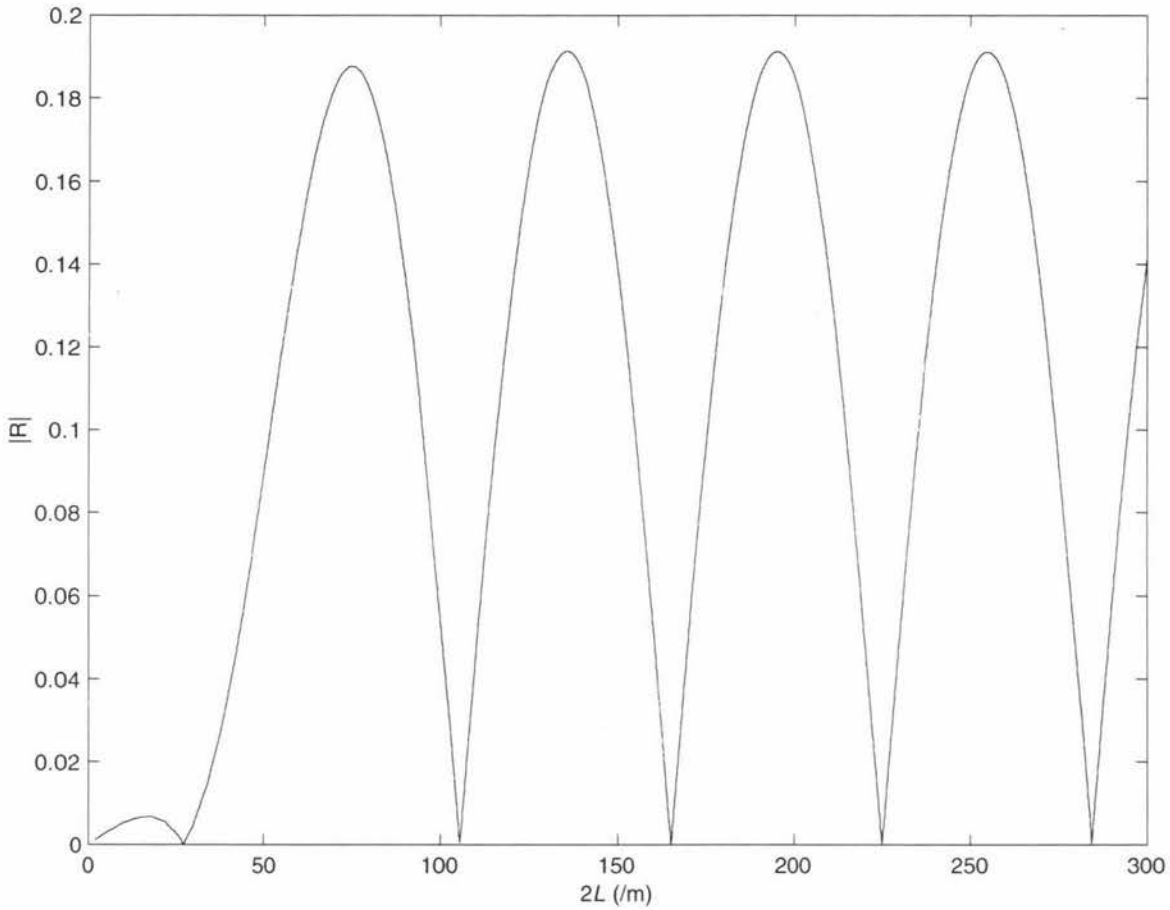

Figure 6.2. The reflection amplitude $|R|$ versus the length of the ice sheet $2L$ with $H_1 = H_2 = 5$ m, $h = 1$ m, $\lambda = 100$ m, and 5 evanescent modes. Perfect transmission occurs when $|R| = 0$.

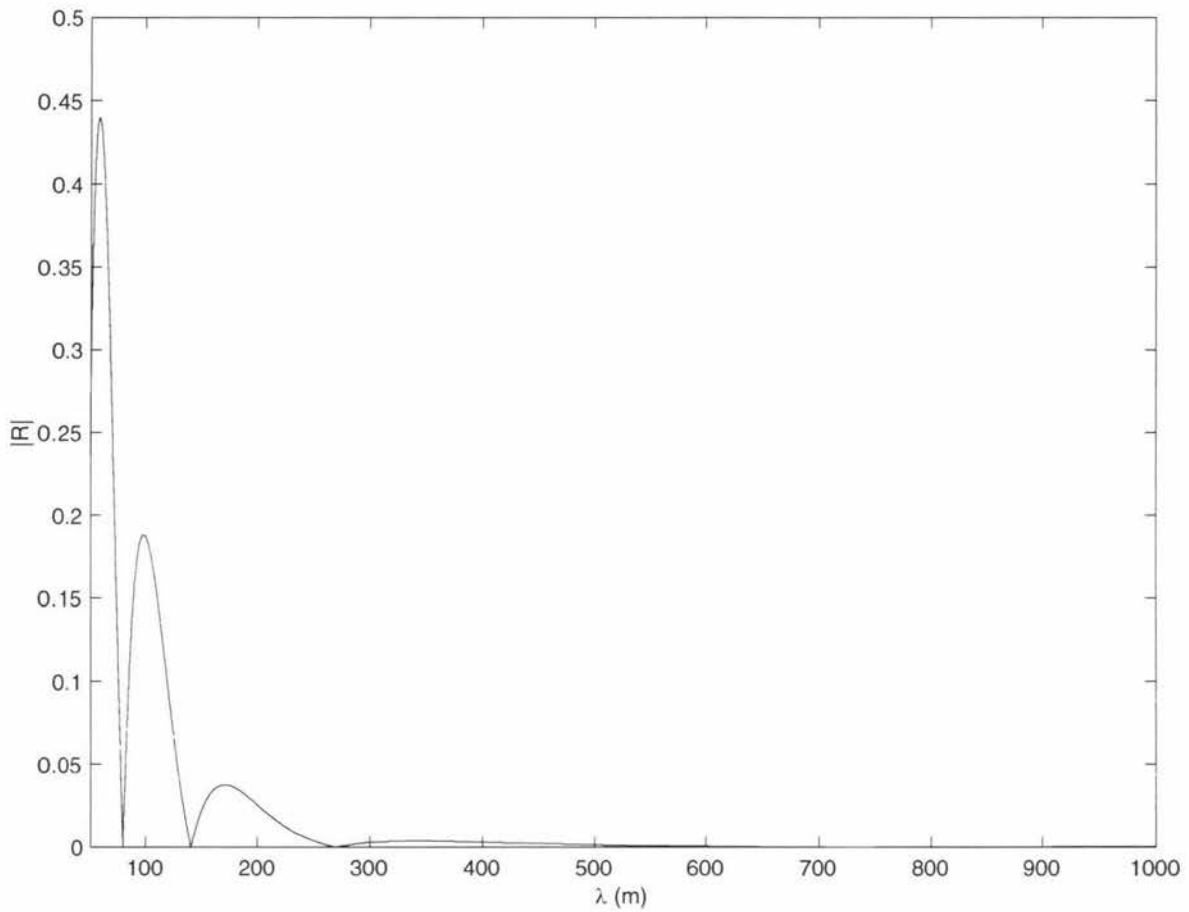

Figure 6.3. The reflection amplitude $|R|$ versus the wavelength λ for an ice sheet on water of constant depth with $H_1 = H_2 = 5$ m, $h = 1$ m, $2L = 200$ m, 5 evanescent modes, and discretization step size of 1 m.

6.2 Water of Free Surface and Variable Depth

In this experiment we aim to check our solution by solving the problem in *Staziker, Porter, and Stirling* [7] and comparing the results. The problem domain consists of a varying region on the bottom without any plate on the surface. The varying seabed is described by equation $d(x)$. We consider two profiles which are taken from Staziker and we call them the *Staziker's humps*. As well as the Staziker's humps, we also have a depth profile whose heights are different at its ends. We call this the *simple sloping plane*.

For the Staziker's humps we use $H_1 = H_2 = 5$ m and the wavelength is $\lambda = 26.1870$ m (accurate to 5 digits). This is chosen so that $\nu = 1$ (this number arises because we first non-dimensionalize $H_1 = 1$ then let $\nu H_1 = 1$). We do this because we want to draw the same figure as their paper and compare them.

6.2.1 First Staziker's Hump

The first Staziker's hump is described by the following equation

$$d(x) = -H_1 \left(\frac{1}{2} \left(\frac{x+l}{l} \right)^2 - \frac{x+l}{l} + 1 \right), \qquad \forall x \in [a_1, a_2], \tag{6.2.1}$$

where $H_1 = H_2 = 5$ m.

The first test uses 5 evanescent modes and 0.05 m discretization step size. The result is shown in Figure 6.4 as the plot of the reflected amplitude versus the length of the hump. This is identical to *Staziker* [7] and hence, again, indicates our numerical method is correct.

Next we test the same hump using parameters $l = 101$ (the length of the hump is 202 m), 5 evanescent modes, and 1 m discretization step size. We do this test because the result

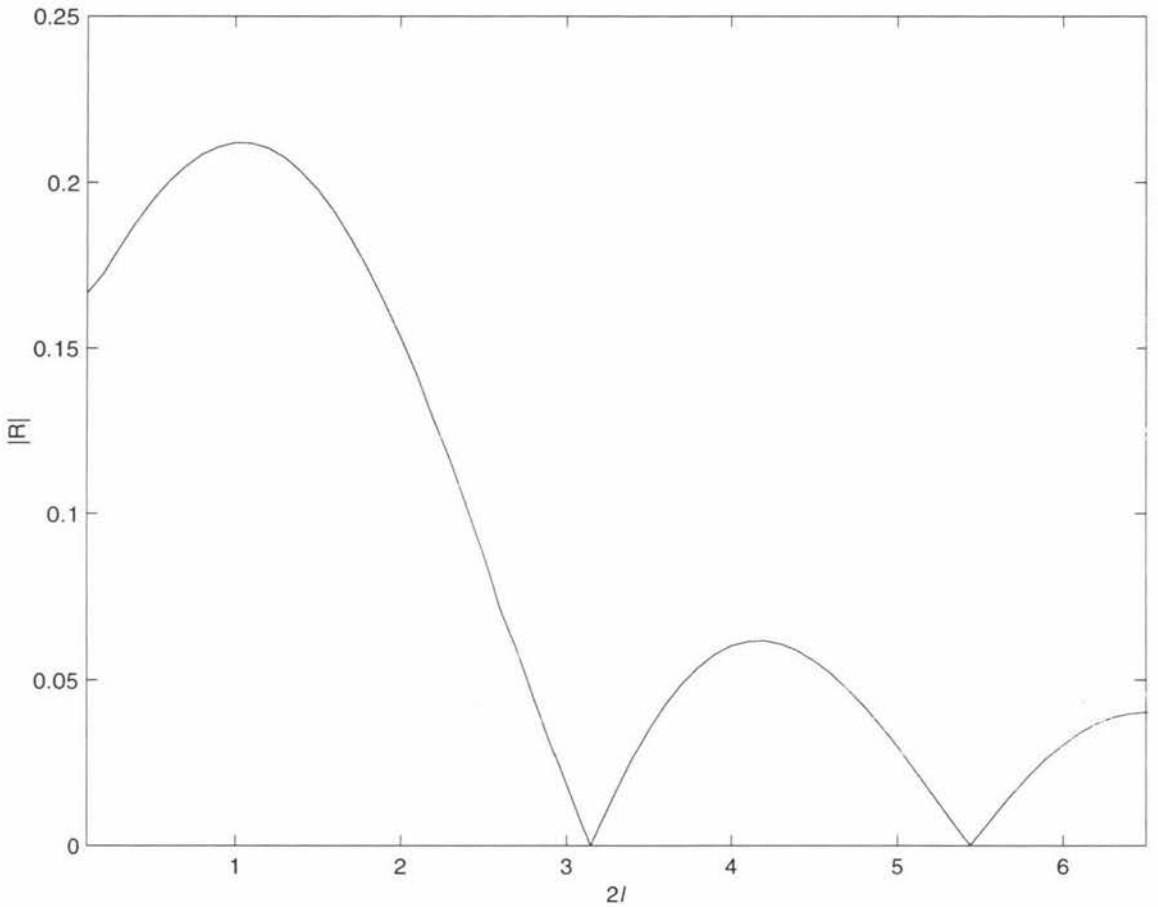

Figure 6.4. The reflection amplitude $|R|$ versus the length of the first Staziker's hump $2l$ with $H_1 = H_2 = 5$ m, $\nu = 1$, $\lambda = 26.1870$ m, 5 evanescent modes, and discretization step size of 0.05 m.

is useful for comparison with a later problem which uses the same hump plus a plate on the water surface. The result is shown in Figure 6.5 as a plot of the reflected amplitude versus the wavelength.

6.2.2 Second Staziker's Hump

The second Staziker's hump is described by the following equation

$$d(x) = H_1 \left(\frac{3}{4} + \frac{1}{4} \cos \left(\pi \left(\frac{x+l}{l} \right) \right) \right), \qquad \forall x \in [-a_1, a_2], \tag{6.2.2}$$

where $H_1 = H_2 = 5$ m. We use 5 evanescent modes and 0.05 m discretization step size. The result is shown in Figure 6.6 as a plot of the reflected amplitude versus the length of the hump.

From Figures 6.4 and 6.6 the reflected amplitude decreases as the hump becomes longer which means that a less steep hump reflects less wave. From Figure 6.5 we see that the hump reflects more when the wave is sufficiently long. There is no perfect resonance point ($|R| = 0$) after $\lambda = 400$ m. The next $|R| = 0$ occurs outside the range of the plot. Therefore the hump is important for a large wavelength.

6.2.3 Simple Sloping Plane

The purpose for this experiment is to help us analyze the later result for problem involving the same sloping plane plus the plate on the water surface. The simple sloping plane is a plane on the seabed which is inclined at a slope of $1/2$. It goes from the depth H_1 to the

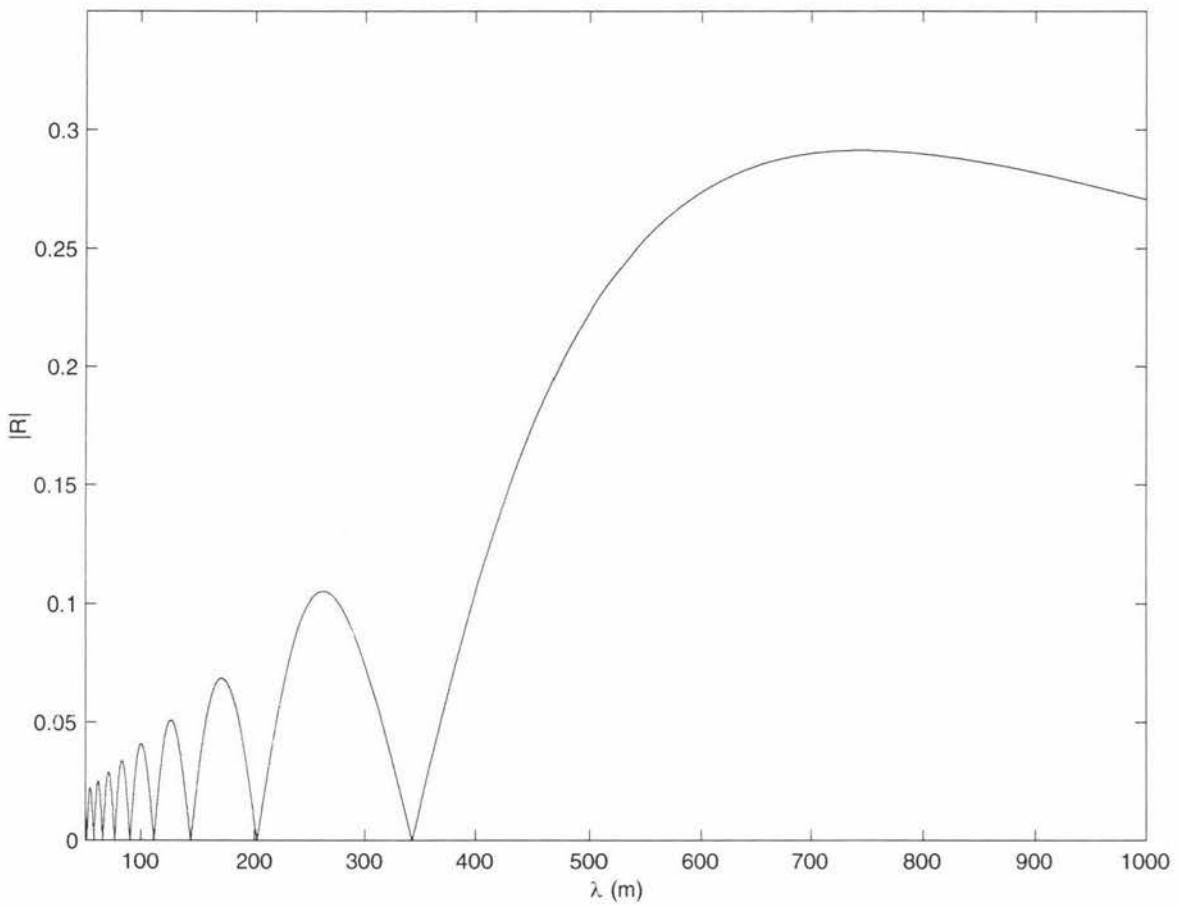

Figure 6.5. The reflection amplitude $|R|$ versus the wavelength λ for the first Staziker's hump with $H_1 = H_2 = 5$ m, $h = 1$ m, $2L = 200$ m, 5 evanescent modes, and discretization step size of 1 m.

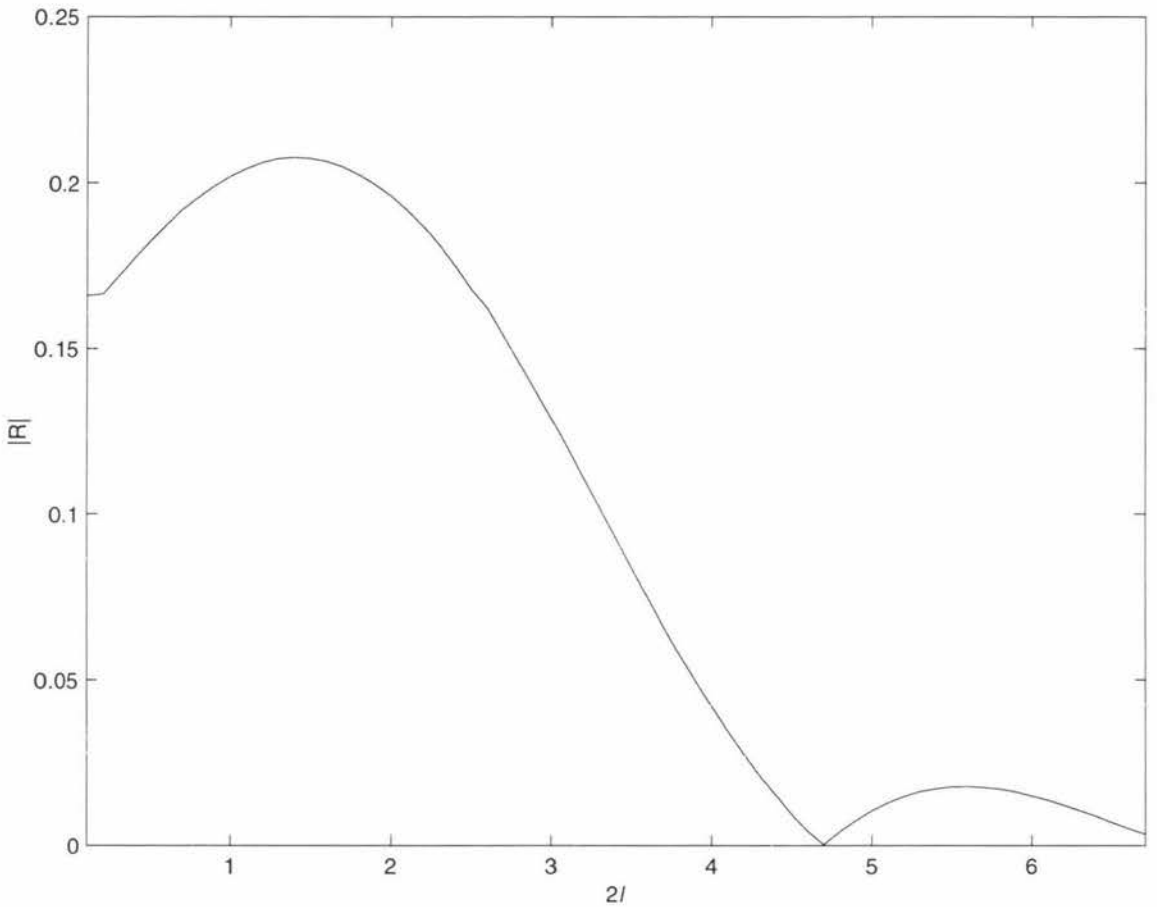

Figure 6.6. The reflection amplitude $|R|$ vs the length of the second Staziker's hump $2l$ with $H_1 = H_2 = 5$ m, $\nu H_1 = 1$, 5 evanescent modes, and discretization step size of 0.05 m.

depth $\frac{1}{2}H_1$. It is defined by the following equation

$$d(x) = H_1\left(\frac{x-a_1}{2(a_2-a_1)} - 1\right), \qquad \forall x \in [a_1, a_2]. \tag{6.2.3}$$

We notice that the plane is sloping upwards from $H_1 = 5$ m to $H_2 = 2.5$ m. The parameters used are: wavelength $\lambda = 100$ m, $l = 101$ m (the length of the sloping plane is 202 m), 5 evanescent modes, and 1 m discretization step size. The result is shown in Figure 6.7 as a plot of the reflection amplitude versus the wavelength.

From Figure 6.7 we notice that the tilted seabed reflects a large proportion of the wave, due to the different depth of the water.

In Figure 6.7 there is no point of perfect resonance ($|R| = 0$). Some points may appear to have reached zero however they are not zero. The lowest magnitude of the reflected amplitude from Figure 6.7 is 4.2564×10^{-5} (accurate to 5 digits) at $\lambda = 61$ m. As the wave becomes longer ($\lambda > 500$ m) the reflected amplitude curves increases.

We believe that the reason why the resonance in Figure 6.7 does not behave as well as Figure 6.3 and Figure 6.5 is because the water domain in this case is *not symmetric*, while previous ones are. We say that water domain is *symmetric* if the domain can be split into half, and the half part on the left-hand side is the mirror reflection of the right-hand side and vice versa.

6.3 Single Ice Sheet on Water of Variable Depth

In this section we present the result of the experiment where both the plate and the varying seabed exist in the problem domain. The plate is a thin sea ice sheet. It is floating on

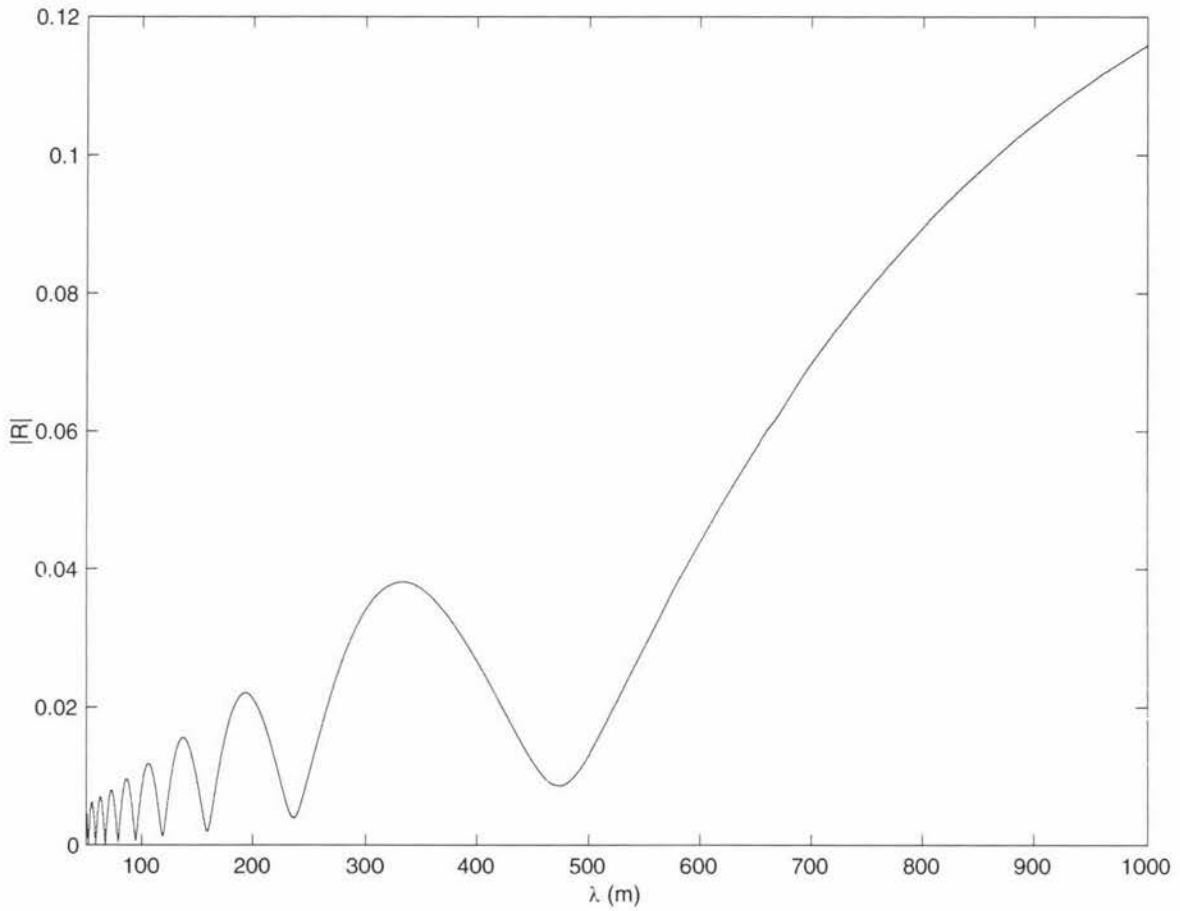

Figure 6.7. The reflection amplitude $|R|$ versus the wavelength λ for the simple sloping plane with $H_1 = 5$ m, $H_2 = 2.5$ m, $l = 101$ m, 5 evanescent modes, and discretization step size of 0.5 m.

the surface of water with depth described by a function $d(x)$. The relevant parameters are: Young's modulus for sea ice $E = 6$ G Pa, sea ice density $\rho' = 922.5\,\text{kg/m}^3$, density of sea water $\rho = 1025.0\,kg/m^3$, Poisson's ratio $\nu = 0.3$, and the bending rigidity $D = \frac{1}{12} E h^3/(1-\nu^2)$, where h is the thickness of the ice sheet. For sea ice $D = 5.4945 \times 10^8$ Pa.m^3. The wavelength is $\lambda = 100$ m.

The first test uses the first Staziker's first hump which is defined by (6.2.1) and the second uses the simple sloping plane defined by (6.2.3). In both tests the parameters are $h = 1$ m, $H_1 = 5$, $2L = 200$ m, 5 evanescent modes, and the dimensionless constants are $\beta \approx 87.5183$ and $\gamma \approx 0.1800$ (β and γ are defined in Chapter 3). For the first test the water depths are $H_2 = H_1 = 5$ m and the discretization step size is 1 m. For the second test the water depths are $H_1 = 5$ m, $H_2 = 2.5$ m, and discretization step size is 0.5 m.

6.3.1 Staziker's Hump

For the first test we use the Staziker's hump which is defined by (6.2.1). The result is shown in Figure 6.8 as a plot of the reflection amplitude versus the wavelength at $H_1 = H_2 = 5$ m and discretization step size 1 m.

From Figure 6.8 we see that the separation of λ-coordinate of points where $|R| = 0$ (perfect resonance) increases with respect to wavelength. The reflection curve increases after passing $\lambda = 342$ m and it starts to decrease after $\lambda \approx 700$ m. From the behaviour of the data we conclude that there will be other points of $|R| = 0$ outside the presented range.

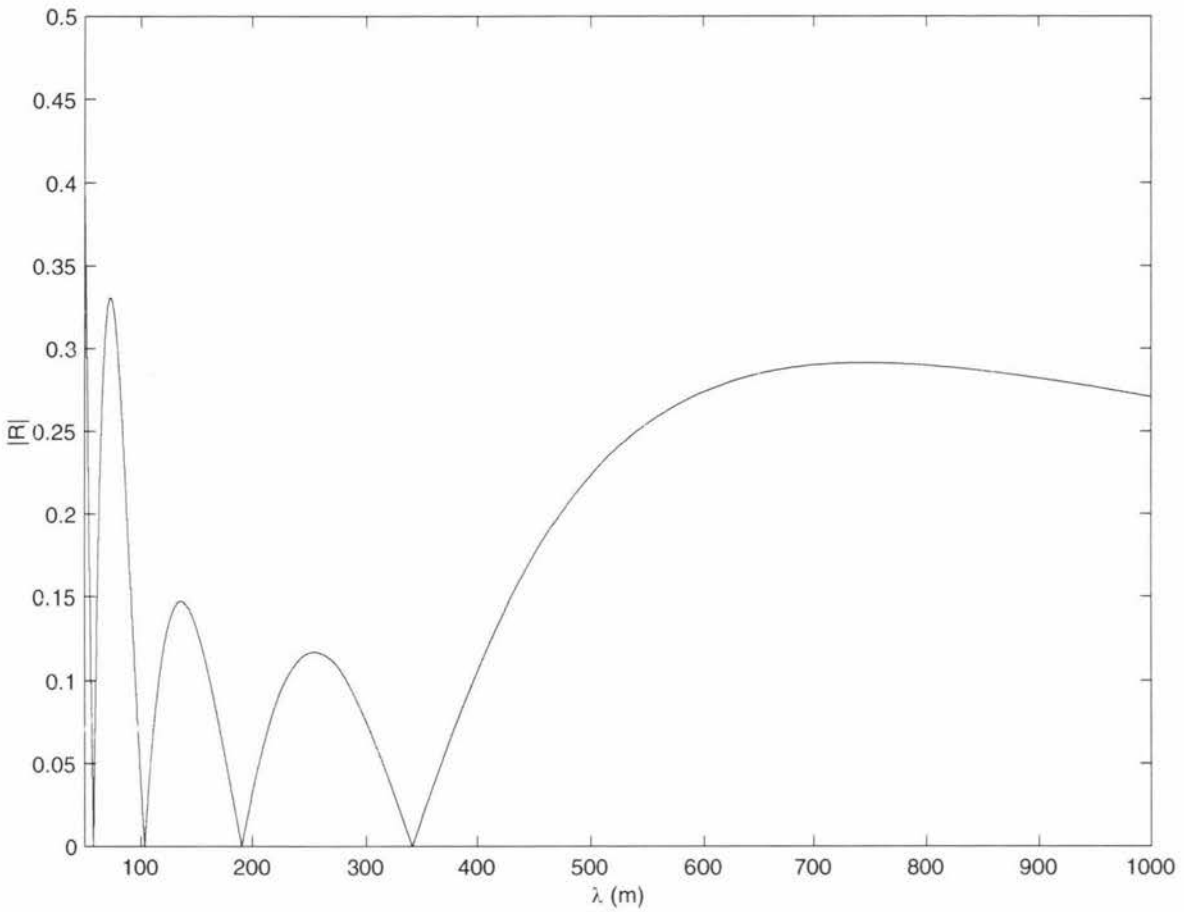

Figure 6.8. The reflection amplitude $|R|$ versus the wavelength λ for an ice sheet floating on water with the first Staziker's hump with $H_1 = H_2 = 5$ m, $h = 1$ m, $2L = 200$ m, $2l = 202$ m, $\lambda = 100$ m, 5 evanescent modes, and discretization step size of 1 m.

The comparison between the results for water domain with the ice sheet only, the first Staziker's hump only, and both the ice sheet and the Staziker's first hump can be seen in Figure 6.9 as a superimposed plot between Figure 6.3, Figure 6.5, and Figure 6.8.

By comparing the reflection amplitude curves in Figure 6.9 we see that for a short wavelength the reflected wave is caused by the ice sheet on the water surface. As the wave becomes longer the reflecting effect by the ice sheet becomes less and the reflecting effect by the varying seabed becomes significant. For wavelength $\lambda > 300$ m the reflection amplitude curves produced by the hump only and by both the hump and the ice sheet coincide. Therefore for a sufficiently long wave the ice sheet has very little or no effect at all on the reflected wave compared to the hump. We also notice that for $\lambda > 300$ m the reflection amplitude for the system with both the hump and the ice sheet may be deduced from the result for the hump only case.

6.3.2 Simple Sloping Plane

For the second test we use the simple sloping plane which is defined by (6.2.3). The result is presented in Figure 6.10 as a plot of the reflection amplitude versus the wavelength at $H_1 = 5$ m, $H_2 = 2.5$ m, and discretization step size of 0.5 m.

Figure 6.10 shows that there is no point of perfect resonance ($|R| = 0$) because the domain is not symmetric. After passing $\lambda = 470$ m the reflection amplitude curve increases in an unbounded manner (it never goes down again like in the case of Staziker's hump in Figure 6.8). This is because for large wavelength the reflection is mainly due to the varying seabed, therefore it behaves like Figure 6.7.

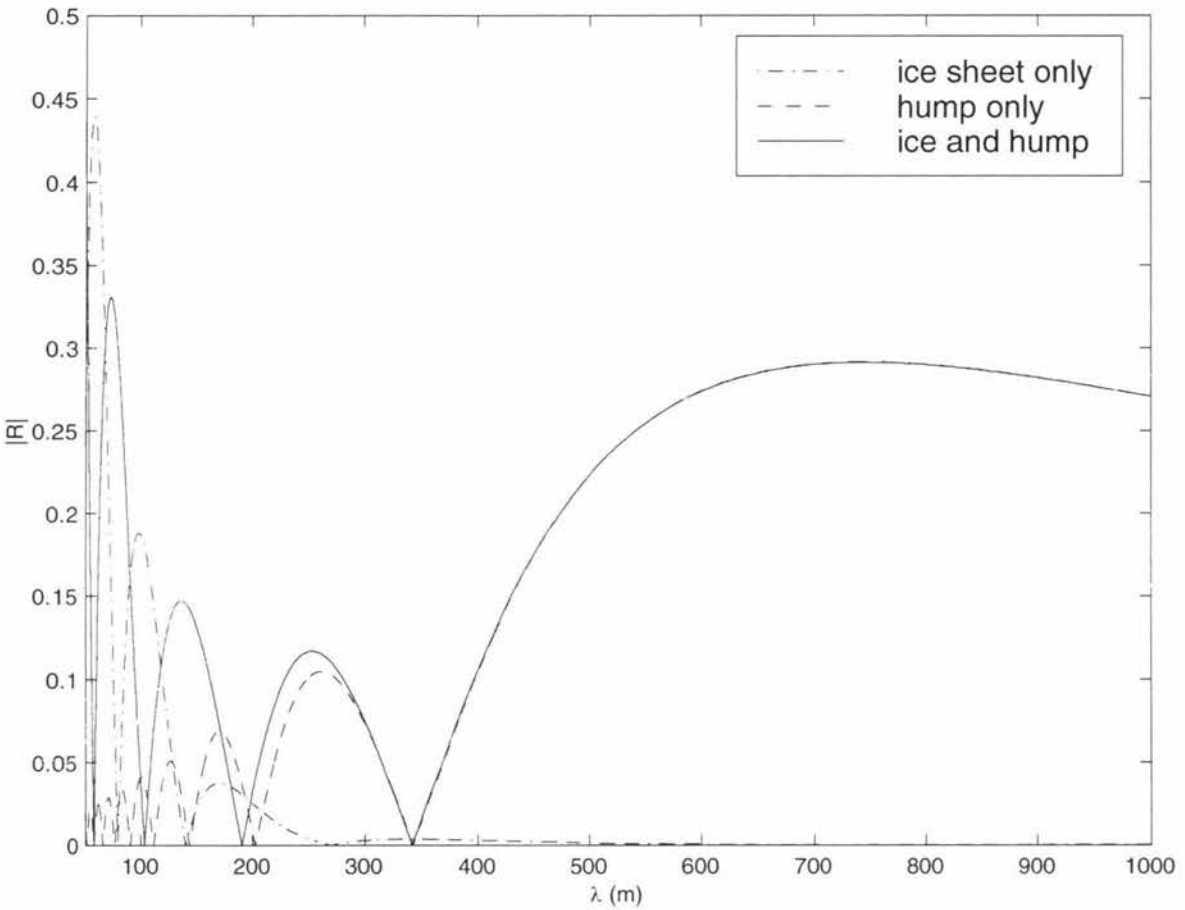

Figure 6.9. The superimposed plot of the reflection amplitude versus the wave length for water domain with the ice sheet only, the first Staziker's hump only, and both the ice sheet and the hump with $H_1 = H_2 = 5$ m, $h = 1$ m, $2L = 200$ m, $2l = 202$ m, 5 evanescent modes, and discretization step size of 1 m.

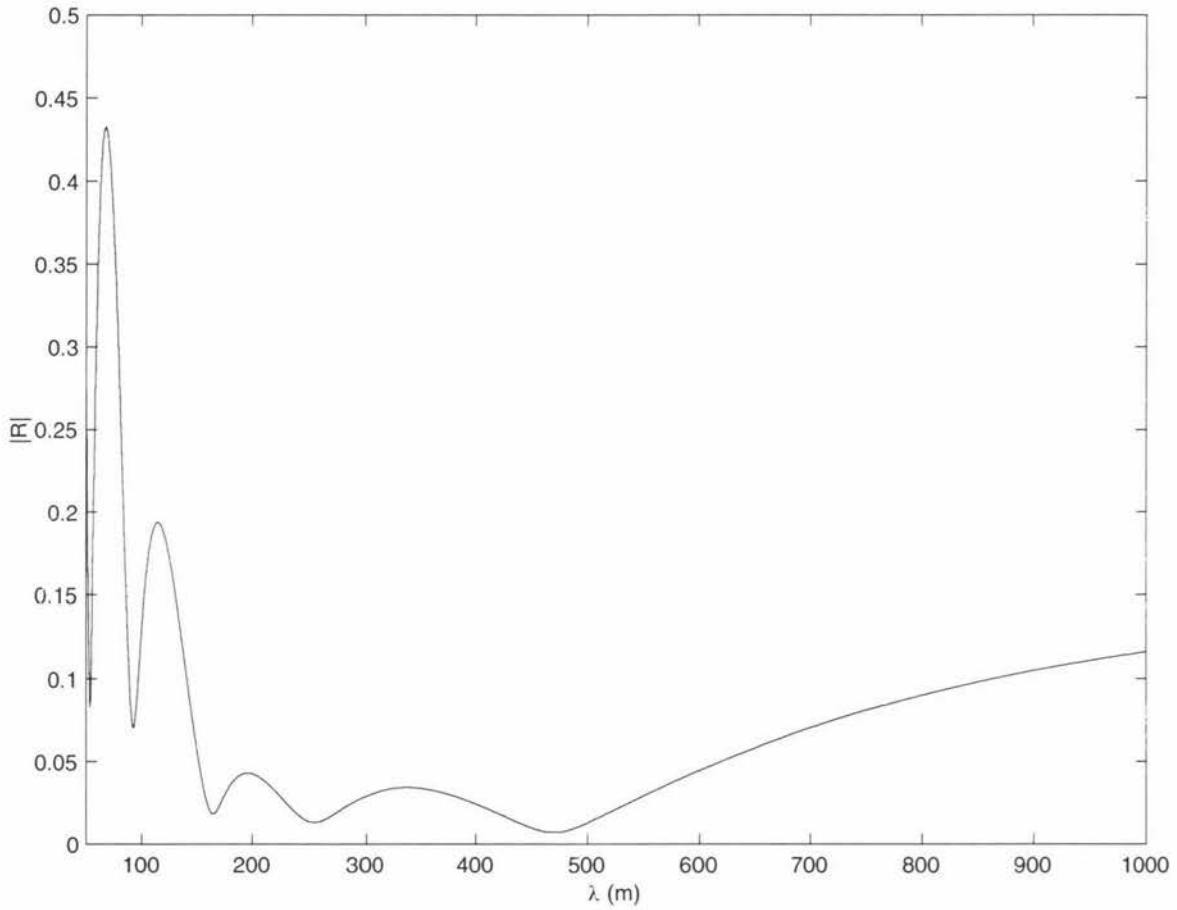

Figure 6.10. The reflection amplitude $|R|$ versus the wavelength λ for an ice sheet floating on water with the simple sloping plane with $H_1 = 5$ m, $H_2 = 2.5$ m, $h = 1$ m, $2L = 200$ m, $2l = 202$ m, $\lambda = 100$ m, 5 evanescent modes, and discretization step size of 1 m.

The comparison between the results for water domain with the ice sheet only, the sloping plane only, and both the ice sheet and the sloping plane can be seen in Figure 6.11 as a superimposed plot between Figure 6.3, Figure 6.7, and Figure 6.10.

The same analysis as previous section applies for Figure 6.11. For $\lambda > 250$ m the reflection amplitudes for both the ice sheet and the sloping plane may be deduced from the result for the sloping plane only case.

6.4 A Floating Runway on Water of Variable Depth

In this section we present the result for the floating runway plus the varying seabed. The parameters for the floating runway were taken from *Namba and Ohkusu* [6].The bending rigidity parameter D is defined by $D/\rho g\,(2L)^2 = 2.404 \times 10^{-4}$ (this is dimensionless). Since D contains all the information needed for the floating runway, we omit the parameters E, ν, and ρ'. The water density is $\rho = 1025.0$ kg/m^3, the water depth is $H = 5$ m. The length of plate is $2L = 200$ m and the length of the varying seabed is $2l = 202$ m. For a floating runway on sea water, the bending rigidity is approximately $D \approx 2.4148 \times 10^8$ Pa.m^3 and the dimensionless constant $\beta \approx 38.4640$. Following Namba and Ohkusu the dimensionless constant γ is relatively small therefore we will neglect γ.

The experiment is done using the first Staziker's hump in Section 6.2.1 and the simple sloping plane in Section 6.2.3. The result is presented as a plot of the reflection coefficient versus the wavelength.

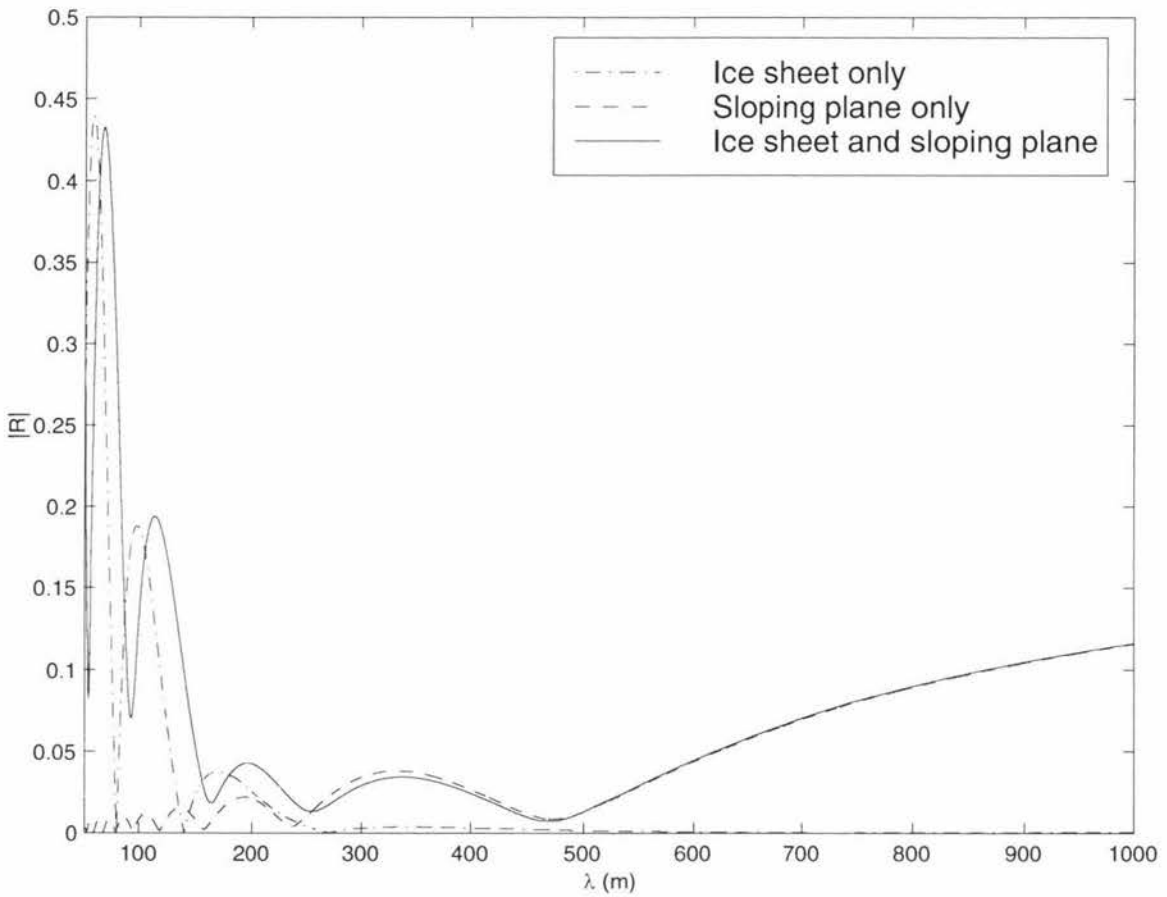

Figure 6.11. The superimposed plot of the reflection amplitude versus the wavelength for water domain with the ice sheet only, the simple sloping plane only, and both the ice sheet and the sloping plane with $H_1 = 5$ m, $H_2 = 2.5$ m, $h = 1$ m, $2L = 200$ m, $2l = 202$ m, 5 evanescent modes, and discretization step size of 0.5 m.

6.4.1 Staziker's Hump

For the first test we use the first Staziker's hump which is described by (6.2.1). There are 5 evanescent modes and the discretization step size is 1 m. The result is shown in Figure 6.12 as a plot of the reflection amplitude versus the length of the wavelength at discretization step size 1 m.

Figure 6.13 is a superimposed plot comparing the reflection amplitude for the case of the ice sheet and the runway.

6.4.2 Simple Sloping Plane

For the second test we use the simple sloping plane which is described by (6.2.3). There are 5 evanescent modes and the discretization step size is 0.5 m. The result is shown in Figure 6.14 as a plot of the reflection amplitude versus the wavelength.

Figure 6.15 is a superimposed plot of the reflection coefficient produced by the ice plate and the runway plate.

The runway has smaller bending rigidity constant (D) than the ice sheet by a factor of 2. Therefore from Figure 6.13 and Figure 6.15 we see that the runway reflects relatively less than the ice sheet. However for large wavelength ($\lambda > 300$ m) the elasticity of the plate does not have any effect to the solution curve (the curve produced by the ice sheet coincides with one by the runway) because the wave only 'notices' the varying seabed and not the plate.

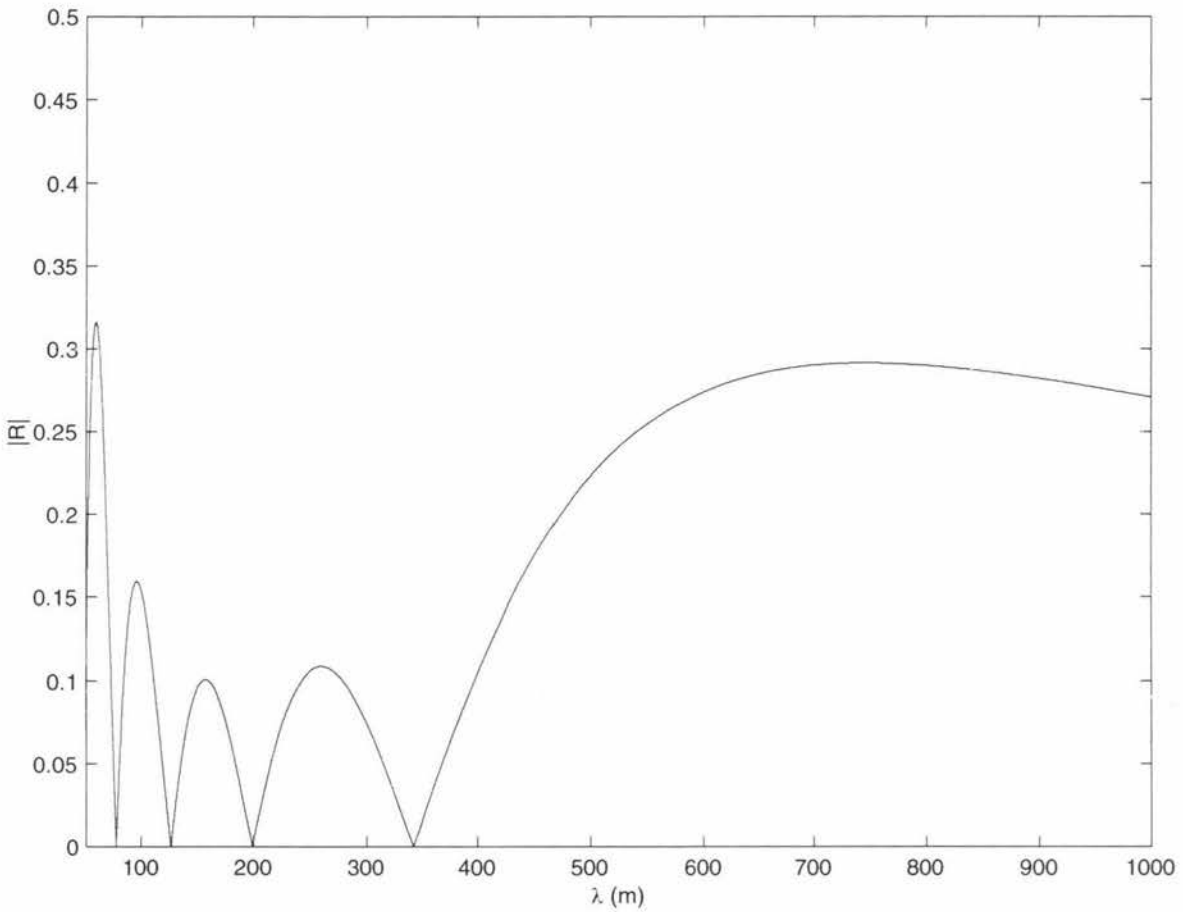

Figure 6.12. The reflection amplitude $|R|$ versus the wavelength λ for a floating runway on water with the first Staziker's hump with $H_1 = H_2 = 5$ m, $2L = 200$ m, $2l = 202$ m, $D/4\rho g L^2 = 2.404 \times 10^{-14}$, 5 evanescent modes, and discretization step size of 1 m.

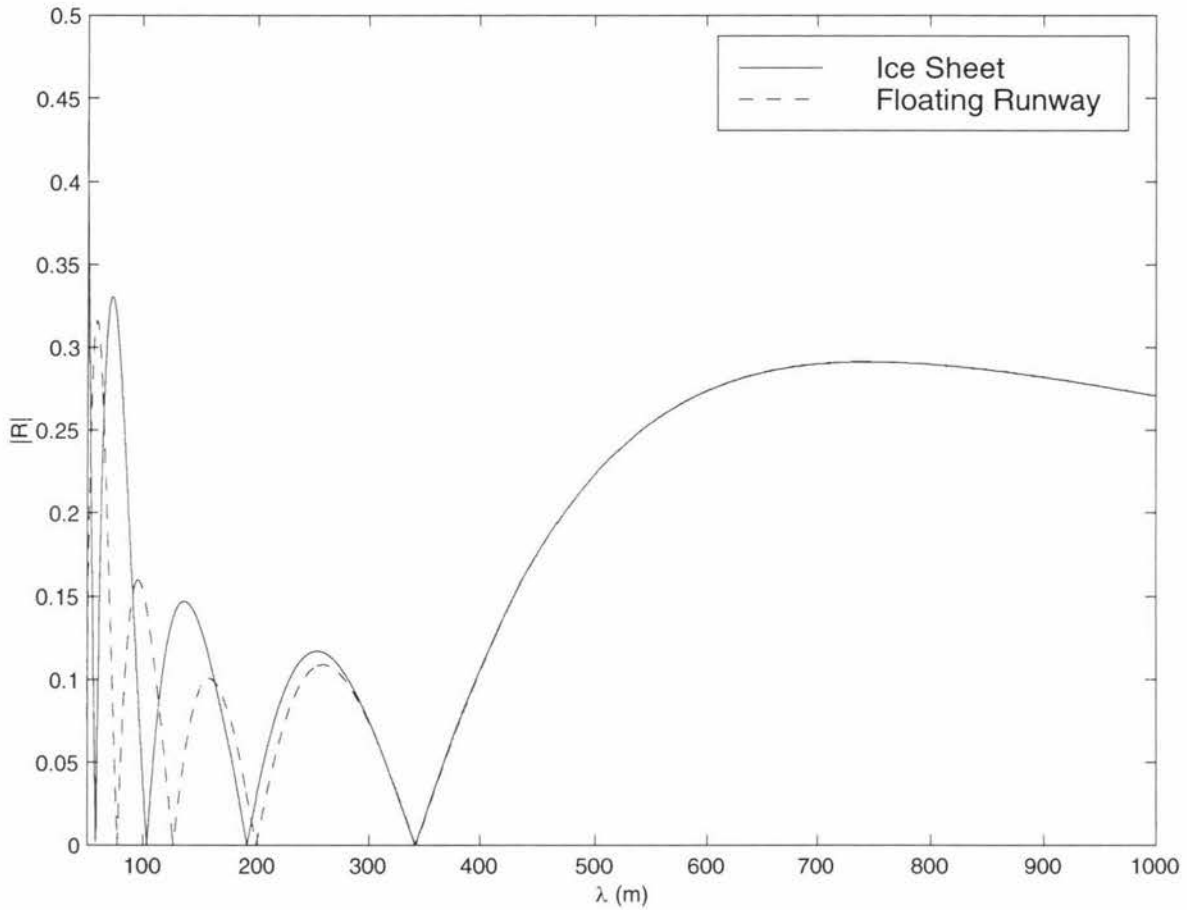

Figure 6.13. The superimposed plot of the reflection amplitude versus the wavelength for the ice sheet and the floating runway on water with the first Staziker's hump.

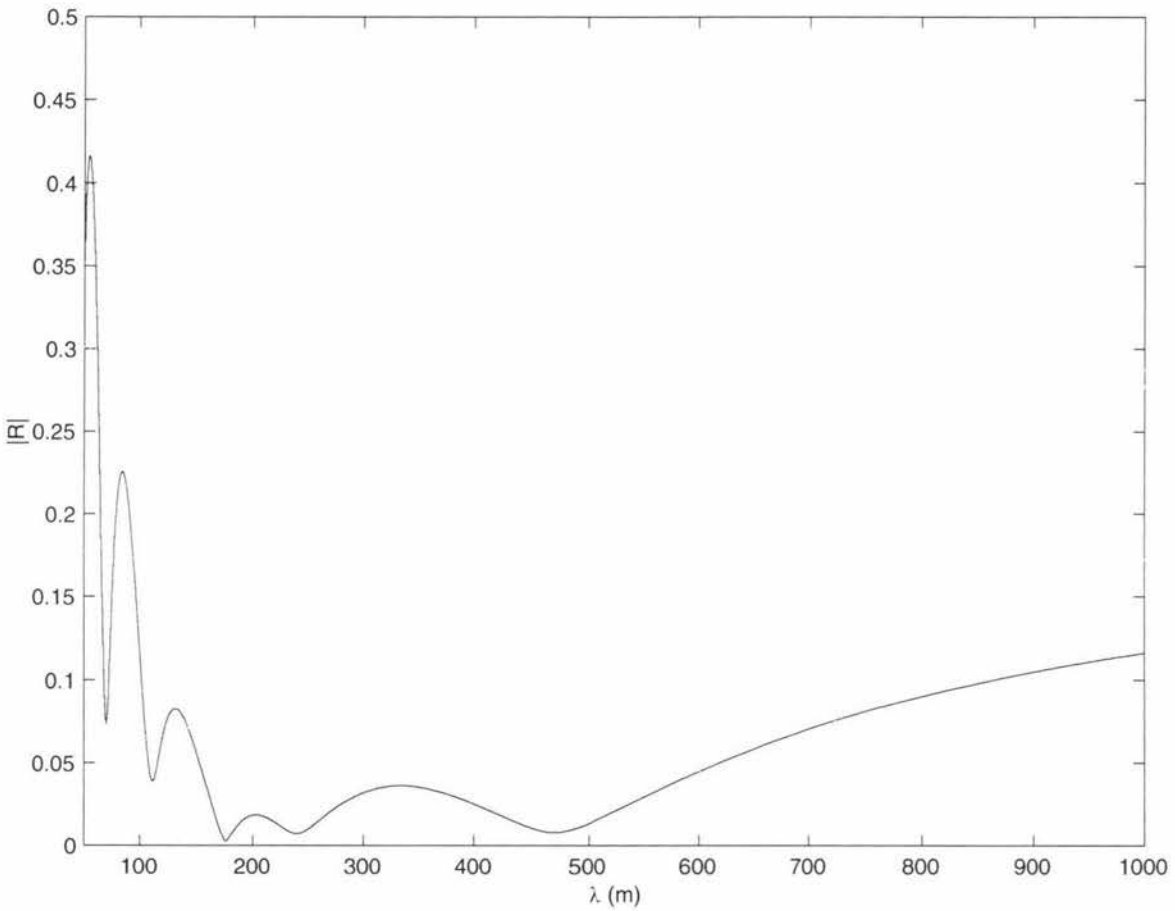

Figure 6.14. The reflection amplitude $|R|$ versus the wavelength λ for a floating runway on water with the simple sloping plane with $H_1 = 5$ m, $H_2 = 2.5$ m, $2L = 200$ m, $2l = 201$ m, $D/4\rho g L^4 = 2.404 \times 10^{-14}$, 5 evanescent modes, discretization step size of 0.5 m.

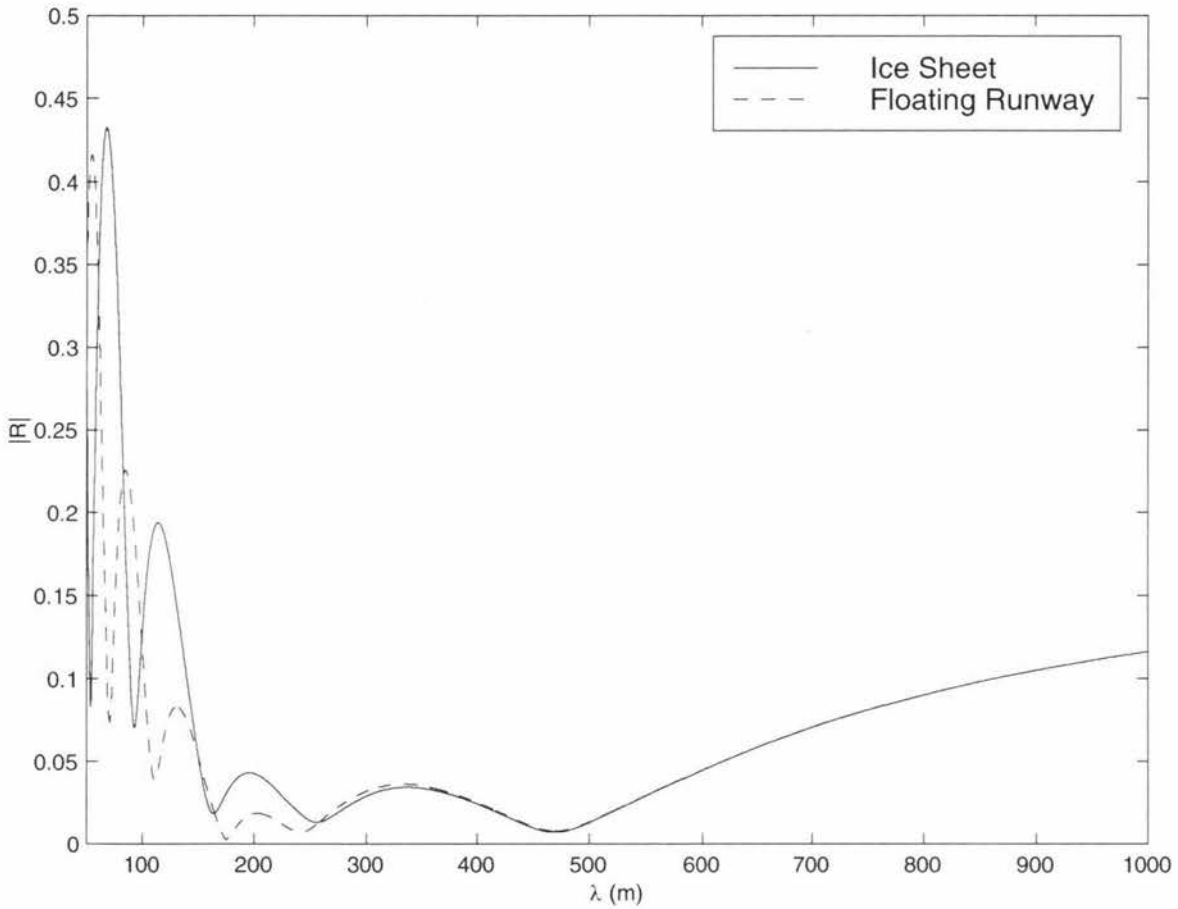

Figure 6.15. The superimposed plot of the reflection amplitude versus the wavelength for the ice sheet and the floating runway on water with the simple sloping plane.

Chapter 7
Summary and Conclusion

We recall that our aim for this thesis was to model the motion of the wave with an elastic floating body and varying seabed by calculating the scattered wave.

In the first chapter we introduced the problem of wave scattering by a thin plate on water with a varying seabed on the bottom. Then this is reduced to a single frequency problem. From the single frequency model we obtained the incident wave and the transient wave. We solved the incident wave and imposed that it only had one direction.

The focus of the second chapter was to solve the wave scattering problem for finite and semi-infinite domains. In the first half of this chapter the water domain was divided into finite and semi-infinite regions by a pair of artificial (vertical) boundaries. In the semi infinite domains the solution was obtained by separation of variables. This gave rise to the coupling operator which defined the boundary condition on the artificial (vertical) boundaries. In the second half of this chapter we solved the problem in the finite domain using the boundary element method (BEM). The BEM transformed the Laplace's equation and the boundary conditions into equivalent integral equations involving the free-space Green's function and the Green's function for the plate.

In the third chapter the integral equation from the second chapter was solved numerically. This was done by dividing the boundary encircling the finite domain into six segments. Then we solved the integral equation for each individual segment. This gave us

a linear equation involving matrices of exact integration of the free-space Green's function and the normal derivative, and the vectors of the wave potential and the constants.

The fourth chapter provided a method to interpret the solution from the preceeding three chapters. In this chapter we defined two forms of the scattered wave, one was the reflected wave and the other was the transmitted one. From the two quantities we derived the energy flux equation and Stoker's time-reversal model, both of which were useful for checking the numerical solution.

The numerical solution was presented in the last chapter. At the beginning of this chapter we tested our numerical method by comparing it with the known results from *Meylan* [5] and *Staziker, Porter, and Stirling* [7]. Both publications have simpler problem domain than ours (Meylan solved for the thin plate only and Staziker, Porter, and Stirling solved for the varying seabed only). We saw that our numerical solutions were in perfect agreement with those known results. Then we presented the solution for the wave scattering problem with the thin plate as well as the varying seabed. The accuracy of these solutions depend on many factors such as the number of evanescent modes of the wave and the discretization step size.

In conclusion we have solved a problem which has never been solved by anyone before; that is the scattering of wave by both an elastic floating plate and a varying seabed. So far no one has ever considered the problem of wave scattering by two scatterers (the plate and the varying seabed) and hence the presented solution method is one original work. We also have shown that this method is reliable and robust for any plate and any arbitrary

seabed shape. This can be seen from the comparison with the known result. Therefore this method is capable of solving real-life problems.

Appendix A
Green's Function for A Floating Thin Plate

For a Green's function to be the solution of (3.4.9) it must satisfy

$$\frac{\partial^4 G_{plate}}{\partial x^4} - \alpha^4 G_{plate} = \frac{\nu}{\beta}\,\delta\left(x-\xi\right).$$

By the definition of the delta function $\dfrac{\partial^4}{\partial x^4} G_{plate}\left(x,\xi\right) - \alpha^4 G_{plate}\left(x,\xi\right) = 0$ except at $x = \xi$. Hence we seek a solution

$$G_{plate}\left(x,\xi\right) = \begin{cases} A_1 e^{i\alpha x} + B_1 e^{-i\alpha x} + C_1 e^{\alpha x} + D_1 e^{-\alpha x}, & x < \xi, \\ A_2 e^{i\alpha x} + B_2 e^{-i\alpha x} + C_2 e^{\alpha x} + D_2 e^{-\alpha x}, & x > \xi. \end{cases} \tag{A.1}$$

We impose the condition that (A.1), its first, and its second derivative must be continuous at $x = \xi$. This gives us

$$e^{i\alpha\xi}\left(A_1 - A_2\right) + e^{-i\alpha\xi}\left(B_1 - B_2\right) + e^{\alpha\xi}\left(C_1 - C_2\right) + e^{-\alpha\xi}\left(D_1 - D_2\right) = 0, \tag{A.2}$$

$$i\alpha\, e^{i\alpha\xi}\left(A_1 - A_2\right) - i\alpha\, e^{-i\alpha\xi}\left(B_1 - B_2\right) + \alpha\, e^{\alpha\xi}\left(C_1 - C_2\right) - \alpha\, e^{-\alpha\xi}\left(D_1 - D_2\right) = 0, \tag{A.3}$$

$$-\alpha^2 e^{i\alpha\xi}\left(A_1 - A_2\right) - \alpha^2 e^{-i\alpha\xi}\left(B_1 - B_2\right) + \alpha^2 e^{\alpha\xi}\left(C_1 - C_2\right) + \alpha^2 e^{-\alpha\xi}\left(D_1 - D_2\right) = 0. \tag{A.4}$$

We must also have

$$\int_{x=\xi^-}^{x=\xi^+} \left(\frac{\partial^4 G_{plate}}{\partial x^4} - \alpha^4 G_{plate}\right) dx = \frac{\nu}{\beta}. \tag{A.5}$$

Since the function G_{plate} is continuous at $x = \xi$ then $\alpha^4 \int_{x=\xi^-}^{x=\xi^+} G_{plate} = 0$. This reduces (A.5) to

$$\int_{x=\xi^-}^{x=\xi^+} \frac{\partial^4 G_{plate}}{\partial x^4}\, dx = \frac{\nu}{\beta}. \tag{A.6}$$

Substituting (A.1) into (A.6) and solving gives us

$$i\alpha^3\, e^{i\alpha\xi}\,(A_1 - A_2) - i\alpha^3 e^{-i\alpha\xi}\,(B_1 - B_2) - \alpha^3\, e^{\alpha\xi}\,(C_1 - C_2) + \alpha^3\, e^{-\alpha\xi}\,(D_1 - D_2) = \frac{\nu}{\beta}. \tag{A.7}$$

Equations (A.2), (A.3), (A.4), and (A.7) provide a set of relationships between the unknown constants, which can be represented as a set of linear equation, which is

$$\begin{bmatrix} 1 & 1 & 1 & 1 \\ i\alpha & -i\alpha & \alpha & -\alpha \\ -\alpha^2 & -\alpha^2 & \alpha^2 & \alpha^2 \\ i\alpha^3 & -i\alpha^3 & -\alpha^3 & \alpha^3 \end{bmatrix} \begin{bmatrix} (A_1 - A_2)\, e^{i\alpha\xi} \\ (B_1 - B_2)\, e^{-i\alpha\xi} \\ (C_1 - C_2)\, e^{\alpha\xi} \\ (D_1 - D_2)\, e^{-\alpha\xi} \end{bmatrix} = \begin{bmatrix} 0 \\ 0 \\ 0 \\ \frac{\nu}{\beta} \end{bmatrix}. \tag{A.8}$$

If we let

$$\mathbb{A} = \begin{bmatrix} 1 & 1 & 1 & 1 \\ i\alpha & -i\alpha & \alpha & -\alpha \\ -\alpha^2 & -\alpha^2 & \alpha^2 & \alpha^2 \\ i\alpha^3 & -i\alpha^3 & -\alpha^3 & \alpha^3 \end{bmatrix},$$

then the inverse of $\mathbb{A}$ is,

$$\mathbb{A}^{-1} = \begin{bmatrix} \frac{1}{4} & -\frac{1}{4}\frac{i}{\alpha} & -\frac{1}{4}\frac{1}{\alpha^2} & -\frac{1}{4}\frac{i}{\alpha^3} \\ \frac{1}{4} & \frac{1}{4}\frac{i}{\alpha} & -\frac{1}{4}\frac{1}{\alpha^2} & \frac{1}{4}\frac{i}{\alpha^3} \\ \frac{1}{4} & \frac{1}{4}\frac{i}{\alpha} & \frac{1}{4}\frac{1}{\alpha^2} & -\frac{1}{4}\frac{i}{\alpha^3} \\ \frac{1}{4} & -\frac{1}{4}\frac{i}{\alpha} & \frac{1}{4}\frac{1}{\alpha^2} & \frac{1}{4}\frac{i}{\alpha^3} \end{bmatrix}.$$

By applying $\mathbb{A}^{-1}$ to the right-hand side of (A.8) we obtain

$$\begin{bmatrix} (A_1 - A_2)\, e^{i\alpha\xi} \\ (B_1 - B_2)\, e^{-i\alpha\xi} \\ (C_1 - C_2)\, e^{\alpha\xi} \\ (D_1 - D_2)\, e^{-\alpha\xi} \end{bmatrix} = \begin{bmatrix} -\frac{1}{4}\frac{i\nu}{\alpha^3\beta} \\ \frac{1}{4}\frac{i\nu}{\alpha^3\beta} \\ -\frac{1}{4}\frac{\nu}{\alpha^3\beta} \\ \frac{1}{4}\frac{\nu}{\alpha^3\beta} \end{bmatrix}. \tag{A.9}$$

where constants with index 2 are related to ones with index 1 by equations

$$\left.\begin{aligned} A_2 &= A_1 + \frac{1}{4}\frac{i\nu}{\alpha^3\beta}\, e^{-i\alpha\xi}, \\ B_2 &= B_1 - \frac{1}{4}\frac{i\nu}{\alpha^3\beta}\, e^{i\alpha\xi}, \\ C_2 &= C_1 + \frac{1}{4}\frac{\nu}{\alpha^3\beta}\, e^{-\alpha\xi}, \\ D_2 &= D_1 - \frac{1}{4}\frac{\nu}{\alpha^3\beta}\, e^{\alpha\xi}. \end{aligned}\right\} \tag{A.10}$$

Next we substitute (A.10) into (A.1) to obtain

$$G_{plate}(x,\xi) = \begin{cases} A_1 e^{i\alpha x} + B_1 e^{-i\alpha x} + C_1 e^{\alpha x} + D_1 e^{-\alpha x}, & x \le \xi, \\ \left(A_1 + \frac{1}{4}\frac{i\nu}{\alpha^3\beta}\, e^{-i\alpha\xi}\right) e^{i\alpha x} + \left(B_1 - \frac{1}{4}\frac{i\nu}{\alpha^3\beta}\, e^{i\alpha\xi}\right) e^{-i\alpha x} & \\ + \left(C_1 + \frac{1}{4}\frac{\nu}{\alpha^3\beta}\, e^{-\alpha\xi}\right) e^{\alpha x} + \left(D_1 - \frac{1}{4}\frac{\nu}{\alpha^3\beta}\, e^{\alpha\xi}\right) e^{-\alpha x}, & x > \xi. \end{cases} \tag{A.11}$$

Equation (A.11) must satisfy the boundary conditions of system (3.4.9) which are

$$\left.\frac{\partial^2}{\partial x^2} G_{plate}(x,\xi)\right|_{x=-L} = \left.\frac{\partial^2}{\partial x^2} G_{plate}(x,\xi)\right|_{x=L} = \left.\frac{\partial^3}{\partial x^3} G_{plate}(x,\xi)\right|_{x=-L} = \left.\frac{\partial^3}{\partial x^3} G_{plate}(x,\xi)\right|_{x=L} = \tag{A.12}$$

By substituting (A.11) into (A.12) we obtain

$$-A_1\alpha^2 e^{-i\alpha L} - B_1\alpha^2 e^{i\alpha L} + C_1\alpha^2 e^{-\alpha L} + D_1\alpha^2 e^{\alpha L} = 0,$$

$$-iA_1\alpha^3 e^{-i\alpha L} + iB_1\alpha^3 e^{i\alpha L} + C_1\alpha^3 e^{-\alpha L} - D_1\alpha^3 e^{\alpha L} = 0,$$

$$\begin{aligned} & -A_1\alpha^2 e^{i\alpha L} - B_1\alpha^2 e^{-i\alpha L} + C_1\alpha^2 e^{\alpha L} + D_1\alpha^2 e^{-\alpha L} \\ = \; & \frac{1}{4}\frac{i\nu}{\alpha^3\beta}\,\alpha^2 e^{i\alpha(L-\xi)} - \frac{1}{4}\frac{i\nu}{\alpha^3\beta}\,\alpha^2 e^{-i\alpha(L-\xi)} - \frac{1}{4}\frac{\nu}{\alpha^3\beta}\,\alpha^2 e^{\alpha(L-\xi)} + \frac{1}{4}\frac{\nu}{\alpha^3\beta}\,\alpha^2 e^{-\alpha(L-\xi)}, \end{aligned}$$

$$\begin{aligned} & -iA_1\alpha^3 e^{i\alpha L} + iB_1\alpha^3 e^{-i\alpha L} + C_1\alpha^3 e^{\alpha L} - D_1\alpha^3 e^{-\alpha L} \\ = \; & -\frac{1}{4}\frac{\nu}{\alpha^3\beta}\,\alpha^3 e^{i\alpha(L-\xi)} + \frac{1}{4}\frac{\nu}{\alpha^3\beta}\,\alpha^3 e^{-i\alpha(L-\xi)}\alpha^3 e^{-i\alpha L} - \frac{1}{4}\frac{\nu}{\alpha^3\beta}\,\alpha^3 e^{\alpha(L-\xi)} - \frac{1}{4}\frac{\nu}{\alpha^3\beta}\,\alpha^3 e^{-\alpha(L-\xi)}. \end{aligned}$$

Then we can write these equations as a linear equation

$$\begin{bmatrix} -\alpha^2 e^{-i\alpha L} & -\alpha^2 e^{i\alpha L} & \alpha^2 e^{-\alpha L} & \alpha^2 e^{\alpha L} \\ -i\alpha^3 e^{-i\alpha L} & i\alpha^3 e^{i\alpha L} & \alpha^3 e^{-\alpha L} & -\alpha^3 e^{\alpha L} \\ -\alpha^2 e^{i\alpha L} & -\alpha^2 e^{-i\alpha L} & \alpha^2 e^{\alpha L} & \alpha^2 e^{-\alpha L} \\ -i\alpha^3 e^{i\alpha L} & i\alpha^3 e^{-i\alpha L} & \alpha^3 e^{\alpha L} & -\alpha^3 e^{-\alpha L} \end{bmatrix} \begin{bmatrix} A_1 \\ B_1 \\ C_1 \\ D_1 \end{bmatrix}$$

$$= -\frac{\nu}{4\alpha^3\beta} \begin{bmatrix} 0 \\ 0 \\ -i\,\alpha^2 e^{i\alpha(L-\xi)} + i\,\alpha^2 e^{-i\alpha(L-\xi)} + \alpha^2 e^{\alpha(L-\xi)} - \alpha^2 e^{-\alpha(L-\xi)} \\ \alpha^3 e^{i\alpha(L-\xi)} - \alpha^3 e^{-i\alpha(L-\xi)} \alpha^3 e^{-i\alpha L} + \alpha^3 e^{\alpha(L-\xi)} + \alpha^3 e^{-\alpha(L-\xi)} \end{bmatrix}. \tag{A.13}$$

Let matrix $\mathbb{M}$ be the inverse of the matrix on the left-hand side of (A.13)

$$\mathbb{M} = \begin{bmatrix} -\alpha^2 e^{-i\alpha L} & -\alpha^2 e^{i\alpha L} & \alpha^2 e^{-\alpha L} & \alpha^2 e^{\alpha L} \\ -i\alpha^3 e^{-i\alpha L} & i\alpha^3 e^{i\alpha L} & \alpha^3 e^{-\alpha L} & -\alpha^3 e^{\alpha L} \\ -\alpha^2 e^{i\alpha L} & -\alpha^2 e^{-i\alpha L} & \alpha^2 e^{\alpha L} & \alpha^2 e^{-\alpha L} \\ -i\alpha^3 e^{i\alpha L} & i\alpha^3 e^{-i\alpha L} & \alpha^3 e^{\alpha L} & -\alpha^3 e^{-\alpha L} \end{bmatrix}^{-1}.$$

By applying $\mathbb{M}$ to the right-hand side of (A.13) gives us an explicit equations for A_1, B_1, C_1, and D which are

$$A_1 = -\frac{\nu}{4\alpha^3\beta} \begin{bmatrix} m_{13}\left(-i\,\alpha^2 e^{i\alpha(L-\xi)} + i\,\alpha^2 e^{-i\alpha(L-\xi)} + \alpha^2 e^{\alpha(L-\xi)} - \alpha^2 e^{-\alpha(L-\xi)}\right) \\ \ldots + m_{14}\left(\alpha^3 e^{i\alpha(L-\xi)} - \alpha^3 e^{-i\alpha(L-\xi)} \alpha^3 e^{-i\alpha L} + \alpha^3 e^{\alpha(L-\xi)} + \alpha^3 e^{-\alpha(L-\xi)}\right) \end{bmatrix},$$

$$B_1 = -\frac{\nu}{4\alpha^3\beta} \begin{bmatrix} m_{23}\left(-i\,\alpha^2 e^{i\alpha(L-\xi)} + i\,\alpha^2 e^{-i\alpha(L-\xi)} + \alpha^2 e^{\alpha(L-\xi)} - \alpha^2 e^{-\alpha(L-\xi)}\right) \\ \ldots + m_{24}\left(\alpha^3 e^{i\alpha(L-\xi)} - \alpha^3 e^{-i\alpha(L-\xi)} \alpha^3 e^{-i\alpha L} + \alpha^3 e^{\alpha(L-\xi)} + \alpha^3 e^{-\alpha(L-\xi)}\right) \end{bmatrix},$$

$$C_1 = -\frac{\nu}{4\alpha^3\beta} \begin{bmatrix} m_{33}\left(-i\,\alpha^2 e^{i\alpha(L-\xi)} + i\,\alpha^2 e^{-i\alpha(L-\xi)} + \alpha^2 e^{\alpha(L-\xi)} - \alpha^2 e^{-\alpha(L-\xi)}\right) \\ \ldots + m_{34}\left(\alpha^3 e^{i\alpha(L-\xi)} - \alpha^3 e^{-i\alpha(L-\xi)} \alpha^3 e^{-i\alpha L} + \alpha^3 e^{\alpha(L-\xi)} + \alpha^3 e^{-\alpha(L-\xi)}\right) \end{bmatrix},$$

$$D_1 = -\frac{\nu}{4\alpha^3\beta} \begin{bmatrix} m_{43}\left(-i\,\alpha^2 e^{i\alpha(L-\xi)} + i\,\alpha^2 e^{-i\alpha(L-\xi)} + \alpha^2 e^{\alpha(L-\xi)} - \alpha^2 e^{-\alpha(L-\xi)}\right) \\ \ldots + m_{44}\left(\alpha^3 e^{i\alpha(L-\xi)} - \alpha^3 e^{-i\alpha(L-\xi)} \alpha^3 e^{-i\alpha L} + \alpha^3 e^{\alpha(L-\xi)} + \alpha^3 e^{-\alpha(L-\xi)}\right) \end{bmatrix},$$

where m_{ia}, $1 \leq i, a, \leq 4$, are the entries of matrix $\mathbb{M}$.

References

[1] Fox, C. & Squire, V.A. 1994. *On The Oblique Reflexion and Transmission of Ocean Waves at Shore Fast Sea Ice*. Phil.Trans. R.Soc. Lond. A. **347**, pp. 185-218.

[2] Greenberg, M. D. 1971. *Application of Green's Functions in Science and Engineering*. Prentice-Hall. New Jersey.

[3] Hazard, C. & Lenoir, M. 1993. *Determination of Scattering Frequencies for An Elastic Floating Body*. Siam J. Math Anal. **Vol.24**, No.6, pp. 1456-1514.

[4] Liu, P. L-F. & Liggett, J. A. 1982. *Applications of Boundary Element Methods To Problems of Water Waves*. In Developments in Boundary Elements Methods - 2 ed. Applied Science Publishers. London.

[5] Meylan, M. 1993. *The Behaviour of Sea Ice in Ocean Waves*. Ph.D Thesis. University of Otago.

[6] Namba, Y. & Ohkusu, M. 1999. *Hydroelastic Behaviour of Floating Artificial Island in Waves*. International Journal of Offshore and Polar Engineering. **Vol. 9**, No.1, pp. 40-47.

[7] Staziker, D. J., Porter, D., & Stirling, D. S. G. 1996. *The Scattering of Surface Waves by Local Bed Elevations*. Applied Ocean Research. **18**, pp. 283-291.

[8] Stoker, J. J. 1957. *Water Waves: The Mathematical Theory with Applications*. Interscience Publishers, Inc. New York.

[9] Zwillinger, D. 1992. *Handbook of Differential Equations*. Academic Press, Inc. Harcourt Brace Jovanovich Publisher. New York.